c.1

LIGHTNING SURGE PROPAGATION IN OVERHEAD LINES AND GAS INSULATED BUS-DUCTS AND CABLES

by

LEE KAI-CHUNG

B.Sc., University of Wisconsin, 1973
M.Sc., University of British Columbia, 1975
M.A.Sc., University of British Columbia, 1977

A THESIS SUBMITTED IN PARTIAL FULFILMENT OF

THE REQUIREMENT FOR THE DEGREE OF

DOCTOR OF PHILOSOPHY
in
The Faculty of Graduate Studies

in the Department

of

Electrical Engineering

We accept this thesis as conforming

to the required standard

THE UNIVERSITY OF BRITISH COLUMBIA

July, 1980

In presenting this thesis in partial fulfilment of the requirements for an advanced degree at the University of British Columbia, I agree that the Library shall make it freely available for reference and study. I further agree that permission for extensive copying of this thesis for scholarly purposes may be granted by the Head of my Department or by his representatives. It is understood that copying or publication of this thesis for financial gain shall not be allowed without my written permission.

Department of EE

The University of British Columbia
2075 Wesbrook Place
Vancouver, Canada
V6T 1W5

Date Oct 14/88

ABSTRACT

The propagation characteristics of lightning surges in compressed SF_6 gas insulated power substation was studied using an electromagnetic transients program. Numerical models were developed to represent the behaviour of different system components especially under lightning over-voltage conditions.

The characteristics of lightning surge propagation in overhead multi-phase untransposed transmission lines was analysed first. Modal analysis, together with special rotation techniques to fit time domain solutions were then used to simulate the wave propagation in multi-phase untransposed line in an electromagnetic transients program. Non-linear voltage-dependent corona attenuation and distortion phenomena were also investigated. Available field test results could be duplicated to within 5%.

The characteristics of lightning surge propagation in multi-phase single-core SF_6 cables was studied next. A program was developed to obtain the cable parameters for typical cable configurations. The amount of core current returning through its own sheath and through the earth were computed to illustrate the single phase cable representation for wave propagation in single core SF_6 cables.

TABLE OF CONTENTS

ACKNOWLEDGEMENT

I would like to show my deepest appreciation to my thesis supervisor Professor Hermann W. Dommel for providing such a unique chance in doing research in electromagnetic transients of power systems. Dr. Dommel's valuable criticism, and countless hours of discussion during research are also gratefully acknowledged.

I am grateful to the B.C. Hydro Engineers, Messrs. Jack Sawada, Brent Hughes, Ken Nishikawara and Nick Cuk for their helpful discussions. I am also thankful to my fellow graduate students and colleagues Messrs. Obed Abledu, But-Chung Chiu, Shi Wei for their different points of view.

The financial support from the University of British Columbia in form of teaching and research assistantship and fellowship is very much appreciated. The financial assistance of the Systems Engineering Division of the British Columbia Hydro and Power Authority through a Power Systems Research Agreement, and the British Columbia Telephone Company Graduate Scholarship are also gratefully acknowledged.

Special thanks are expressed to Miss Gail Hrehorka in the Electrical Engineering Main Office for producing this excellently typed thesis.

Finally, I am indebted to my parents for their continuous encouragement and my wife for her patience.

INTRODUCTION

Every year, atmospheric lightning discharges cause numerous disturbances and damages to electric power systems, such as, destroying transformers and causing black-outs of large areas. This thesis is devoted to the analysis of lightning surge propagation into compressed SF_6 gas-insulated substations. The MICA project of the British Columbia Hydro and Power Authority was chosen as a test example.

Insulation co-ordination requirements are usually derived from simulated surge propagation studies. This thesis shows that the present practice of insulation co-ordination design can be improved with the numerical models developed in this thesis. The contributions of this thesis to insulation co-ordination design and related power system studies includes the following:

1. Determination of wave propagation in untransposed lines - Analysis is used, with a special rotation of modal parameters and transformation matrices to make the method suitable for time-domain solutions of wave propagation in multi-phase untransposed line. The suitability of different simplified transmission line models is clarified by comparing simulation results with those from an exact multi-phase representation.
2. Representation of non-linear voltage-dependent corona effects - Corona distortion and attenuation has been simulated with voltage dependent velocities and correction factors in the past[44,12], or with finite difference methods. However, these methods are inefficient for digital computer applications. More efficient computational algorithms, using compensation methods, are developed in this thesis to

investigate the non-linear voltage dependent corona effects.

3. Determination of wave propagation in multi-phase single core SF_6 cables - Published methods for the calculation of cable constants give inconsistent results. A new cable constants program for multi-phase single core SF_6-cables has been developed by the author, using various converging infinite series. The complete shielding effect of the externally grounded sheath at frequencies above 1 k Hz has been confirmed with this program.

The problem of transient groundrise caused by internal breakdowns or by lightning impulses, as studied by Ontario Hydro[51], is not included in this thesis. These transient potential differences between SF_6 bus-ducts and ground occur mainly at the junction with the overhead line. As this thesis shows, the current return in the SF_6 bus-duct is completely through the sheath at frequencies above 1 kHz, whereas the current return of the lightning impulse on the overhead line isin the ground. At the junction, the return current must therefore pass from the sheath into the ground through the ground leads, which in turn causes the transient groundrise problem. These transient groundrises are an important factor in the design of the grounding system, because they can cause damage to an auxiliary wiring or shocks to personnel.

CHAPTER 1: LIGHTNING CHARACTERISTICS AND STROKES TO POWER TRANSMISSION LINES

1. Introduction

The first important experiment on lightning was done by Benjamin Franklin, who used flying kites to show that lightning is electrical in nature. For more than two centuries, lightning has been the subject of active research. Much of this research has been concerned with the protection of people and property against the effects of lightning stroke.

2. Lightning discharge mechanisms

Lightning strokes are first initiated inside thunder-clouds. A thunder-cloud usually contains several negative and positive charge centres distributed in different locations as shown in Figure 1.1a. As soon as the electron is jumping over to neutralize the positive charge, a step leader starts to move down the earth in discrete zig-zag steps of about 50 meters in length as shown in Figure 1.1b. This downward pilot stroke is about 1 cm in diameter and is not visually detectable by the human eye.

As this stepped leader continues to progress downwards, positive charges are induced and accumulated on the ground surface. Eventually, these positive charges jump upwards and form the return stroke to meet the downward stepped leader as shown in Figure 1.1c. This highly luminous return stroke produces most of the thunder which is heard. The return stroke is about 10 cm in diameter and at a temperature of around 30,000°K. Once all the positive charges transfer to the thunder-cloud as shown in Figure 1.1d, the discharged charge centre completely becomes

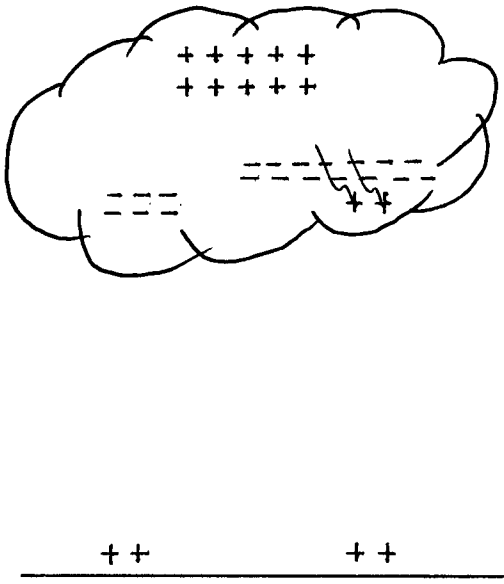

a. Charge neutralization within the cloud.

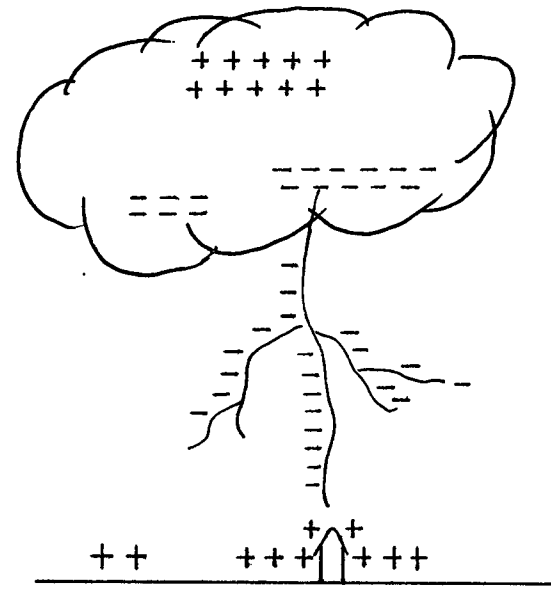

b. Stepped leader moving downwards.

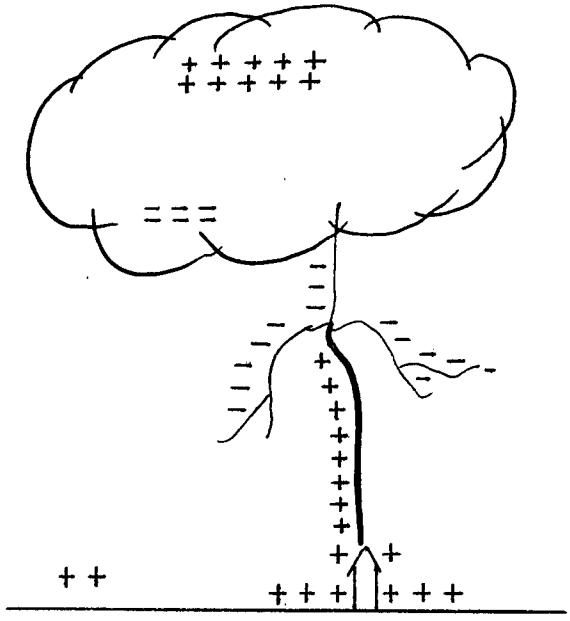

c. Initialization of upward moving return leader.

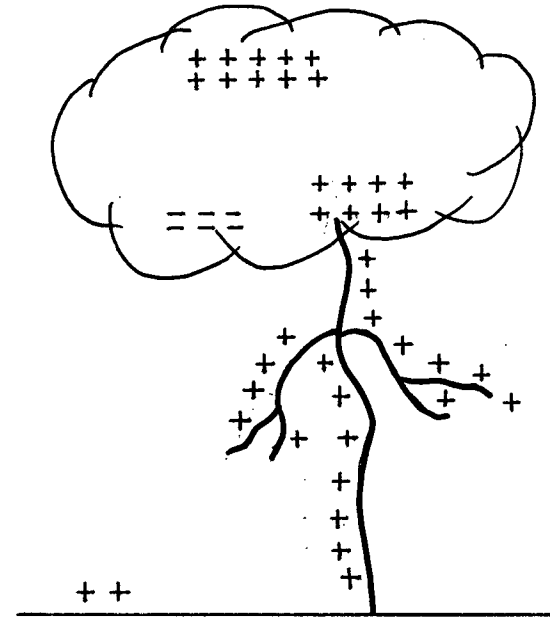

d. Complete upward propagation of return leader to cloud (charge centre becomes positive).

Figure 1.1: Charge distribution and propagation during initial lightning discharge.

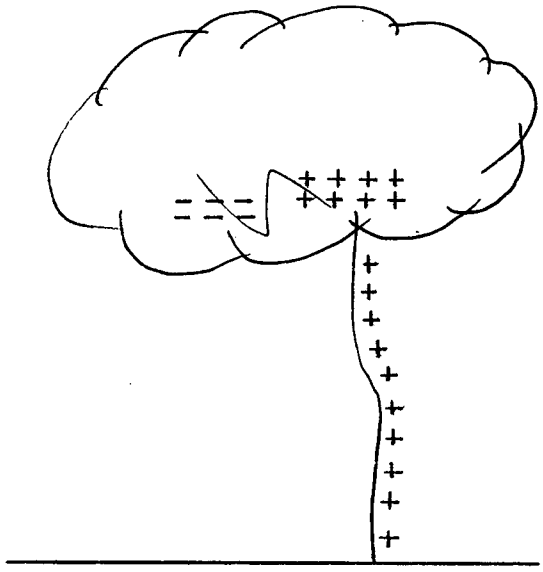

a. Discharge between 2 charge centres.

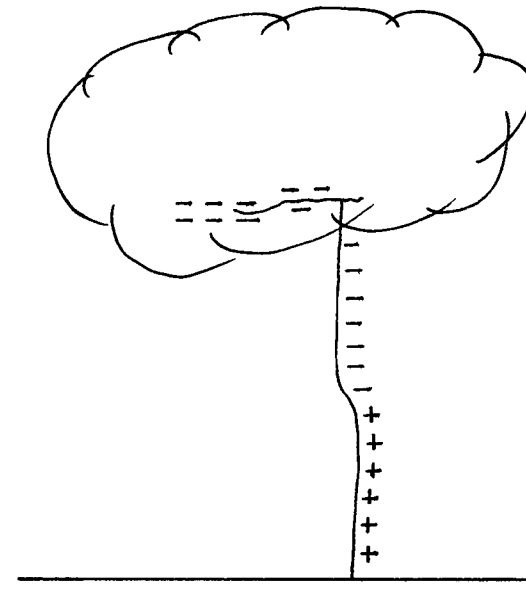

b. Negative charge dart stroke flowing down the continuous earth path.

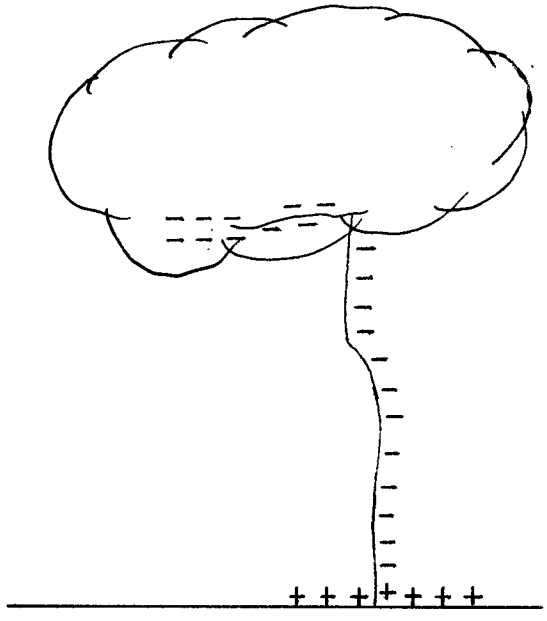

c. Negative charge dart stroke about to hit the ground.

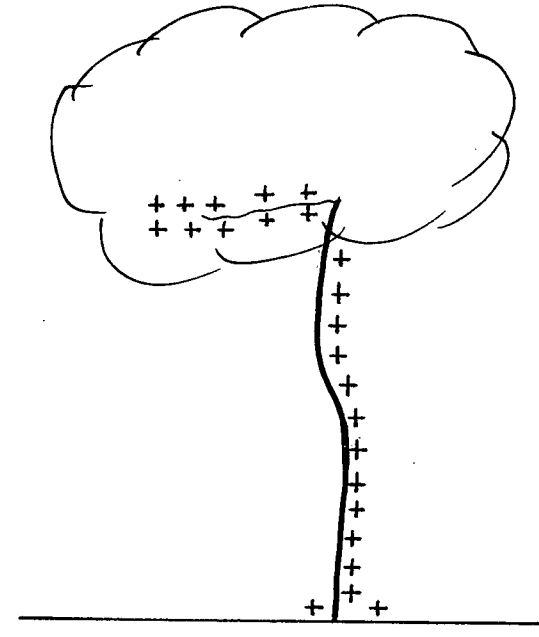

d. Formation of subsequent return leader from ground to cloud charge centres.

Figure 1.2: Charge distribution and propagation during subsequent dart leader (multipli-stroke lightning).

positive and single stroke lightning discharge is completed.[1]

However, about 50% of all lightning flashes are multi-strokes[2,3] and contain 3 or 4 subsequent strokes, typically separated by 30 to 40 ms. About less than 100 ms after the first stroke, a high potential difference is again established between the charge centres. Discharges again occur and a dart leader is formed which moves earthwards in the previous main stream as shown in Figure 1.2a to 1.2c. Similarly, a return stroke is also formed and more positive charges transfer to the thunder-clouds as shown in Figure 1.2d.

The whole process of multi-strokes with relative stroke magnitudes and time scales is illustrated in Figure 1.3a and 1.3b. Typical subsequent strokes are $\frac{1}{5}$ of the initial stroke magnitude and are well separated (about 30 - 40 ms) in time. The initial stroke is the prime factor in the insulation co-ordination studies, but subsequent strokes must be taken into account as arresters must be able to handle repetitive discharges, and the dead times of the auto-reclosing switchgear must be set longer.

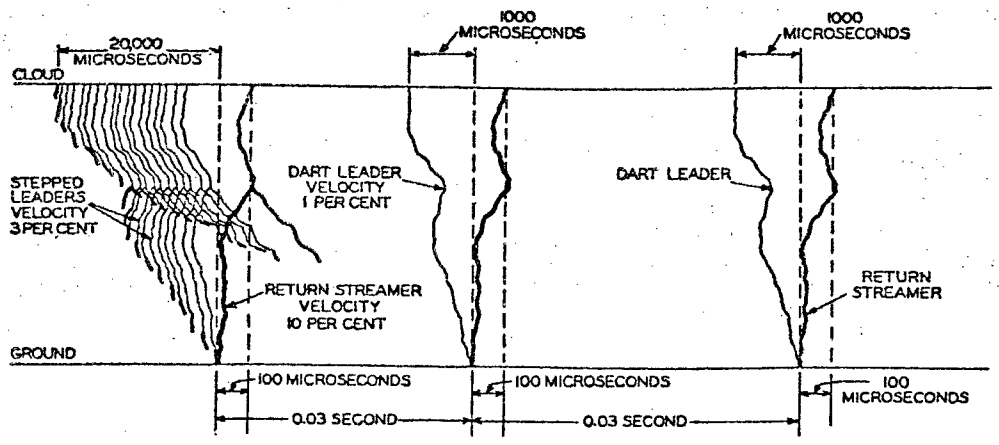

Velocity 100% = 300 m/μs

Figure 1.3a: Diagram showing time intervals between initial and subsquent strokes. (Ref. 3)

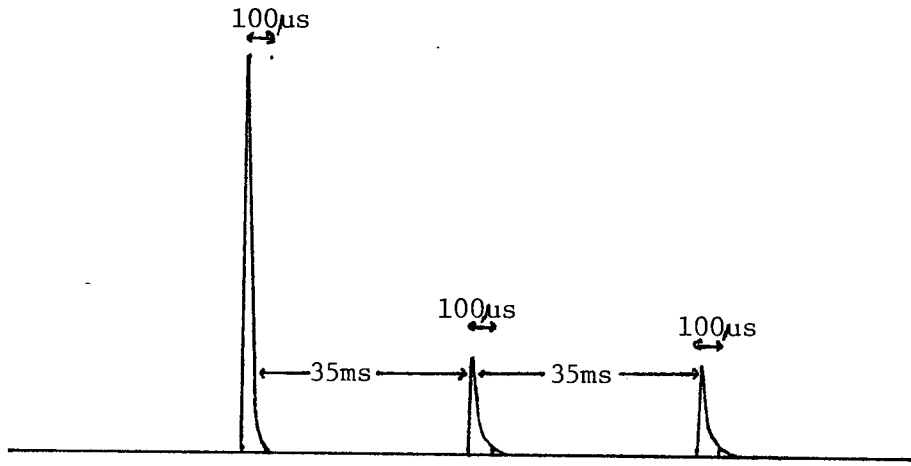

Figure 1.3b: Current magnitudes of initial and subsequent strokes in typical lightning flashes.

3. Statistical characteristics of lightning strokes

Due to the different distributions and intensities of charge centres inside the thunder-cloud, the characteristics of lightning strokes show a large statistical variation in both magnitude and shape.

a. Magnitude of lightning strokes

The voltage stress on the power system depends on the magnitude of the lightning current, which is therefore a critical factor in determining insulation requirements. Recorded measurements[4,52] are shown in Figure 1.4. It can be seen that 80% of the lightning current magnitudes are within 10 to 100 kA, and only 5% exceed magnitude of 100 kA.

It is suggested[52] that the lightning stroke has to be simulated as an incident current source to the power line with a maximum current magnitude of 100 kA for insulation co-ordination studies. However, this current source will become an overvoltage wave when propagating down the power line due to the inherent surge impedance of the line. Thus, for

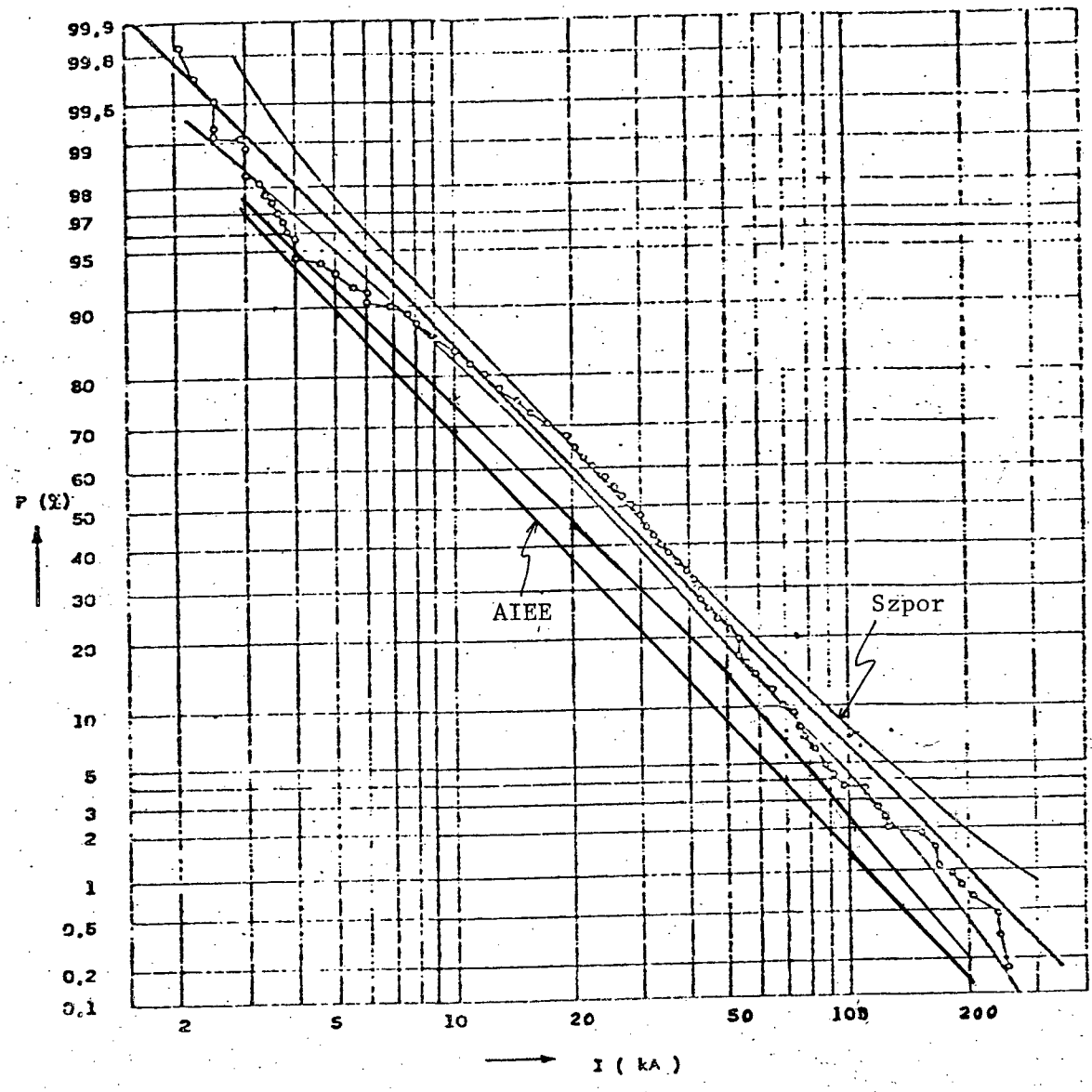

Figure 1.4: Cumulative Probability of Occurrence of the Amplitudes of Lightning Currents obtained by summarising results from more than 624 measured incidents from 9 countries (Ref. 4).

equipment test purposes, overvoltage waves are prescribed.

b. Waveshape of lightning stroke

The lightning waveshapes measured by different researchers essentially resemble a double exponential waveshape of different rise time and decay time. The observed spread of rise time is from very short to 10 μs. The observed decay time also spreads from 2 to 100 μs [5] (see Figure 1.5a). The electric power industry therefore agreed many years ago to use a lightning overvoltage wave for equipment insulation testing purpose of a shape 1.2 x 50 μs (explanation of designation in Figure 1.5b and 1.5c). Some testing precriptions also specify that this full wave be chopped with a spark gap in the tail to expose the equipment to the higher frequencies which are contained in the voltage collapse.

4. Frequency of lightning strokes to earth

The thunderstorm activity on earth is measured by the isokeraunic level. This isokeraunic level (IKL) gives the number of days per year that thunder has been heard. Usually, thunder cannot be heard outside a 7-24 km radius. An updated world map of isokeraunic level [6] is shown in Figure 1.6. As expected, higher IKL is found within the tropical and sub-tropical regions close to the equator.

After obtaining the IKL of a given place, the number of strokes to earth per km^2 (N) in a particular location is given by [7]

$$N = A\ (IKL)\ \text{stroke}/(km^2 - yr)$$

where

$$A = 0.1 \text{ to } 0.2$$

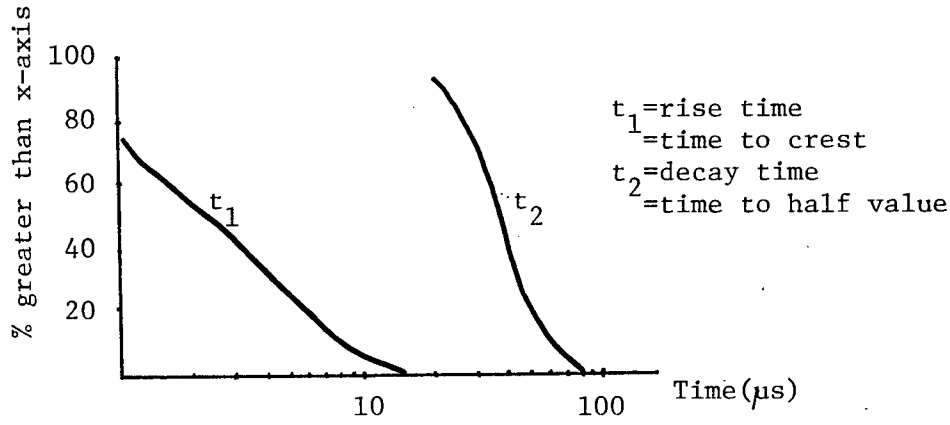

a. Wave fronts and tails of lightning surges

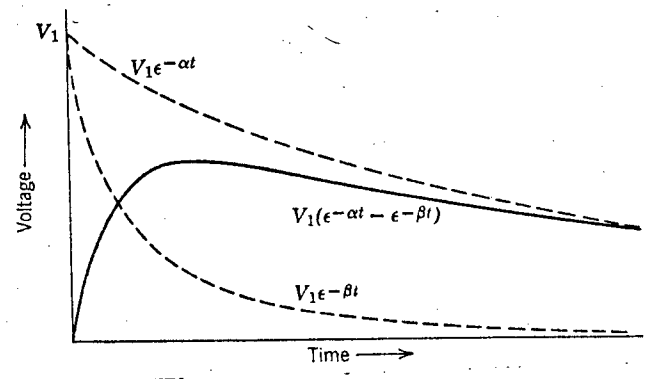

b. Double exponential wave $V = v_0 (e^{-\alpha t} - e^{-\beta t})$.

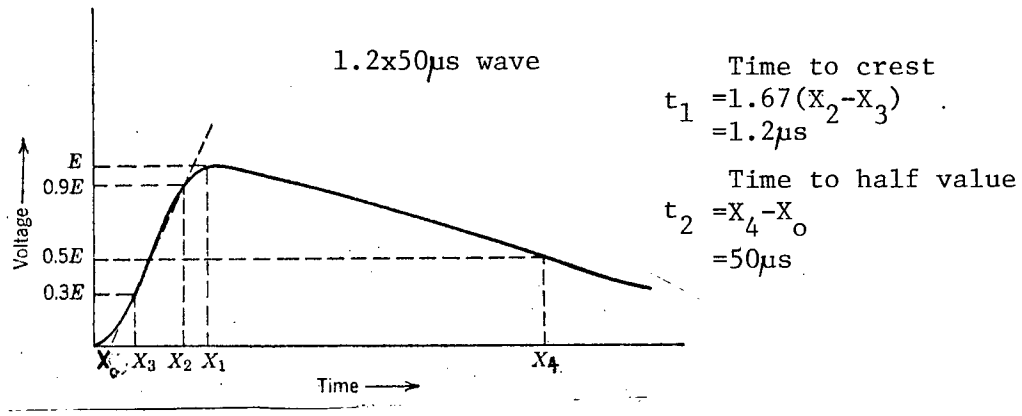

c. Typical surge waveform impulse generator

Figure 1.5: Waveshape of lightning strokes.(Ref.5)

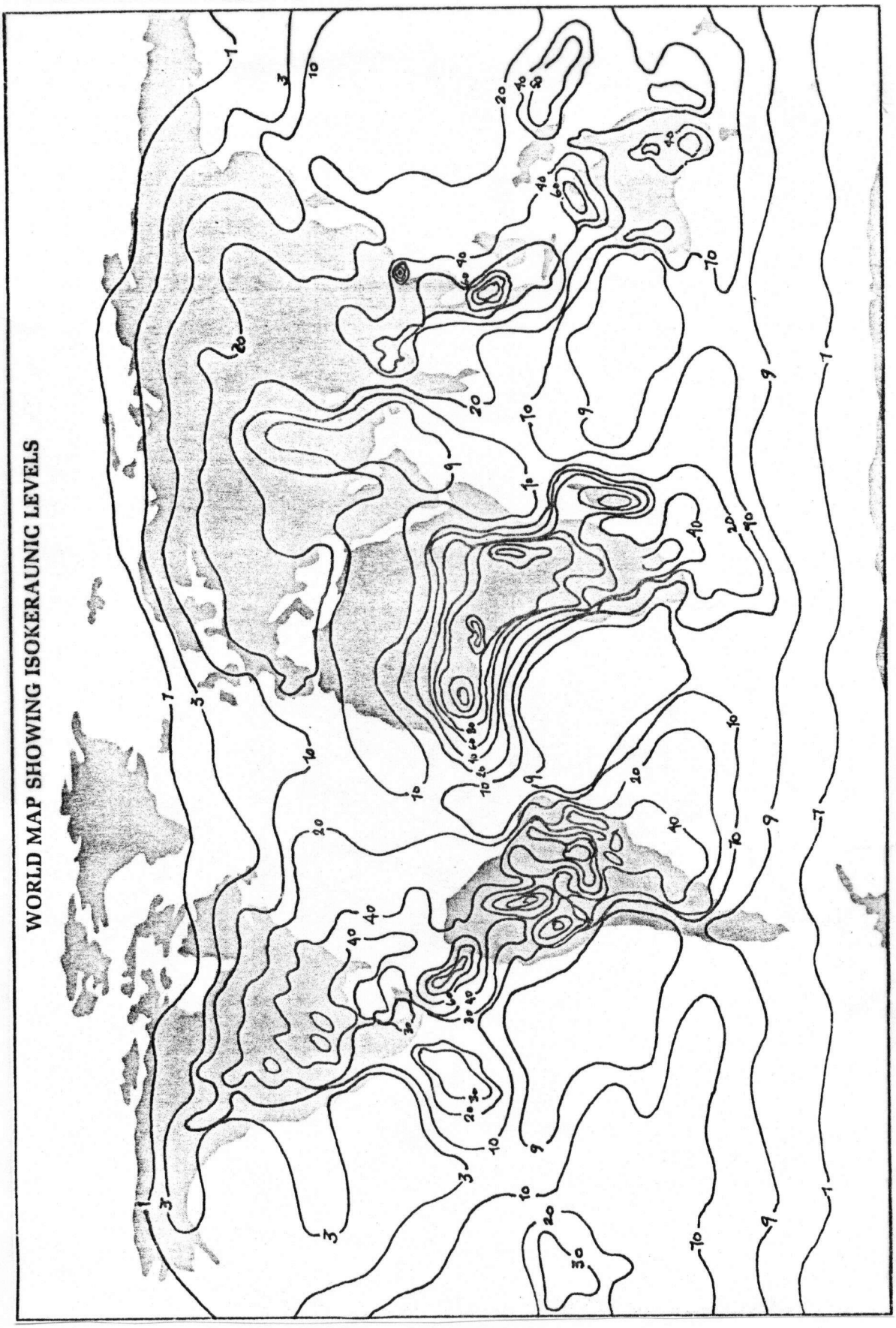

Figure 1.6: World Distribution of Thunderstorm Days (Ref.6)

5. Frequency of lightning strokes to power lines

For estimating the number of lightning strokes to power lines, we can start from the 'electrical shadow' cast on the ground by the tall tower structure with power lines. The frequency of lightning strokes on the 'electrical shadow' is assumed to be the frequency of strokes to the power lines. The width (w) of the shadow area estimated by reference 6 is chosen. For a power line with two ground wires, the width is given by (see Figure 1.7)

$$w = 4h + b$$

where h = height of ground wire in m

b = separation between ground wires

Similarly, for a power line with only 1 ground wire, the width is given by

$$w = 4h$$

where h = height of ground wire in m

and for power lines without ground wires, the width is given by

$$w = 4h + b$$

where h = height of phase wire in m

b = separation between outermost phase wires

Thus, the number of strokes/km - yr to the power line (N_L) is

$$N_L = 0.1\ (IKL)\ \frac{W}{1000}\ \text{stroke /km -yr} \qquad (1.1)$$

For a typical 500 kV tower of the MICA Dam Project, for the line close to the substation, we have

$$N_L = (0.1)(30)\frac{4 \times 37.5 + 18.64}{1000} \qquad (1.2)$$

$$= 0.5 \text{ strokes/km - yr}$$

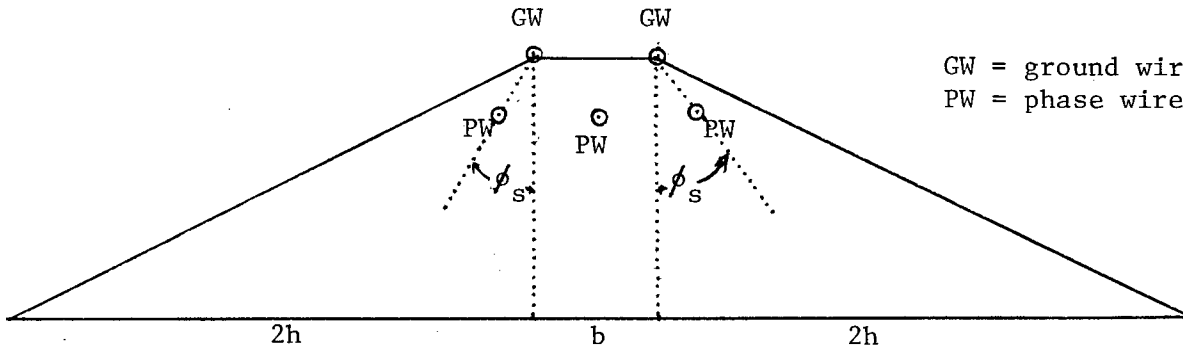

GW = ground wire
PW = phase wire

ϕ_s = shielding angle

= 23°

h = height of ground wire

= 37.5 m

b = width between ground wire

= 18.64 m

Figure 1.7: Lightning stroke 'Electrical shadows' of a typical 500 kV transmission line.

6. Shielding failure phenomenon of lightning strokes

As shown in Figure 1.7, ground wires are designed for shielding of the phase wire from direct lightning strokes. However, lightning strokes

could still 'sneak' through the ground wire and hit the phase wire. Such shielding failures have been recorded in various countries for different tower configurations.

Maikopar[6] derived a shielding failure curve based on observed field data (see Figure 1.8). However, the graph does not shows the fact that shielding failures occur mainly on lower lightning strike currents. At higher currents, (e.g. >14.2kA for MICA), the phase wire is effectively shielded from lightning strokes.

As seen from Figure 1.1 and 1.2, the pilot downward stepped leader from the thundercloud is formed and propagates earthward freely regardless of the structure on earth initially. Later, the return strokes is formed from a ground object closest to the leader tip, (ground wire, phase wire, or the ground) and propagates upward to meet the stepped leader to complete the lightning path. This ground object is the object which will be struck by the lightning stroke.

Brown[8] analysed results from the 120,000 km - yr line in the Pathfinder Project and deduced that the target is not chosen until the distance between the stepped leader tip and the prospective object is shorter than the striking distance r_s. This striking distance is related only to the stroke current as

$$r_s = 7.1\ I^{0.75} \quad m$$

where

I = current in kA

From this striking distance concept, we can develop the electrogeometric model as shown in Figure 1.9a. The shielding failure of ground wire at lower current amplitudes can correctly explained by this more refined method. The degree of exposure of different conductors is

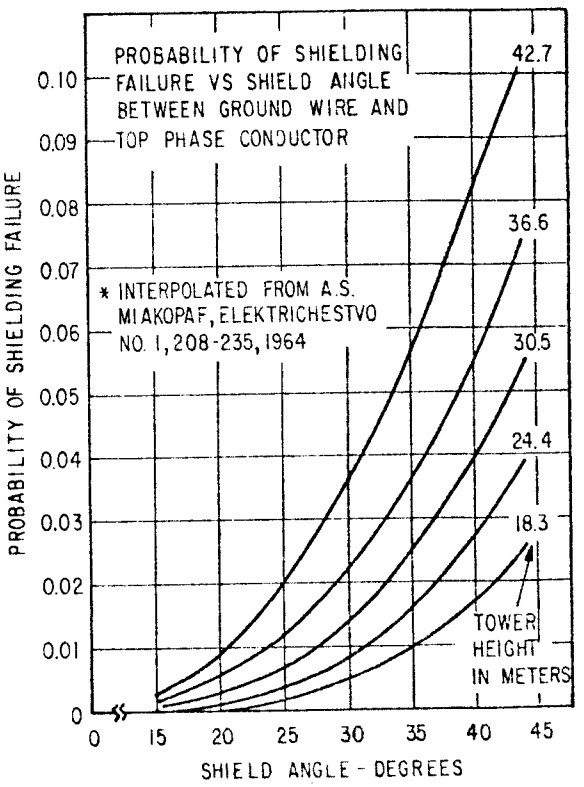

Figure 1.8: Probability of Shielding Failure vs. Shield Angle between Ground Wire and Top Phase Conductor.[7]

represented by drawing exposure arcs of striking distance radius, and centred at each individual conductors. The initial power frequency voltage of the phase conductor is ignored as this voltage is comparatively small to the discharge voltage of the lightning strokes.

For lightning currents of 10 kA and 14.2 kA, the corresponding exposure of the phase conductor PW is shown. It can be seen that the phase conductor exposure to lightning stroke is decreased with increases in striking current. For current of amplitudes higher than 14.2 kA, for this tower structure in MICA project, the phase conductor is effectively shielded by the ground wire and the ground as the exposure arc is negligible in size (See Figure 1.9a).

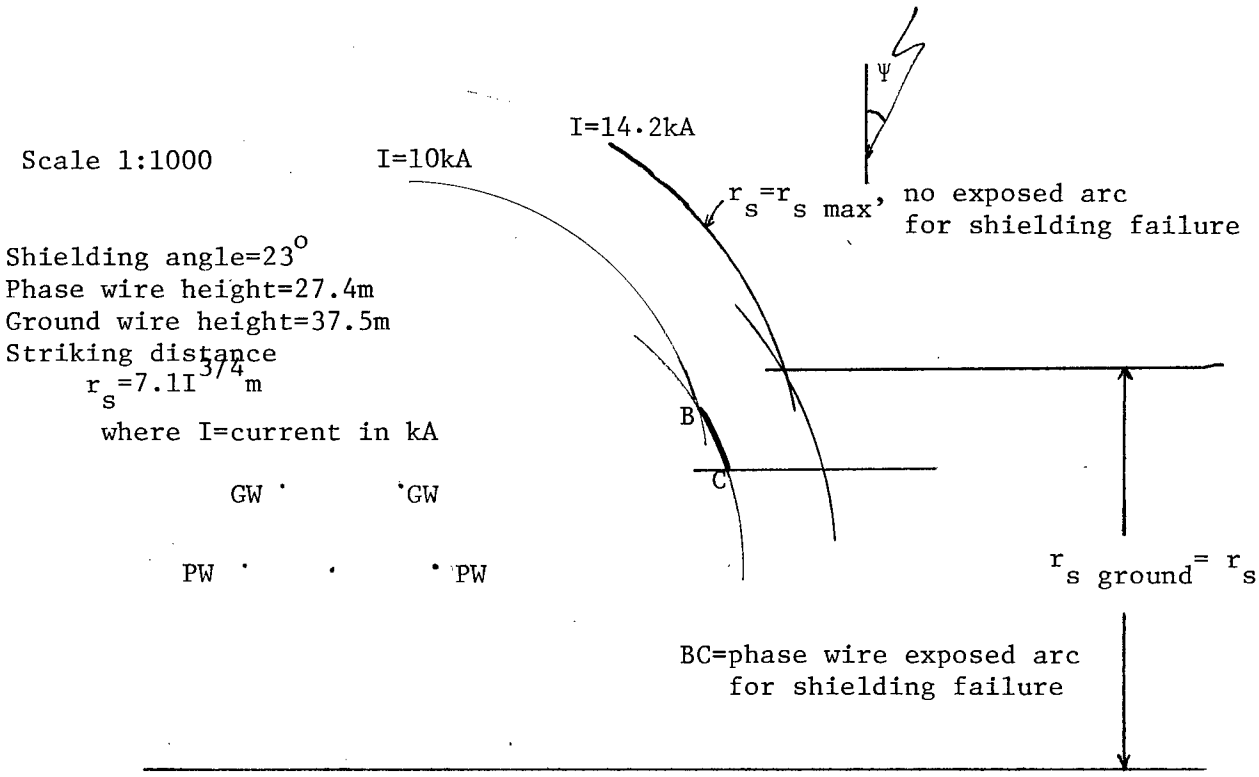

Figure 1.9a: Electrogeometric model with maximum striking distance of 53.3m.

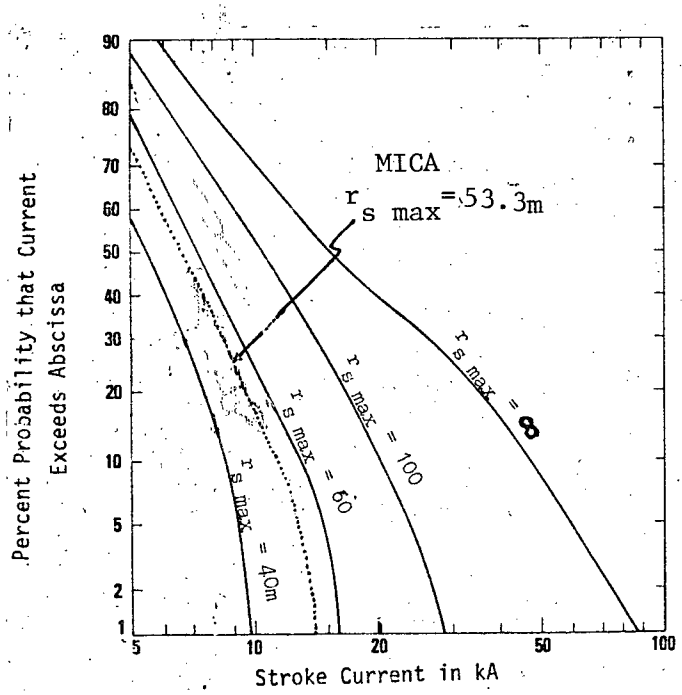

Max striking distance

$$r_{s\ max} \cong \frac{h+y}{2(1-\sin\phi_s)}$$

where h=ground wire height
y=phase wire height
ϕ_s=shielding angle

Figure 1.9b: Frequency Distribution of Shielding Failure Stroke Currents in case of Shielding Failure

Brown et al further investigated this situation by taking the angular distribution of the lightning stroke $g(\psi)$ into account and evaluated the phase wire exposed arc for different stroke currents as

$$x = r_s \int_{\phi_1}^{\phi_2} \int_{\psi_2(\phi)}^{\psi_1(\phi)} \frac{\sin(\phi-\psi)}{\cos\psi} g(\psi) d\psi d\phi \qquad (1.3)$$

where:

$$g(\psi) = \frac{2}{\pi} \cos^2\psi \qquad (1.4)$$

The detailed analytical results are shown in Figure 1.9b. For our MICA tower of maximum striking distance of 53.3 m (I =14.2kA), the result shows that less than 1% of shielding failure lightning currents to the phase wire will exceed 14 kA. This agrees well with the geometric interpretation shown in Figure 1.9a.

The lightning stroke usually hit the ground wire or the tower. In this case, a voltage will build up across the insulator because of the potential rise on the tower crossarms. If the insulator flash over (' backflashover') to the phase conductors, then lightning overvoltage surges will appear on the conductors.

CHAPTER 2: LIGHTNING SURGE PROPAGATION IN OVERHEAD TRANSMISSION LINES

1. Introduction

Propagation of lightning surges due to direct strokes or backflashovers in overhead lines influences the choice of insulation requirements. One must know the attenuation and distortion characteristics of the line in order to find the overvoltages entering the substation where most of the equipment is concentrated. This section tries to answer the questions whether it is possible to represent untransposed overhead lines as equivalent single phase lines for the stricken conductor with accuracy, and whether self, positive or zero sequence impedances should be used in such single-phase representations?

At first, field tests results are duplicated by using a Fourier transformation method.[9] This method not only includes the frequency-dependence of the line parameters, but it also uses the exact complex, frequency-dependent transformation matrix which requires recomputation at each frequency within the frequency range typical of lightning surges (e.g. 10 k Hz to 1MHz). This method is recommended for the simulation of distant strokes where the frequency dependent characteristics must be included.

For close-by lightning strokes, the above frequency-domain solution can be replaced by a simpler time-domain solution method. This method is based on modal analysis with frequency-independent parameters and real-valued transformation matrices. The results obtained with the simpler time-domain simulation method agree very well (< 4% deviation) with the accurate frequency-domain simulation method.

After confirming the correctness in the time-domain simulation with the exact N - phase representation of the overhead line for close-by lightning strokes, the results obtained are thus compared against single-phase approximate representations as presently used. Furthermore, additional recommendations are made on how to remove uncertainties in the choice of surge impedance values of overhead lines.[10] It is also found that frequency dependence effect of nearby lightning stroke can be ignored. Line parameters can be chosen at high frequency e.g. at 1 M Hz, and line resistance can be ignored as contradictory to the previous findings.[11,12]

2. Modal analysis for N - phase untransposed line

The well known transmission line equations describe the propagation of electromagnetic waves on overhead transmission lines. However, contrary to the single phase case, the solution to the N- phase case cannot be obtained easily since each of the N overhead conductors is mutually coupled to the other conductors. The following two sets of simultaneous second-order partial differential matrix equations describing the change in voltages and currents along the N - phase line must be solved:

$$-\left[\frac{dV^{phase}}{dx}\right]_{nx1} = [Z^{phase}]_{nxn}[I^{phase}]_{nx1} \qquad (2.1)$$

$$-\left[\frac{dI^{phase}}{dx}\right]_{nx1} = [Y^{phase}]_{nxn}[V^{phase}]_{nx1} \qquad (2.2)$$

where

$[Z^{phase}]_{nxn}$ = impedance matrix in phase domain

$[Y^{phase}]_{nxn}$ = admittance matrix in phase domain

$[I^{phase}]_{nx1}$ = phase current vector

$[V^{phase}]_{nx1}$ = phase voltage vector

The N coupled differential equations in equations (2.1) and (2.2) can be transformed into N decoupled equations by replacing phase quantities with modal quantities,

$$[V^{phase}] = [T_v]\,[V^{mode}] \tag{2.3}$$

$$[I^{phase}] = [T_i]\,[I^{mode}] \tag{2.4}$$

and by choosing $[T_v]$ and $[T_i]$ in a certain way, as described later. Applying equations (2.3) and (2.4) to equations (2.1) and (2.2) gives

$$-\left[\frac{dV^{mode}}{dx}\right] = [T_v]^{-1}\,[Z^{phase}]\,[T_i]\,[I^{mode}] \tag{2.5}$$

$$= [Z^{mode}]\,[I^{mode}] \tag{2.6}$$

and

$$-\left[\frac{dI^{mode}}{dx}\right] = [T_i]^{-1}\,[Y^{phase}]\,[T_v]\,[V^{mode}] \tag{2.7}$$

$$= [Y^{mode}]\,[V^{mode}] \tag{2.8}$$

To find $[T_v]$, we first differentiate equation (2.1) with respect to x, and replace $\left[\frac{dI^{phase}}{dx}\right]$ with equation (2.2):

$$\left[\frac{d^2V^{phase}}{dx^2}\right] = [Z^{phase}]\,[Y^{phase}]\,[V^{phase}] \tag{2.9}$$

With equation (2.3), this can be written in modal quantities as

$$\left[\frac{d^2V^{mode}}{dx^2}\right] = [T_v]^{-1}\,[Z^{phase}]\,[Y^{phase}]\,[T_v]\,[V^{mode}] \tag{2.10}$$

$$= [\Lambda]\,[V^{mode}] \tag{2.11}$$

If $[T_v]$ is the matrix of eigenvectors of $[Z^{phase}]\ [Y^{phase}]$, then $[\Lambda]$ becomes a diagonal matrix, with its elements being the eigenvalues of $[Z^{phase}]\ [Y^{phase}]$.

Similarly, for the current quantities, we have

$$\left[\frac{d^2 I^{mode}}{dx^2}\right] = [T_i]^{-1}\ [Y^{phase}]\ [Z^{phase}]\ [T_i]\ [I^{mode}] \tag{2.12}$$

$$= [\Lambda]\ [I^{mode}] \tag{2.13}$$

where $[T_i]$ = matrix of eigenvectors of $[Y^{phase}]\ [Z^{phase}]$, with $[\Lambda]$ being identical to that in equation (2.11).

Taking the transpose of the expression for $[\Lambda]$ in equation (2.12) and comparing it with that for $[\Lambda]$ in equation (2.10), while remembering that $[Z^{phase}]$ and $[Y^{phase}]$ are symmetric, gives:

$$[\Lambda] = [T_i]^t\ [Z^{phase}]\ [Y^{phase}]\ ([T_i]^t)^{-1}$$

$$= [T_v]^{-1}\ [Z^{phase}]\ [Y^{phase}]\ [T_v]$$

or
$$[T_v] = ([T_i]^t)^{-1} \tag{2.14}$$

Thus, only one of the matrices $[T_i]$ or $[T_v]$ is needed. Using only the $[T_i]$-matrix, we can obtain the modal parameters of $[Z^{mode}]$ and $[Y^{mode}]$ from equation (2.6) as

$$[Z^{mode}] = [T_i]^t\ [Z^{phase}]\ [T_i] \tag{2.15}$$

and from equation (2. 8) as

$$[Y^{mode}] = [T_i]^{-1}\ [Y^{phase}]\ ([T_i]^t)^{-1} \tag{2.15a}$$

or
$$[Y^{mode}]^{-1} = [T_i]^t\ [Y^{phase}]^{-1}\ [T_i] \tag{2.16}$$

In the computer program developed for this modal analysis,[13,14] equation (2.16) is used for these two reasons: it does not require the inverse of $[T_i]$ and secondly, the program calculates $[Y^{phase}]^{-1}$ first anyhow, from which $[Y^{phase}]$ is obtained by inversion. $[Y^{mode}]$ is then easily obtained by taking the reciprocal of the diagonal elements of the right-hand side of equation (2.16). $[Z^{mode}]$ is not calculated from equation (2.15), but in a simpler way from

$$[Z^{mode}] = [\Lambda]\ [Y^{mode}]^{-1} \tag{2.17}$$

that is, each component is simply

$$Z^{mode}_{i} = \frac{\Lambda_i}{Y^{mode}_{i}} \tag{2.18}$$

This is valid because $[\Lambda]$ from equation (2.11) can be rewritten as

$$\begin{aligned}[\Lambda] &= [T_v]^{-1}\ [Z^{phase}]\ [Y^{phase}]\ [T_v] \\ &= [T_v]^{-1}\ [Z^{phase}]\ [T_i].\ [T_i]^{-1}\ [Y^{phase}]\ [T_v] \\ &= [Z^{mode}].\ [Y^{mode}]\end{aligned} \tag{2.19}$$

3. Rotation of eigenvectors for zero shunt conductance

It has to be noted that the eigenvectors (columns of $[T_i]$ or $[T_v]$) are only determined to within a multiplicative constant. Each eigenvector can, therefore, be multiplied with any non-zero complex scalar, and it will still be the correct eigenvector.

Since we assume zero phase shunt conductances (corona losses will be discussed later in Chapter 4), the modal conductances should also be zero. This can be achieved by multiplying the eigenvectors with a properly chosen constant. Then equation (2.8), which is defined in the frequency domain,

can be rewritten in the time domain as follows

$$-\left[\frac{\partial i^{mode}}{\partial x}\right] = [C^{mode}] \left[\frac{\partial v^{mode}}{\partial t}\right]$$

In order to obtain zero modal conductances, a rotation scheme is used which makes the modal admittance matrix $[Y^{mode}]$ purely imaginary,

$$[Y^{mode}]_{rotate} = [0] + j[B^{mode}]_{rotate}$$

This rotation is equivalent to dividing the i-th eigenvector (i-th column of $[T_i]$) by a factor D_i. First, find the angle θ_i of Y_i^{mode}, as shown in Figure 2.1.

Then

$$D_i = e^{j\frac{90° - \theta_i}{2}} \tag{2.20}$$

With all D_i's forming a diagonal matrix [d], the modified matrix of eigenvectors becomes

$$[T_i]_{rotate} = [T_i]\ [D] \tag{2.21}$$

Then from equation (2.15a),

$$[Y^{mode}]_{rotate} = [D]\ [T_i]^{-1}\ [Y^{phase}]\ ([T_i]^t)^{-1}\ [D] \tag{2.22}$$

or

$$[Y^{mode}]_{rotate} = [D]\ [Y^{mode}]\ [D] \tag{2.23}$$

Since all matrices in equation (2.23) are diagonal, equation (2.23) is simply a totation of Y_i^{mode} by an angle $(90° - \theta_i)$, which according to Figure 2.1, makes $[Y^{mode}]_{rotate}$ purely imaginary.

After $[Y^{mode}]_{rotate}$ is found from equation (2.23), and $[T_i]_{rotate}$ from equation (2.21), $[Z^{mode}]_{rotate}$ is calculated from

$$[Z^{mode}]_{rotate} = [\Lambda]\,[Y^{mode}]^{-1}_{rotate} \tag{2.24}$$

These modal quantities and transformation matrices obtained are characteristics of the particular design of the untransposed line. These modal parameters and modal transformation matrices are needed as input for the representation of untransposed distributed - parameter lines in the time domain solution, such as in the UBC version of the Electromagnetic Transients Program as described in [13,14].

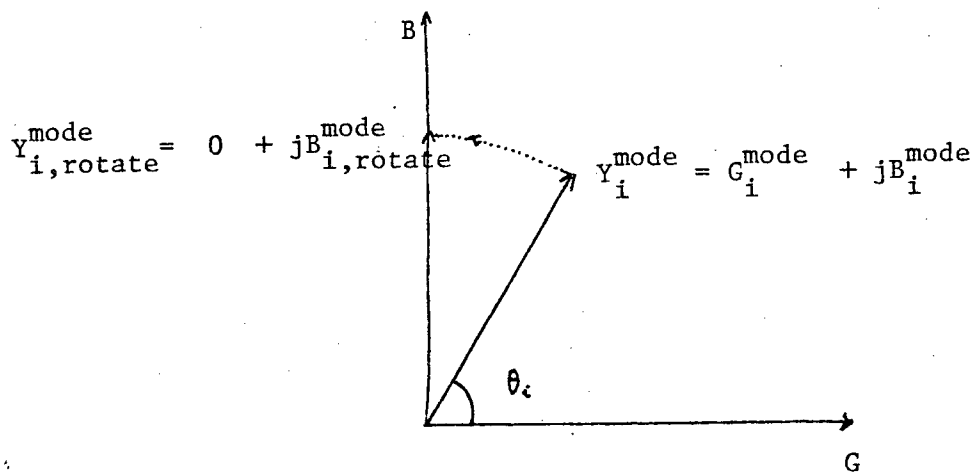

Figure 2.1: Complex Y^{mode}_i before and after rotation

4. Confirmation of accuracy of eigenvalue and eigenvector subroutine

The UBC Computing Centre library subroutine DCEIGN[15] is chosen to compute the eigenvalues and engenvectors of the $[Y]\cdot[Z]$ matrix. This double precision subroutine first reduces the complex matrix to a Hessenburg matrix H. The subdiagonal elements of H are then forced to converge to zero by the modified LR method.[49] Hence the diagonal elements of H converge to the eigenvalues. The eigenvectors can then be obtained by backward substitution.

The correctness of the program has been checked by comparing its output with published results for a double-circuit line[16]. Both results of modal attenuations and modal velocities agree to within three digits (see Table 2.1). The modal matrices $[T_v]$ differ only slightly (see Table 2.2).

Table 2.1

UBC & BPA modal analysis results for a 735 kV line[16].

Modal attenuation	neper/mile	Modal velocity	miles/s
	BPA	UBC	BPA
.15998E6	.15998E6	.61227E-1	.612E-1
.18438E6	.18437E6	.19050E-2	.191E-2
.18497E6	.18497E6	.18209E-2	.182E-2
.18606E6	.18605E6	.54529E-3	.544E-3
.18615E6	.18614E6	.50169E-3	.502E-2
.18614E6	.18614E6	.47704E-3	.475E-3

5. Real-valued frequency - independent transformation matrix

Time domain solutions with the transformation matrix $[T_i]$ become difficult in theory since $[T_i]$ is complex as well as frequency-dependent.

Table 2.2

UBC and BPA modal matrix $[T_v]$ results for a 735 kV line[16]

BPA:

$$[T_v] = \begin{bmatrix} .3412-j.0022 & .5558+j.0 & -.4959-j.0262 & .1730-j.0017 & .3209+j.0008 & .6827+j.0 \\ .3948-j.0157 & .3324+j.0230 & .5486-j.0 & .4647-j.0247 & .4804+j.0 & -.3550-j.0021 \\ .4822-j.0 & -.3128+j.0248 & -.1118+j.0056 & .5410-j.0 & -.4145+j.0304 & .0812+j.0061 \\ .3412-j.0022 & .5558+j.0 & -.4959-j.0262 & -.1730+j.0017 & -.3209-j.0008 & -.6827+j.0 \\ .3948-j.0157 & .3324+j.0230 & .5486-j.0 & -.4647+j.0247 & -.4804+j.0 & .3550+j.0021 \\ .4822-j.0 & -.3128+j.0248 & -.1118+j.0056 & -.5410+j.0 & .4145-j.0304 & -.0812-j.0061 \end{bmatrix}$$

UBC:

$$[T_v] = \begin{bmatrix} .3412-j.0022 & .5558+j.0612 & -.4959+j.0452 & .1730-j.0298 & .3209+j.0208 & .6827+j.0737 \\ .3955-j.0157 & .3294+j.0594 & .5453-j.0784 & .4681-j.0598 & .4659+j.0285 & -.3637-j.0422 \\ .4832-j.0 & -.3153-j.0095 & -.1105+j.0215 & .5469-j.0408 & -.4064+j.0048 & .0869+j.0159 \\ .3412-j.0022 & .5558+j.0612 & -.4959+j.0452 & -.1730+j.0298 & -.3209-j.0208 & -.6827+j.0737 \\ .3955-j.0157 & .3294+j.0594 & .5453-j.0784 & -.4681+j.0598 & -.4659-j.0285 & .3637-j.0422 \\ .4832-j.0 & -.3153-j.0095 & -.1105+j.0215 & -.5469+j.0408 & .4064-j.0048 & -.0869+j.0159 \end{bmatrix}$$

However, the imaginary part of the matrix $[T_i]$ is always small ($\sim$ 5%) compared with its real part. By taking the real part or the magnitude of the matrix itself, we obtain modal parameters which are still accurate enough ($\sim$ 2% deviation).

Furthermore, the attenuation caused by corona may be much higher than that caused by the series resistance and for close-by strokes, transmission lines should be represented as lossless. With the approximations, the frequency dependence of the modal transformation matrix disappears. It is therefore recommended that the complex matrix be approximated by a real-valued, frequency-independent matrix. This makes simulations much easier for two reasons:

a) A frequency independent modal matrix does not require recomputation of the modal matrix at each frequency considered within the lightning frequency range, e.g. 10 kHz to 100 kHz.

b) A real-valued modal matrix enables direct transient simulation to be performed in the time domain.

6. Frequency dependent effects in lightning surge propagation

To include frequency dependent effects in transient overvoltage studies is a complicated topic by itself. Meyer, Dommel[17] and Marti[18] have investigated the time domain methods using convolution integrals and weighting functions. However, the frequency domain solutions can also be obtained by the Fourier Transformation methods.[9] Though the frequency domain method is inadequate to account for the non-linear phenomenon (e.g. corona discharge) and the time domain phenomena (e.g. insulator back — flashover or arrester operation), it is sufficient for the purpose

of studying frequency dependent effects on lightning surge propagation in overhead lines.

As discussed in an earlier work[9], the frequency domain solutions includes frequency dependence of line parameters. It also uses the exact complex frequency dependent transformation matrix to be computed at each frequency point, and employs the linear interpolation technique in evaluating the Fourier Transformation integrals. The results from a measured field test by Ametani[19,20] of a laboratory generated distant lightning wavefront 83.212 km from the substation was successfully duplicated by the author using the Fourier Transformation method. (See Figure 2.2). Due to the frequency dependent effect of the line parameters, an initial rise time of 2 μs of the wavefront now increased to about 40 μs as the wave travelled down the line. Thus, the frequency dependent effect must be included for the distant lightning stroke case. The lightning waveshape obtained after the stroke has travelled from the striking point to the substation can then be interfaced with the time domain solutions as used in an electromagnetic transients program.[47]

For close-by lightning strokes, the resulting waveshapes can again be obtained by the Fourier Transformation integrals, and the simpler time domain methods. For the time domain method, the multi-phase untransposed line can be first solved by modal analysis using frequency independent parameters and real-valued transformation matrix (as described in previous sections). Then, this multi-phase line is represented by a single phase line approximation. As shown in Figure 2.3, results obtained by all these methods agree quite well (< 4% deviation). The single phase line representation with frequency independent effect is valid in this close-by stroke case because variations among the modal arrival times at range of lightning frequencies are not apparent in such short distances (e.g. < 2 km).

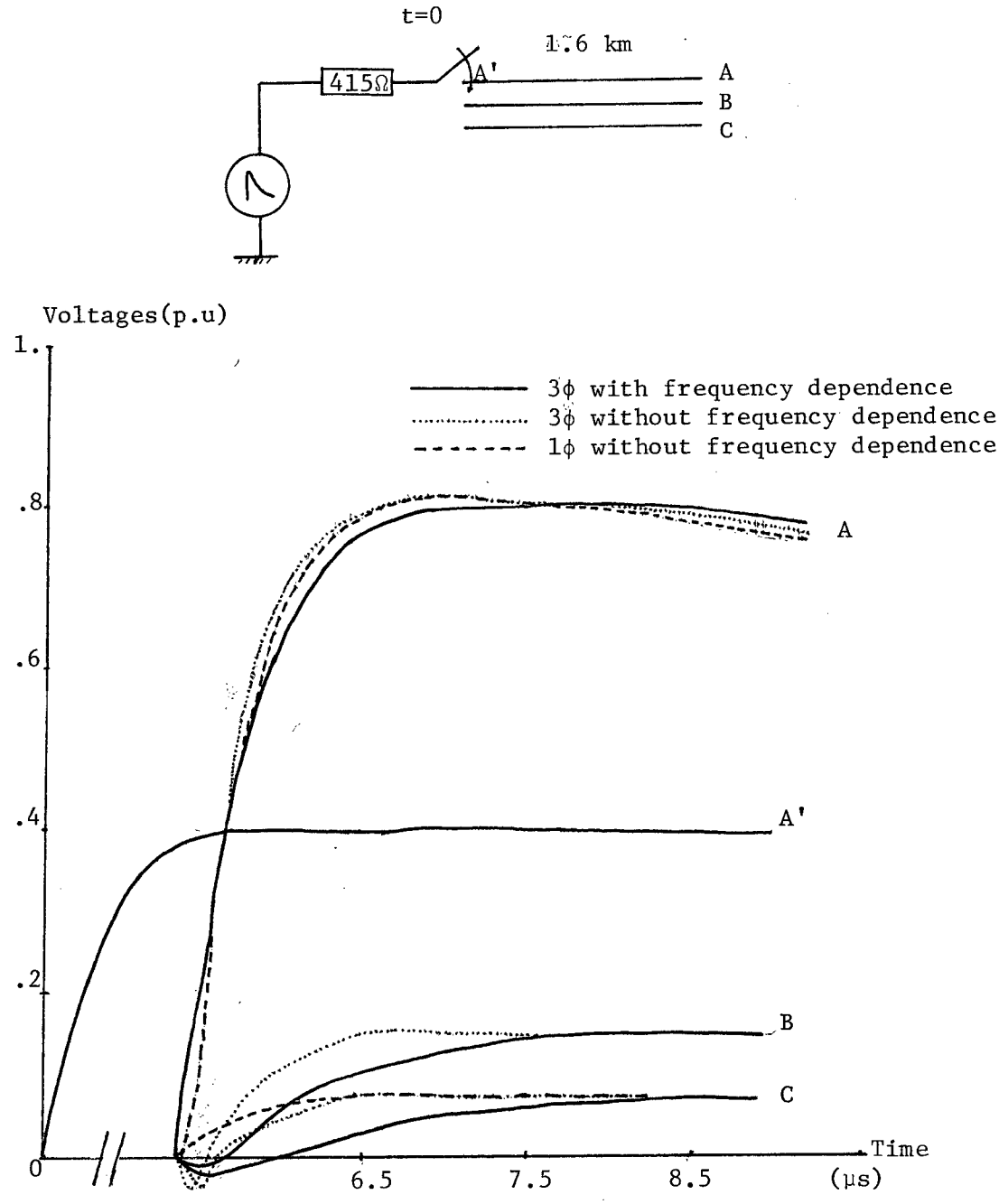

Figure 2.3: Close-by lightning stroke case solved by frequency and time domain methods.

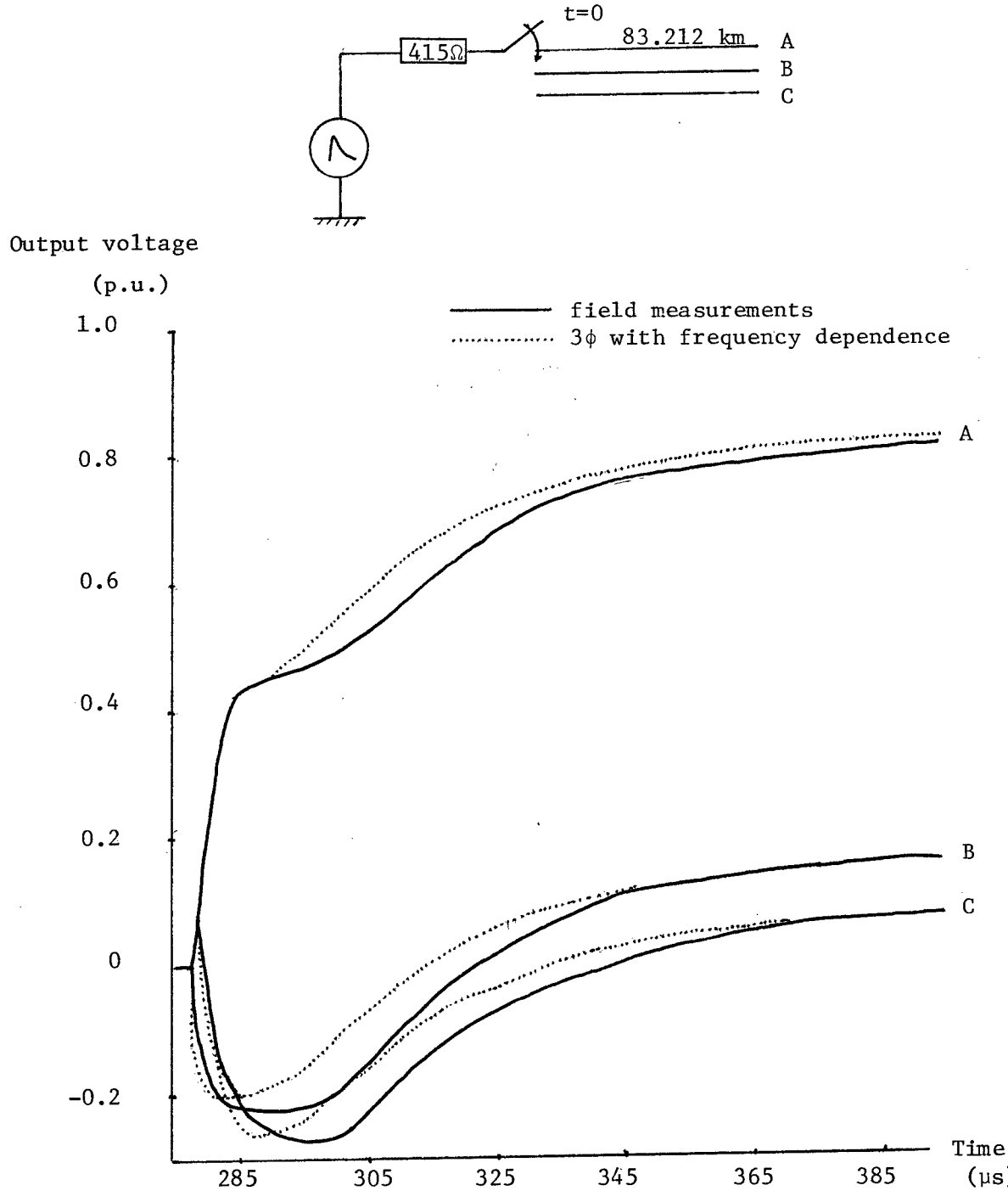

Figure 2.2: Numerical simulation of over-voltage taking untransposition and frequency dependence into account.(Ref. 9)

In such a representation, self impedance parameters calculated at higher frequencies (e.g. 1 MHz) should be used to approximate the frequency dependance characteristics of the line.

However, caution must be taken in choosing line resistance for the lightning surge studies. The frequency dependence of line parameters of one phase for a typical 500 kV line is shown in Table 2.3. It is shown that the attenuation of the wave is negligible (< 5%) up to about 100 kHz for 1 km. The resistance to reactance ratio is also small especially at higher frequencies, e.g. 2.8% at 1 M Hz. Furthermore, since the Bergeron's method of characteristic in solving the transmission line equation is valid only for a lossless transmission line, distributed line losses are usually approximated by lumping the resistance at certain locations. This high resistance at 1 M Hz may cause inaccuracy in the simulation. On the other hand, surge impedances calculated by

$$Z^{surge} = \sqrt{\frac{R + j\omega L}{j\omega C}} \qquad (2.25)$$

where $R/j\omega L = 2.8\%$ at 1 M Hz (See Table 2.3)

or

$$Z^{surge} = \sqrt{\frac{j\omega L}{j\omega C}} \qquad (2.26)$$

are essentially identical for this lossy and lossless cases. Thus, complicated frequency dependent effects for the nearby stroke case can be ignored, and frequency independent and lossless representation give acceptable accuracy (See Figure 2.9).

Therefore, the previous methods of modelling line losses by simple exponential decay in overvoltages[12] or any resistance lumping scheme[11,21] are not acceptable. They should be replaced by detailed weighting function techniques, or Fourier Transformation methods for distant stroke, or by

Frequency (Hz)	Resistance R(Ω/km)	Reactance X(Ω/km)	R/X %	Z^{surge} (Ω)	Velocity (m/μs)	Attenuation $e^{-\gamma \ell}$(/km)
10^6	183.	6525.	2.8	291.	280.	.73
10^5	42.	692.	6.	300.	272.	.93
10^4	7.	78.	9.	317.	257.	.989
10^3	.9	8.9	10.	340.	240.	.999

Table 2.3: Frequency dependence of self quantities of line parameters for a 3 phase 500 kV line.

lossless line representation for a nearby stroke as described in above.

7. Determination of the surge impedance of the struck phase of a transmission line.

An accurate and reliable value of the surge impedance in phase domain must be obtained as due to the following reasons:

a) The amount of overvoltage wave transmitted from the overhead line to the underground SF_6 cable at the cable-line junction is determined by the surge impedances of different components. The refraction coefficient C_R is

$$C_R = \frac{2\ Z_{surge}^{cable}}{Z_{surge}^{line} + Z_{surge}^{cable}} \qquad (2.27)$$

where

Z_{surge}^{cable} = surge impedance of cable (e.g. 60 Ω)

Z_{surge}^{line} = surge impedance of line (e.g. 304 Ω)

b) The exact value of the overvoltage wave on the line, resulting from the lightning stroke (I_k) is directly related to surge impedance of the line Z_{surge}^{line} as

$$\ddot{v} = \frac{I_k}{2} \cdot Z_{surge}^{line} \qquad (2.28)$$

This resulting overvoltage wave impresses electrical stress on external and internal insulation of the system and forms the main concern in the insulation co-ordination study.

In spite of the above important criteria, uncertainties in surge impedance calculations of overhead line do exist.[10,11,12] Reference 11 give relatively lower surge impedance results for the ground wire (352 Ω) as compared to Darveniza's computation.[12] Darveniza claims that the equation for surge impedance in phase domain as is given by:

$$Z_{self}^{surge} = 60 \ln \frac{2h}{r} \tag{2.29}$$

$$Z_{mutual}^{surge} = 60 \ln \frac{a_{ij}}{b_{ij}} \tag{2.30}$$

where h = conductor height

r = conductor radius

a_{ij} = separation between conductors

b_{ij} = separation between conductor and other conductor image

This is readily derived from the potential coefficient P and the inductance term L as:

$$P_{self} = \frac{1}{C_{self}} = \frac{1}{2\pi\varepsilon_0} \cdot \ln \frac{2h}{r} \tag{2.31}$$

$$L_{self} = \frac{\mu_0}{2\pi} \ln \frac{2h}{r} \tag{2.32}$$

and

$$Z_{self}^{surge} = \sqrt{\frac{L_{self}}{C_{self}}} = \sqrt{L_{self} P_{self}} = 60 \ln \frac{2h}{r} \tag{2.33}$$

where μ_o = permeability
$= 4\pi \times 10^{-7}$ H/m

ε_o = permitivity
$= \frac{1}{36\pi} \times 10^{-9}$ F/m

$[C] = [P]^{-1}$

[P] = potential coefficient matrix,
with diagonal term P_{self}.

[L] = inductance matrix,
with diagonal term L_{self}.

However, the above formulae neglect Carson's correction terms, other conductors, and ground wires used for earth return. A detailed calculation for the surge impedance matrix in phase domain $[Z_{surge}^{phase}]$ must be performed to in order to justify this assumption.

If we consider the relationship between the surge impedance matrix in both phase and modal domain as

$$[V^{phase}] = [Z_{surge}^{phase}][I^{phase}] \tag{2.34}$$

and $$[V^{mode}] = [Z_{surge}^{mode}][I^{mode}] \tag{2.35}$$

then by substituting eqs.(2.3) & (2.4) into (2.35), we can get

$$[T_v]^{-1}[V^{phase}] = [Z_{surge}^{mode}][T_i]^{-1}[I^{phase}] \tag{2.36}$$

or $$[V^{phase}] = [T_v][Z_{surge}^{mode}][T_i]^{-1}[I^{phase}] \tag{2.37}$$

Comparing equations (34) and (37), we thus obtain

$$[Z_{surge}^{phase}] = [T_v][Z_{surge}^{mode}][T_i]^{-1} \tag{2.38}$$

The above relation in equation (2.38) is identical to that derived by Wedepohl.[22] In his method, the reflection coefficient for phase current is first obtained. The coefficient is then set to zero to obtain the expression for $[Z_{surge}^{phase}]$ as in equation (2.38).

Results for the surge impedance from equations (2.29) and (2.38) for both the ground and the phase wires are shown in Table 2.4. As can be seen from the table, the surge impedance obtained by Darveniza's formula which neglects the skin effect of the earth return component introduces negligible deviation (about 1%). However, the Darveniza's formula should only be used when the ground wire is treated as another individual phase (e.g. for the close-by lightning stroke case). If one takes the ground wire as another component for earth return (e.g. for the distant stroke case), the formula for self surge impedance must be modified accordingly by treating voltages on ground wire to be zero. This requires reducing the impedance and admittance matrices before surge impedances can be calculated. The surge impedance value obtained in this case is lower than that obtained by Equation (2.29), as shown in Table 2.4.

8. Single phase representation for close-by strokes on double circuited line

After the author has verified that single phase representation with appropriate choice of line parameters is accurate for a three phase line case without ground wire, a double-circuited overhead transmission line of the MICA Project of the B.C. Hydro and Power Authority[23] was used as a more detailed transmission system with ground wires.

	surge impedances	
	ground wire	phase wire
A	547 Ω	342 Ω
B or C	545 Ω	338 Ω
D	-	318 Ω
(A-B)/A*100%	0.4%	1.2%

A = Exact method (2.38) with Carson's Correction terms for earth return skin effect, ground wire treated as another phase.

B = Exact method equation (2.38) without Carson's Correction terms for earth return skin effect.

C = Darveniza approximate equation (2.29).

D = Exact method equation (2.38) with Carson's Correction terms for earth return skin effect, ground wire treated as earth return component.

Table 2.4: Self surge impedances for ground and phase wires for a typical 500 kV line[16,17]

This tranmission system is a double-circuited 500 kV line. Each tower consists of a three phase line with two ground wires (See Figures 2.4 and 2.5). When the lightning stroke hits either one of the ground wires or one of the phase conductors, different line parameters must be chosen because of different line design. The corresponding parameters are shown in Table 2.5. One can see from this table that the self surge impedance of the ground wire is greater than that of the phase conductor. The wave propagation velocity is also lower in the ground wire case.

In Figures 2.6 and 2.7, one can compare the lightning overvoltage wave propagation characteristics for the open and short circuit test by using multi- and single-phase line representation when lightning stroke hits the ground wire. Figure 2.6a shows the result obtained by the multi-phase solution method using modal analysis. It also shows clearly the different modal components on the resulting waveform. Figure 2.6b shows the result for the single phase case and the overall important propagation charactertistics of multi-phase representation is successfully duplicated here. Similar results are obtained for the short-circuit test, as shown in Figures 2.7a and 2.7b. One can observe that the current waveforms obtained from these two different line representations agree very well.

Similarly, the open and short circuit test results are also successfully duplicated for surges on the phase conductor as in case of direct strokes or backflashovers (See Fig.2.8&2.9) Thus, it is recommended to use single phase representation for double-circuited line with ground wires for studying close-by lightning stroke propagations.

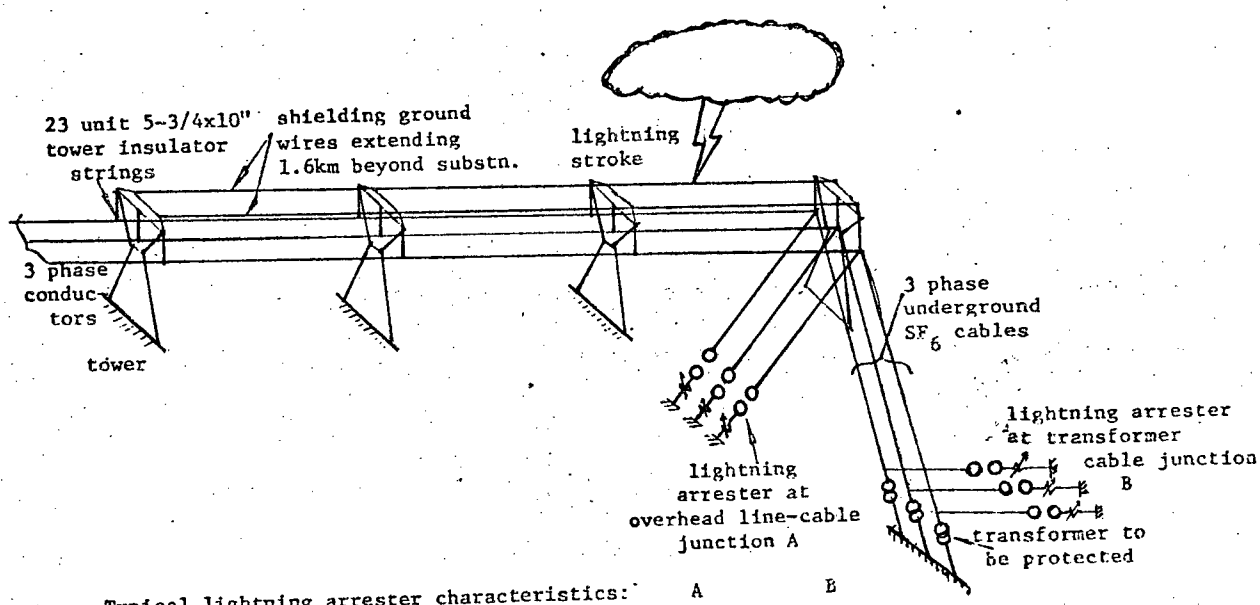

Typical lightning arrester characteristics:

	A	B
nominal rating (reseal voltage)	420 kV	396 kV
switching sparkover	950 kV	960 kV
Min 60 Hz sparkover	588 kV	555 kV
lightning sparkover	985 kV	990 kV

Insulation levels	SF_6 cable	Transformer
60 Hz	800 kV	745 kV
BIL	1550 kV	1675 kV

Figure 2.4: Layout of SF_6 substation protection scheme showing one of the double circuit systems.

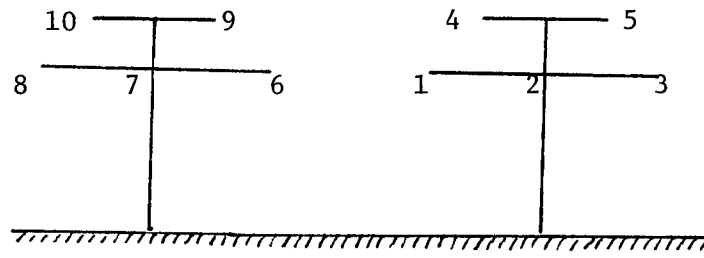

Conductors 1-3, 6-8 phase wires

4,5, 9,10 ground wires

Coupling factor:

$$\text{lightning struck } \phi\text{ - wire } K_{34} = \frac{Z^{\text{phase}}_{\text{surge } 3,4}}{Z^{\text{phase}}_{\text{surge } 3,3}} = \cdot 16 = \frac{V^{\text{induced}}_{\text{ground wire}}}{V_{\text{phase wire}}}$$

$$\text{lightning struck g - wire } K_{43} = \frac{Z^{\text{phase}}_{\text{surge } 4,3}}{Z^{\text{phase}}_{\text{surge } 4,4}} = \cdot 06 = \frac{V^{\text{induced}}_{\text{phase wire}}}{V_{\text{ground wire}}}$$

Figure 2.5: Side view of the MICA 10 ϕ Systems.

		Ground conductor	Phase conductor
Self surge impedance	Z_{self}^{surge}	658 Ω	304 Ω
Wave velocity	v	245 m/μs	293 m/μs
Line resistance		0 Ω/m	0 Ω/m
Length		1609 m	1609 m

where $Z_{self}^{surge} = 60 \ln \frac{2h}{r}$

$$= \sqrt{L_{self} P_{self}}$$

$$\text{velocity} = \sqrt{\frac{P_{self}}{L_{self}}}$$

and L_{self} and P_{self} are diagonal elements of matrix [L] and [P].

Table 2.4: Line parameters of ground and phase conductor for lossless single phase representation.

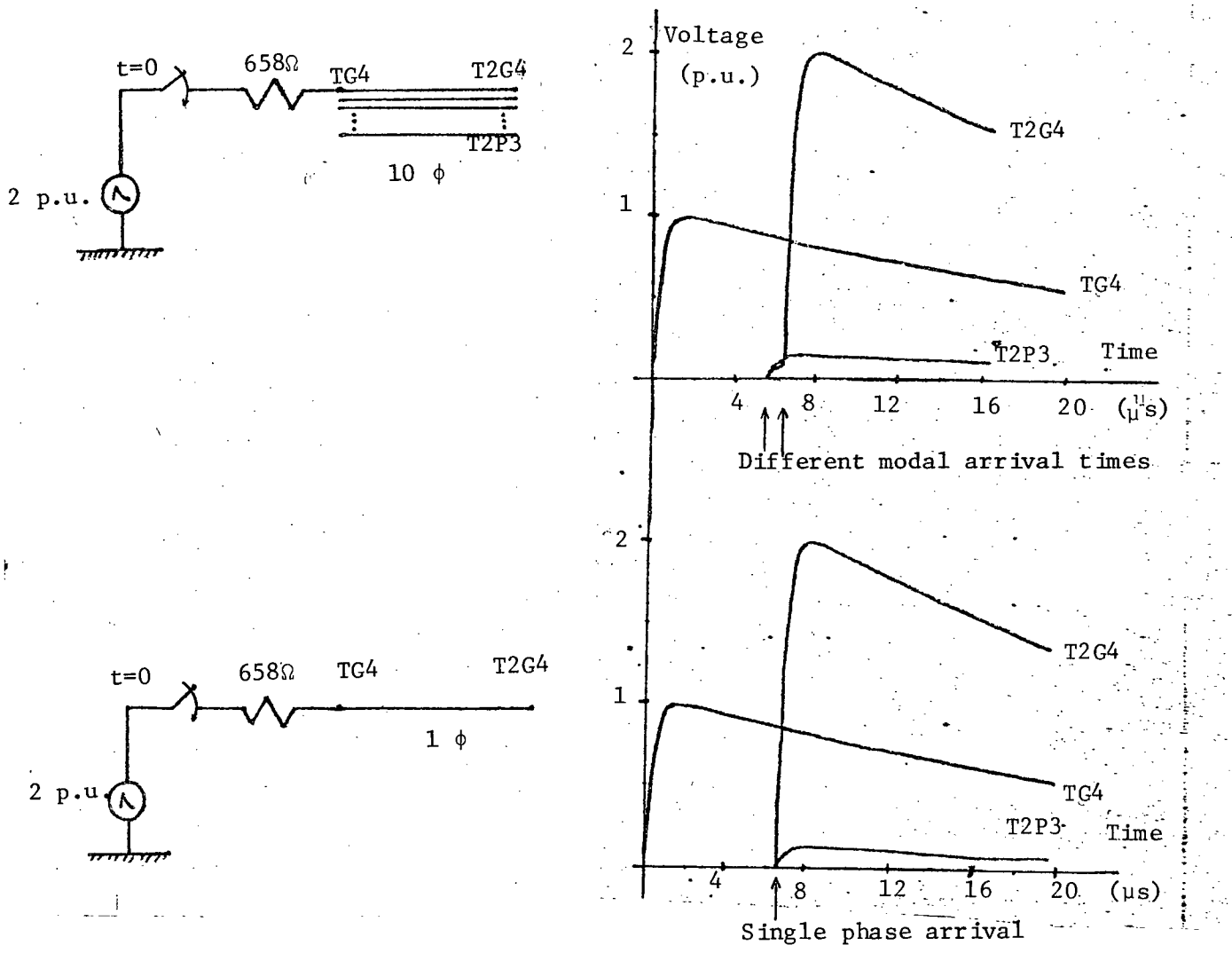

In 1ϕ case: V_{T2P3} = (Coupling factor) V_{T2G4}

$$= \frac{Z^{surge}_{3,4}}{Z^{surge}_{4,4}} \quad V_{T2G4}$$

Figure 2.6: Open circuit test on single and multi-phase representation with stroke on ground wire.

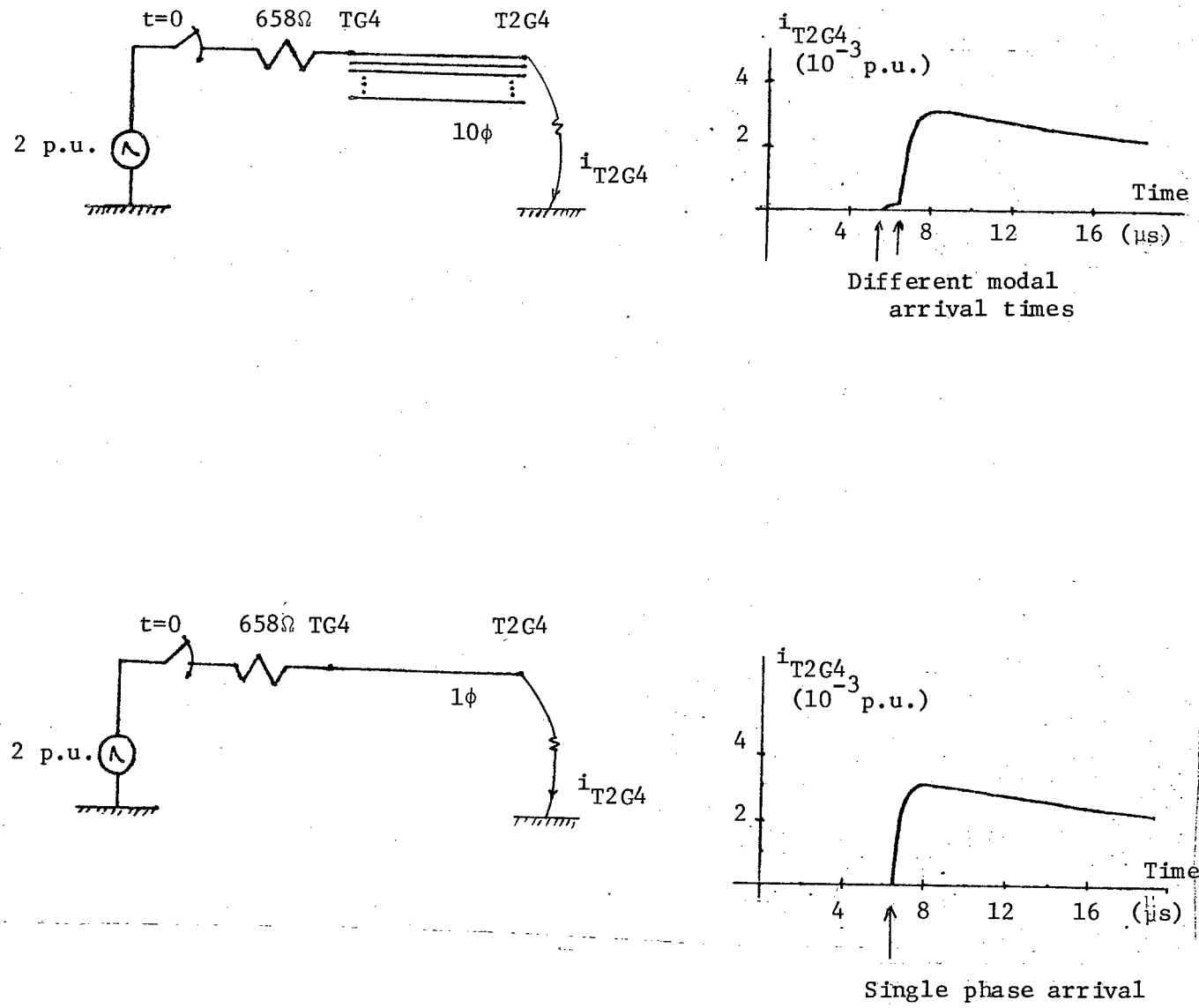

Figure 2.7: Short circuit test on single and multi-phase representation with stroke on ground wire.

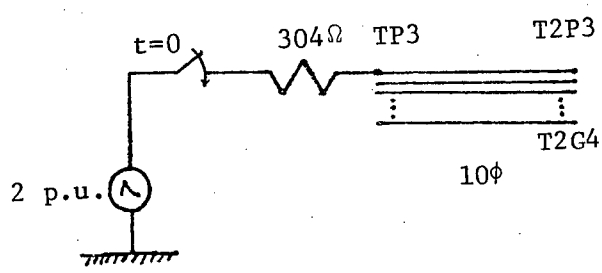

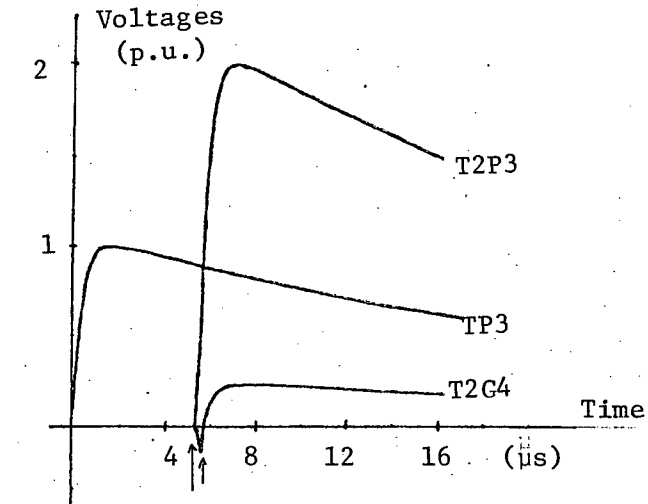

Different modal arrival times

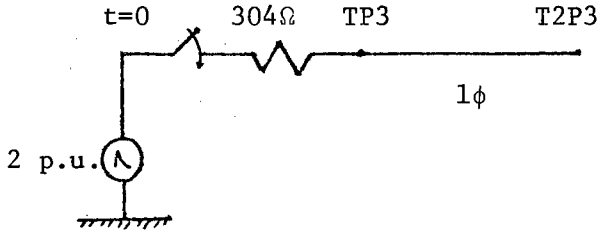

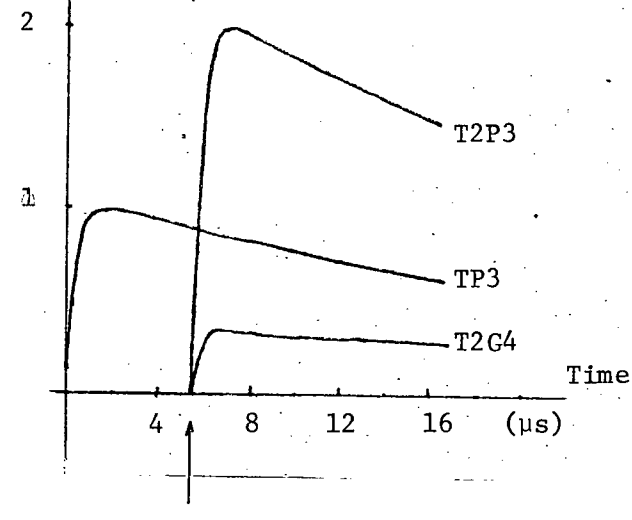

Single phase arrival

In 1 ϕ case: $V_{T2G4} = \frac{Z^{surge}_{3,4}}{Z^{surge}_{3,3}} V_{T2P3}$

Figure 2.8: Open circuit test on single and multi-phase representation with stroke on phase conductors.

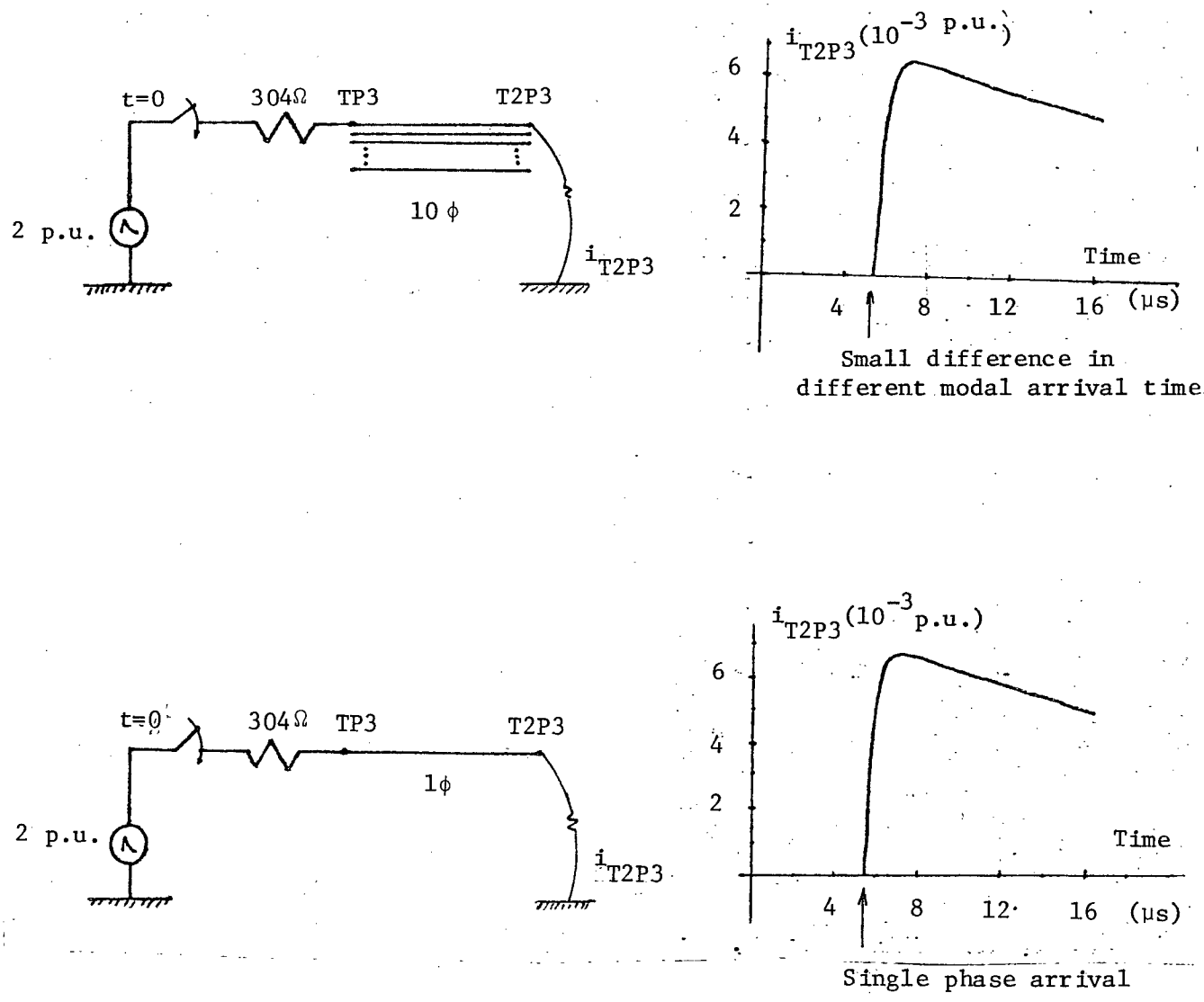

Figure 2.9: Short circuit test on single and multi-phase representation with stroke on phase conductors.

CHAPTER 3: LIGHTNING WAVE PROPAGATION IN SF_6 GAS INSULATED UNDERGROUND TRANSMISSION CABLE SYSTEM.

1. Introduction

The world's first commercial SF_6 gas-insulated cable rated at 345 kV was installed in 1970. Its inherent advantages over conventional underground oil-filled cables with respect to charging current, dielectric losses, thermal performance, voltage rating flexibility and power handling capacity are well-known. It offers additional advantages of reduced substation size. This compactness in size of SF_6-insulated substations and switchgear brings the equipment closer to the protective lightning arrester located at the overhead line and underground cable junction. This is of vital importance, especially when there is no lightning arrester at the transformer terminal, as in certain substation design.

In the SF_6-insulated cable at the MICA Dam,[23] which will be used as a test example, each of the 3 phase cables consists of two concentric aluminum tubes (see Figure 3.1a). The inner tube is the conductor core and the outer grounded tube is the sheath. The three sheaths are solidly bonded together and grounded at many locations. At the high frequencies encountered in lightning surges, the sheath return current will be equal in magnitude and 180° out of phase with the core conductor current. Whether the magnetic field external to the sheaths can be completely neglected in the frequency range of interest must be investigated, however. If the magnetic field is negligible, then there would be no mutual inductive coupling among the phases. There is no electrostatic capacitive coupling between phases as the solidly-grounded sheaths act as electrostatic shields up to 1 Mhz.

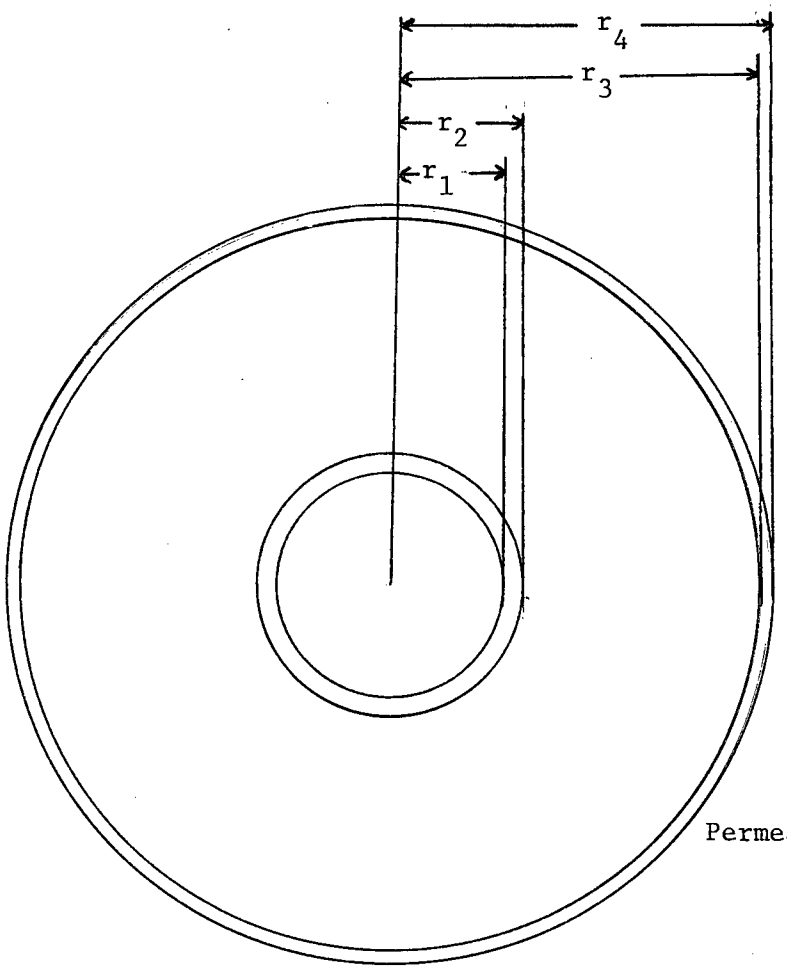

Skin depth of Al

$= (\pi f \sigma \mu)^{-1/2} = \frac{8.1}{\sqrt{f}}$ cm

$= 1.0$ cm at 60Hz

Scale = 1:2.54

r_1 = 3" = 7.62 cm

r_2 = 3.5" = 8.89 cm

r_3 = 9.75" = 24.765 cm

r_4 = 10" = 25.4 cm

sheath thickness=.635 cm

Permeability Al = $\mu_r \mu_0 = \mu_0$

$= 4\pi \times 10^{-7}$ H/m

Figure 3.1a: Individual cable design

Permittivity $SF_6 = \varepsilon_r \varepsilon_0 = \varepsilon_0$

$= \frac{1}{36\pi} \times 10^{-9}$ F/m

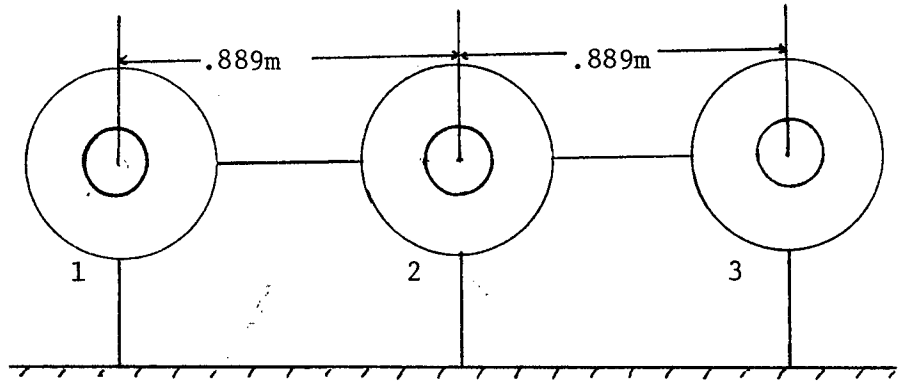

Figure 3.1b: Overall cable layout.

In order to investigate the sheath current return phenomenon of SF_6 cables, and thus to clarify the wave propagation characteristics, the cable parameter must be calculated accurately. In this research work, cable parameters of multi-core cable[24,25] is not investigated. Such multi-core cable systems certainly have coupling between phases at all frequencies. Nevertheless, coupling between phases for the single core cable system in different frequencies needs further investigation.

Commellini[26] and Abledu[27] used finite elements technique to sub-divide the main conductors into smaller sub-conductors of cylindrical shape. The impedance matrix for the main conductors was formed by bundling up the sub-conductors in the matrix elimination process. However, due to the thin tubular shape of the conductors involved in the SF_6 buses, large number of sub-conductors is required. This will demand huge computer core storage space and long computer execution time.

Sunde[28] and Pollaczek[29] had derived analytical expressions for the self and mutual impedance of cables which are constructed overhead, underground or on ground surface. These analytical expressions contain Kelvin functions and an infinite integral known as the Carson's Correction terms. Before the widespread application of digital computers, simplified assumptions and restrictions were made to facilitate the computation process. With the recent popularity and increased application of digital computers, these infinite integrals can be modified and replaced by straight forward numerical computations without significant sacrifice for accuracy.

Wedepohl et al[30] and Ametani[31,32] used different approaches to tackle the analytical expression in the cable parameter calculation. However, both approaches gave different results (20% from each other).

Bianchi[33] proposed to calculate the earth or sea return impedance by approximating the return medium as a tube of infinite outside radius. These approximation results fell somewhere between those of Wedepohl et al and Ametani.

Because of the inconsistency in the above findings, a detailed investigation for numerical calculation of cable parameters must be performed to reveal wave propagation characteristics in SF_6 single core cables. Current return characteristics from core through sheath also must be investigated to confirm single phase or multi-phase representation for the cable system involved.

2. Formation of series impedance matrix for SF_6 cables

The single core SF_6 cable system configuration is shown in Figure 3.1b. Each phase consists of two conductors, core and sheath. We can build up a 6 x 6 series impedance matrix Z, describing the cable system as follows:

$$-\begin{bmatrix} \frac{dV_{c1}}{dx} \\ \frac{dV_{s1}}{dx} \\ \frac{dV_{c2}}{dx} \\ \frac{dV_{s2}}{dx} \\ \frac{dV_{c3}}{dx} \\ \frac{dV_{s3}}{dx} \end{bmatrix} = \left[\begin{array}{cc|cc|cc} Z_{s11} & Z_{s12} & Z_{m12} & Z_{m12} & Z_{m13} & Z_{m13} \\ Z_{s21} & Z_{s22} & Z_{m12} & Z_{m12} & Z_{m13} & Z_{m13} \\ \hline Z_{m12} & Z_{m12} & Z_{s11} & Z_{s12} & Z_{m12} & Z_{m12} \\ Z_{m12} & Z_{m12} & Z_{s21} & Z_{s22} & Z_{m12} & Z_{m12} \\ \hline Z_{m13} & Z_{m13} & Z_{m12} & Z_{m12} & Z_{s11} & Z_{s12} \\ Z_{m13} & Z_{m13} & Z_{m12} & Z_{m12} & Z_{s21} & Z_{s22} \end{array}\right] \cdot \begin{bmatrix} i_{c1} \\ i_{s1} \\ i_{c2} \\ i_{s2} \\ i_{c3} \\ i_{s3} \end{bmatrix}$$

$$= \left[\begin{array}{c|c|c} \bar{Z}_s & \bar{Z}_{m12} & \bar{Z}_{m13} \\ \hline \bar{Z}_{m12} & \bar{Z}_s & \bar{Z}_{m12} \\ \hline \bar{Z}_{m13} & \bar{Z}_{m12} & \bar{Z}_s \end{array}\right] \cdot \begin{bmatrix} i_{c1} \\ i_{s1} \\ i_{c2} \\ i_{s2} \\ i_{c3} \\ i_{s3} \end{bmatrix} \qquad (3.1)$$

where $\bar{Z}_s$ is 'self submatrix' on the diagonal. All $\bar{Z}_s$ matrices are equal because they represent identical cable configurations.

It is assumed that the mutual impedance between cores, between sheaths and between corresponding cores and sheaths are all equal. In other words, all elements in the sub-matrix $\bar{Z}_{m12}$ or $\bar{Z}_{m13}$ are assumed to be equall (See Section 6 for further discussion)

3. Calculation of self and mutual earth return impedance for single core cable

The analytical expressions for the self and mutual earth return impedance of cables was first derived by Sunde and Pollaczek[29], and then by Wedepohl et al.[30] Firstly, the Maxwell's electromagnetic equation can be solved after neglecting end effects as:

$$\nabla \times E = -j\omega\mu_0 H \tag{3.2}$$

$$\nabla \times H = J + \frac{\partial D}{\partial t} = J \left(1 + \frac{\omega\epsilon_o}{\sigma} \right) \tag{3.3}$$

$$= J, \text{ as displacement current can be neglected.}$$

Taking the curl of equation (3.2) and substituting into (3 3) give

$$\nabla \times \nabla \times E = -j\omega\mu_0 \nabla \times H$$

or $$\nabla(\nabla \cdot E) - \nabla^2 E = -j\omega\mu_0(J)$$

Assuming cable separation >> cable radius, we have

$$\nabla^2 E = j\omega\mu_0 \sigma(E + \rho \; i \; \delta(x) \; \delta(y + h))$$

Assuming cables are parallel to ground surface and attenuation of voltage and current is negligible over distances comparable to cable separation, we have

$$\frac{\partial^2 E_1}{\partial x^2} + \frac{\partial^2 E_1}{\partial y^2} = 0 \quad , y \geq 0 \tag{3.4}$$

$$\frac{\partial^2 E_2}{\partial x^2} + \frac{\partial^2 E_2}{\partial y^2} = m^2 E_2 + \rho \; m^2 \; i \; \delta(x) \; \delta(y + h) \; , \quad y < 0. \tag{3.5}$$

where $m = \sqrt{\frac{j\omega\mu}{\rho}}$

ρ = earth resistivity = $\frac{1}{\sigma}$

ω = angular frequency

μ = permeability

δ = Dirac function

E_1, E_2 = electric field above and below ground.

Imposing the restriction of continuity of electric field at y = 0 for E_1 and E_2 as boundary conditions, we can obtain a general expression

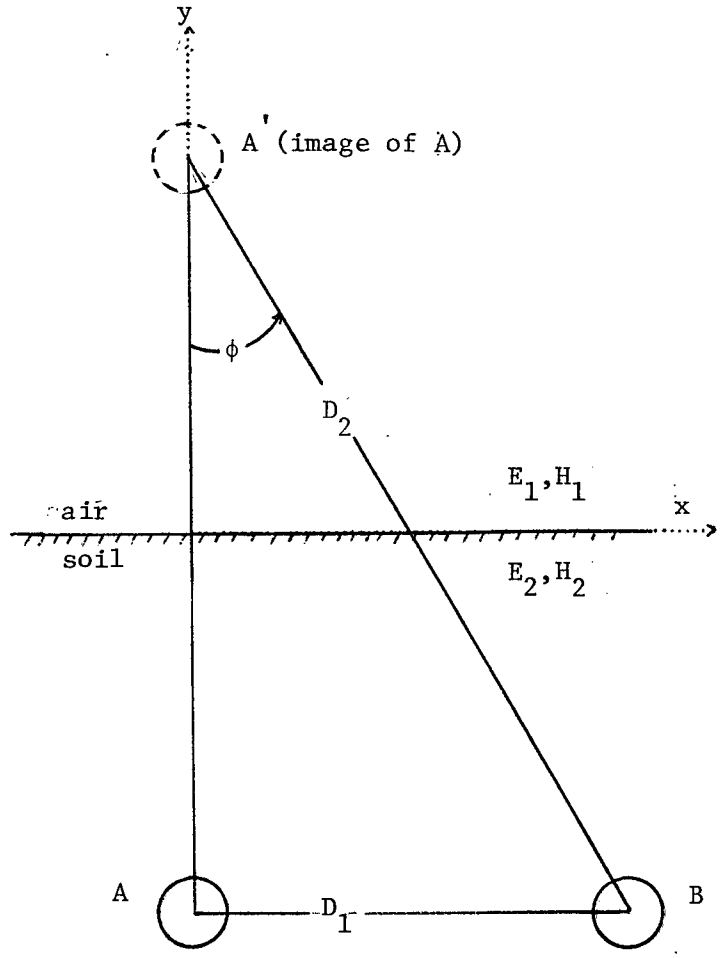

Figure 3.2: Conductor configurations for earth return formula.

for the underground electric field E_2. We can then obtain the expression for the mutual earth-return impedance of underground cables by dividing $E_2(x,h_2)$ by the current $i(0,h_2)$ to get

$$Z_{ij} = \frac{j\omega\mu}{2\pi}\left[\int_{-\infty}^{\infty} \frac{\exp(-\ell\sqrt{\alpha^2+m^2})}{|\alpha| + \sqrt{\alpha^2+m^2}} e^{j\alpha x}\, d\alpha + \int_{-\infty}^{\infty} \frac{\exp(-\ell'\sqrt{\alpha^2+m^2})}{2\sqrt{\alpha^2+m^2}}\, d\alpha - \int_{-\infty}^{\infty} \frac{\exp(-\ell\sqrt{\alpha^2+m^2})}{2\sqrt{\alpha^2+m^2}}\, d\alpha\right] \quad (3.6)$$

$$= \frac{j\omega\mu}{2\pi}\int_{-\infty}^{\infty} \frac{\exp(-\ell\sqrt{\alpha^2+m^2})}{|\alpha| + \sqrt{\alpha^2+m^2}} e^{j\alpha x}\, d\alpha + \frac{j\omega\mu}{2\pi}\left(K_0(mD_1) - (K_0(mD_2)\right)$$

$$= \Delta Z_{ij} + \frac{j\omega\mu}{2\pi}\left(K_0(mD_1) - K_0(mD_2)\right) \quad (3.7)$$

where K_0 = Kelvin function of order zero

$m = \sqrt{\frac{j\omega\mu}{\rho}}$; x = horizontal separation between cables

$D_1 = \sqrt{x^2+(h_1-h_2)^2}$

$D_2 = \sqrt{x^2+(h_1+h_2)^2}$

h_1, h_2 = depths of burial of cables

$\ell' = |h_1 - h_2|$

$\ell = |h_1 + h_2|$

ΔZ_{ij} = Carson's Correction term, identical to that for overhead lines case.

The above formula is also applicable to self earth return impedance components. In such cases, the terms for D_1 and D_2 can be re-defined as

$$D_1 = r$$

$$D_2 = 2h \qquad (3.7a)$$

where r is radius, h = depth of buried cable.

However, the above formula is unsuitable for straight forward calculations. Before digital computers are widely used, approximate results were obtained only after certain limiting conditions[28] were accommodated. Then, Wedepohl et al used Cauchy's integration for the Carson's correction terms and derived approximate formula for the equation given in equation (3.7) as

$$Z_{ij} = \frac{j\omega\mu}{2\pi} \{ \ell n(\gamma \frac{mD_2}{2}) + \frac{1}{2} - \frac{2}{3} m\ell \} \qquad (3.8)$$

for $|mD_1| < 0.25$

and γ = Euler's constant

= 0.5772157.

However, the above formula gives results which are about 20% higher when compared with the direct numerical computation using the original equation as in Ametani's case. The infinite integral for the underground cable is the same as the Carson's correction terms for overhead lines. We can define a new parameter a as

$$a = \sqrt{\frac{\omega\mu}{\rho}} D$$

$$= 4\pi \sqrt{5}\ 10^{-4}\ D\sqrt{\frac{f}{\rho}} \qquad (3.9)$$

where D and ρ are in MKS units

and $D = \begin{cases} 2h_i & \text{for self earth return impedance} \\ D_2 & \text{for mutual earth return impedance} \end{cases}$

This correction term integral can be represented by the following infinite converging series:[34]

1. For $a \leq 5$

$$\Delta R' = 4\omega \cdot 10^{-4} \{ \frac{\pi}{8}$$
$$-b_1 a \cdot \cos\phi$$
$$+b_2[(c_2 - \ln a)a^2 \cos 2\phi + \phi a^2 \sin 2\phi]$$
$$+b_3 a^3 \cos 3\phi$$
$$-d_4 a^4 \cos 4\phi$$
$$-b_5 a^5 \cos 5\phi$$
$$+b_6[(c_6 - \ln a)a^6 \cos 6\phi + \phi a^6 \sin 6\phi]$$
$$+b_7 a^7 \cos 7\phi$$
$$-d_8 a^8 \cos 8\phi$$
$$- \ldots\}$$

$$\Delta X' = 4\omega \cdot 10^{-4} \{ \frac{1}{2}(0.6159315 - \ln a)$$
$$+b_1 a \cdot \cos\phi$$
$$-d_2 a^2 \cos 2\phi$$
$$+b_3 a^3 \cos 3\phi$$
$$-b_4[(c_4 - \ln a)a^4 \cos 4\phi + \phi a^4 \sin 4\phi]$$
$$+b_5 a^5 \cos 5\phi$$
$$-d_6 a^6 \cos 6\phi$$
$$+b_7 a^7 \cos 7\phi$$
$$-b_8[(c_8 - \ln a)a^8 \cos 8\phi + \phi a^8 \sin 8\phi]$$
$$+ \ldots\}$$

Notice that each 4 successive terms form a repetitive pattern. The coefficients b_i, c_i and d_i are obtained from the recursive formulas:

$$b_i = b_{i-2}\,\frac{\text{sign}}{i(i+2)} \quad \text{with the starting value} \begin{cases} b_1 = \frac{\sqrt{2}}{6} & \text{for odd subscripts,} \\ b_2 = \frac{1}{16} & \text{for even subscripts,} \end{cases}$$

$$c_i = c_{i-2} + \frac{1}{i} + \frac{1}{i+2} \quad \text{with the starting value} \quad c_2 = 1.3659315,$$

$$d_i = \frac{\pi}{4} \cdot b_i,$$

with sign = ±1 changing after each 4 successive terms (sign = ±1 for i = 1,2,3,4; sign = -1 for i = 5,6,7,8 etc.).

2. For a > 5

$$\Delta R' = \left(\frac{\cos\phi}{a} - \frac{\sqrt{2}\cos 2\phi}{a^2} + \frac{\cos 3\phi}{a^3} + \frac{3\cos 5\phi}{a^5} - \frac{45\cos 7\phi}{a^7} \right) \cdot \frac{4\omega \cdot 10^{-4}}{\sqrt{2}} \tag{3.11}$$

$$\Delta X' = \left(\frac{\cos\phi}{a} - \frac{\cos 3\phi}{a^3} + \frac{3\cos 5\phi}{a^5} + \frac{45\cos 7\phi}{a^7} \right) \cdot \frac{4\omega \cdot 10^{-4}}{\sqrt{2}}$$

It should be noted that the correction terms will become zero when the parameter a is very big, ie. when frequency or cable distance from ground is very large or when earth resistivity is very small.

The Kelvin functions can also be calculated by another infinite converging series as can be obtained from availabe source.[36] It can also be calculated by a special subroutine CBESK[35] available from the UBC Computing Centre.

After establishing the numerical formula for cable earth return impedance, the discrepancies between the results of Wedepohl et al and

those of Ametani can then be clarified.

The author has confirmed that accurate cable earth return impedance can be calculated by using direct computation of infinite series substitution for infinite integral and Kelvin function.[40] Cable mutual impedance from Ametani's computation is acceptable though different infinite series is used for the Carson's correction terms. Identical results are obtained at least to 4 significant figures for frequencies up to 100 k Hz (See Figure 3.2). The approximate formula given by equation (3.8) on the other hand, gives results about 20% consistently higher.

The author has also confirmed that the earth return impedance for underground cable can be approximated by the equivalent earth return impedance for overhead lines. The expression for earth return impedance for overhead line is

$$Z_{ij} = \frac{j\omega\mu}{2\pi} \ln \frac{D_2}{D_1} + \Delta Z_{ij} \quad , \tag{3.12}$$

for mutual earth return impedance

and

$$Z_{ij} = \frac{j\omega\mu}{2\pi} \ln \frac{2h}{GMR} + \Delta Z_{ij} \quad , \tag{3.13}$$

for self earth return impedance

where D_2 is distance between i^{th} and image of j^{th} conductor;

D_1 is distance between i^{th} and j^{th} conductor;

h is height of conductor above ground;

GMR is geometric mean radius = radius of conductor at high freq.

ΔZ is Carson's correction term.

Identical results up to 3 or 4 figures are obtained for earth resistivity of 1 to 100 Ω-m up to the frequency of 100 K Hz. The

consistency between these two results is due to the fact that the Kelvin functions

$$K_0(\sqrt{j}\,x) = \ker(x) + j\,\mathrm{kei}(x)$$

can be evaluated by the following converging series[36] for $0 \le x \le 8$:

$$\begin{aligned}\ker x = &-\ln(\tfrac{1}{2}x)\,\mathrm{ber}\,x + \tfrac{1}{4}\pi\,\mathrm{bei}\,x - .57721\ 566 \\ &- 59.05819\ 744(x/8)^4 + 171.36272\ 133(x/8)^8 \\ &- 60.60977\ 451(x/8)^{12} + 5.65539\ 121(x/8)^{16} \\ &- .19636\ 347(x/8)^{20} + .00309\ 699(x/8)^{24} \\ &- .00002\ 458(x/8)^{28} + \epsilon \\ &|\epsilon| < 1\times10^{-8}\end{aligned} \tag{3.14}$$

$$\begin{aligned}\mathrm{kei}\,x = &-\ln(\tfrac{1}{2}x)\,\mathrm{bei}\,x - \tfrac{1}{4}\pi\,\mathrm{ber}\,x + 6.76454\ 936(x/8)^2 \\ &- 142.91827\ 687(x/8)^6 + 124.23569\ 650(x/8)^{10} \\ &- 21.30060\ 904(x/8)^{14} + 1.17509\ 064(x/8)^{18} \\ &- .02695\ 875(x/8)^{22} + .00029\ 532(x/8)^{26} + \epsilon \\ &|\epsilon| < 3\times10^{-9}\end{aligned} \tag{3.15}$$

where

$$\begin{aligned}\mathrm{ber}\,x = 1 &- 64(x/8)^4 + 113.77777\ 774(x/8)^8 \\ &- 32.36345\ 652(x/8)^{12} + 2.64191\ 397(x/8)^{16} \\ &- .08349\ 609(x/8)^{20} + .00122\ 552(x/8)^{24} \\ &- .00000\ 901(x/8)^{28} + \epsilon \\ &|\epsilon| < 1\times10^{-9}\end{aligned} \tag{3.16}$$

$$\begin{aligned}\mathrm{bei}\,x = &\ 16(x/8)^2 - 113.77777\ 774(x/8)^6 \\ &+ 72.81777\ 742(x/8)^{10} - 10.56765\ 779(x/8)^{14} \\ &+ .52185\ 615(x/8)^{18} - .01103\ 667(x/8)^{22} \\ &+ .00011\ 346(x/8)^{26} + \epsilon \\ &|\epsilon| < 6\times10^{-9}\end{aligned} \tag{3.17}$$

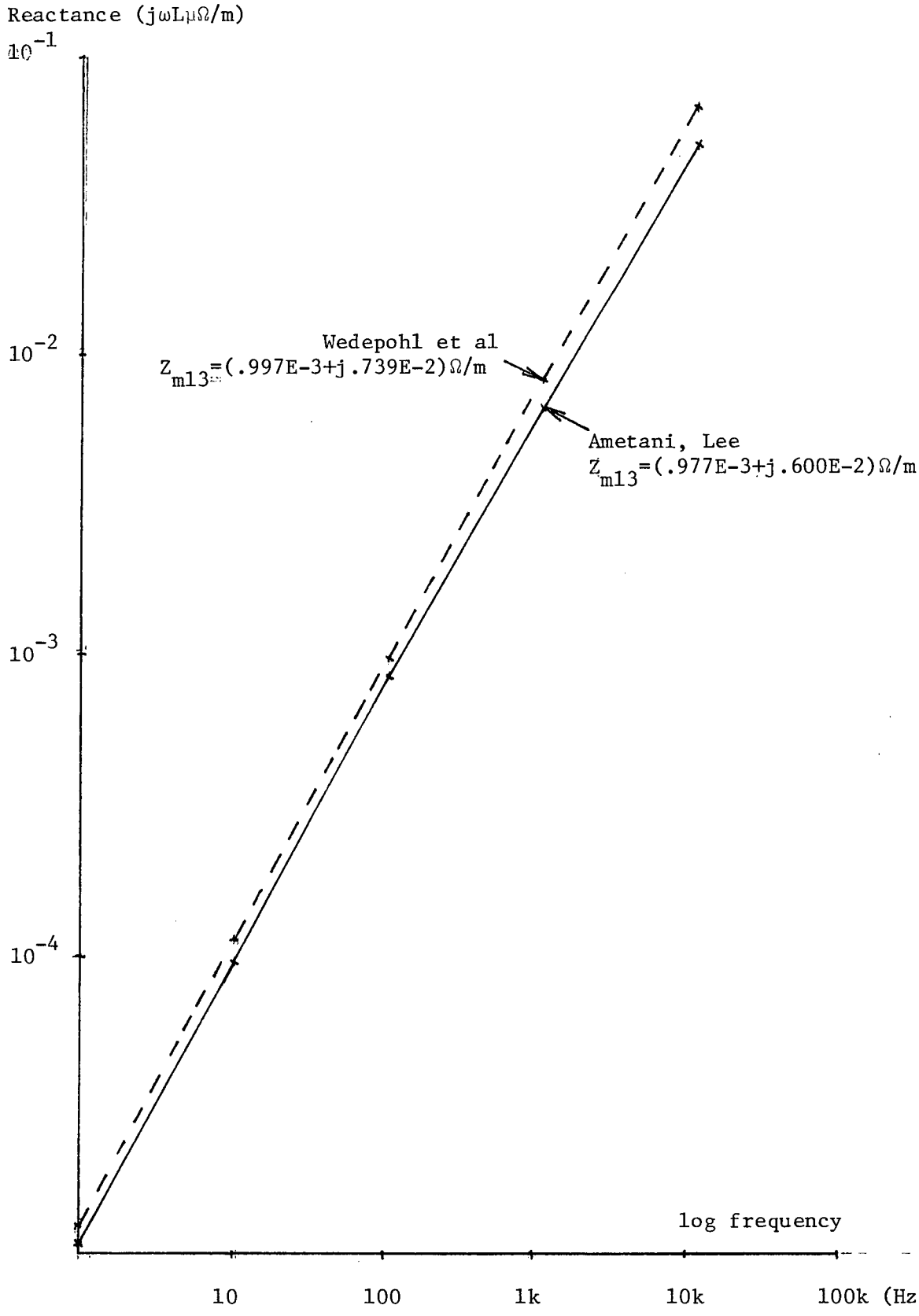

Figure 3.2: Mutual impedance between outermost cables by different computation methods.

and $$x = \sqrt{\frac{\omega\mu}{\rho}}\, D, \tag{3.18}$$

$\mu = 4\pi \times 10^{-7}$ H/m

ω = frequency

D = distance D_1 or D_2

ρ = earth resistivity

For frequencies up to about 1 M Hz and earth resistivity of about 100 Ω-m, and cable separation or cable depth of about 1 m, the term x is relatively small as

$$x \to 0$$

Then, one can rewrite equations (3.14) to (3.17) for $x \to 0$ as

ber = 1

bei = 0

$$\therefore \quad K_o(\sqrt{j}x) = \text{ker } x + j \text{ kei } x$$

$$= -\ln \frac{1}{2} x - 0.57721 - j\frac{\pi}{4} \tag{3.19}$$

Thus, for the earth return impedance as shown in equation (7), we have

$$Z_{ij} = \Delta Z_{ij} + \frac{j\omega\mu}{2\pi} (K_o(mD_1) - K_o(mD_2))$$

$$= \Delta Z_{ij} + \frac{j\omega\mu}{2\pi} \left(\left(-\ln \frac{mD_1}{2} - .57721 - j\frac{\pi}{4} \right) - \left(-\ln \frac{mD_2}{2} - .57721 - j\frac{\pi}{4} \right) \right)$$

$$= \Delta Z_{ij} + \frac{j\omega\mu}{2\pi} \cdot \ln \frac{D_2}{D_1} \quad , \quad x \to 0$$

Carson's correction term; self-term

which is the same as in equations (3.12) and (3.13).

The numerical results for the self-term component of the self and mutual earth return impedance for the underground cable obtained by the different formulae developed earlier are shown in Table 3.1. As can be seen from Table 3.1, the results obtained by these different formulae are very consistent. The final results for mutual impedance from these methods are also shown in Figure 3.3 for frequencies up to 1 M Hz. Because of the observed consistencies, the overhead line formula approximation is therefore recommended for underground cable for all frequencies up to 1 M Hz and earth resistivities above 1 Ω-m.

4. Calculation of self impedance matrix for single core cable

After the self and mutual impedance for earth return of underground cables is obtained, the self impedance of individual cables can be calculated and the obtained results for different current loops can then be transformed to the required form for the impedance diagonal submatrix $\bar{Z}_s$ as shown in equation (3.1).

At first, one can consider the current in each of the individual cables flow in two adjacent loops as shown in Figure 3.4. Loop 1 is formed by the current flowing through the core and returning through the outside sheath. Loop 2 is formed by the current flowing through the sheath and returning through the outside earth. These two loops can be described by equation (3.21) as

$$-\begin{bmatrix} \frac{dv_1}{dx} \\ \\ \frac{dv_2}{dx} \end{bmatrix} = \begin{bmatrix} Z_{11} & Z_{12} \\ \\ Z_{21} & Z_{22} \end{bmatrix} \cdot \begin{bmatrix} i_1 \\ \\ i_2 \end{bmatrix} \qquad (3.21)$$

where $Z_{21} = Z_{12}$ by symmetry.

	Separation in meter		underground	overhead
	D_1	D_2	$K_0(mD_1) - K_o(mD_2)$	$\ell n\frac{D_2}{D_1}$
(1,3)	.889	2.189	.901+j.000 (60Hz)	.901
			.895-j.020 (100Hz)	.901
(1,2)	1.778	2.676	.408+j.000 (60Hz)	.408
			.403-j.018 (100Hz)	.408
(self)	.254	2.0	2.064+j.000 (60Hz)	2.064
			2.057-j.022 (100Hz)	2.064

where

$$f = 60 \text{ Hz}, \quad m = \sqrt{\frac{j\omega\mu}{\rho}} = \sqrt{\frac{j60 \times 2\pi \times 4\pi \times 10^{-7}}{100}} = .0022\sqrt{j}$$

$$f = 100 \text{ Hz}, \quad m = \sqrt{\frac{j\omega\mu}{\rho}} = \sqrt{\frac{j100 \times 2\pi \times 4\pi \times 10^{-7}}{100}} = .089\sqrt{j}$$

underground cable (exact)

$$Z_{ij} = \frac{j\omega\mu}{2\pi}\left(K_0(mD_1) - K_0(mD_2)\right) + \Delta Z_{ij}$$

overhead cable (approximation to above)

$$Z_{ij} = \frac{j\omega\mu}{2\pi}\ell n\frac{D_2}{D_1} + \Delta Z_{ij}, \quad x = \sqrt{\frac{\omega\mu}{\rho}}D \to 0$$

Table 3.1: Mutual and self earth return impedance terms as given by underground and overhead cable formula.

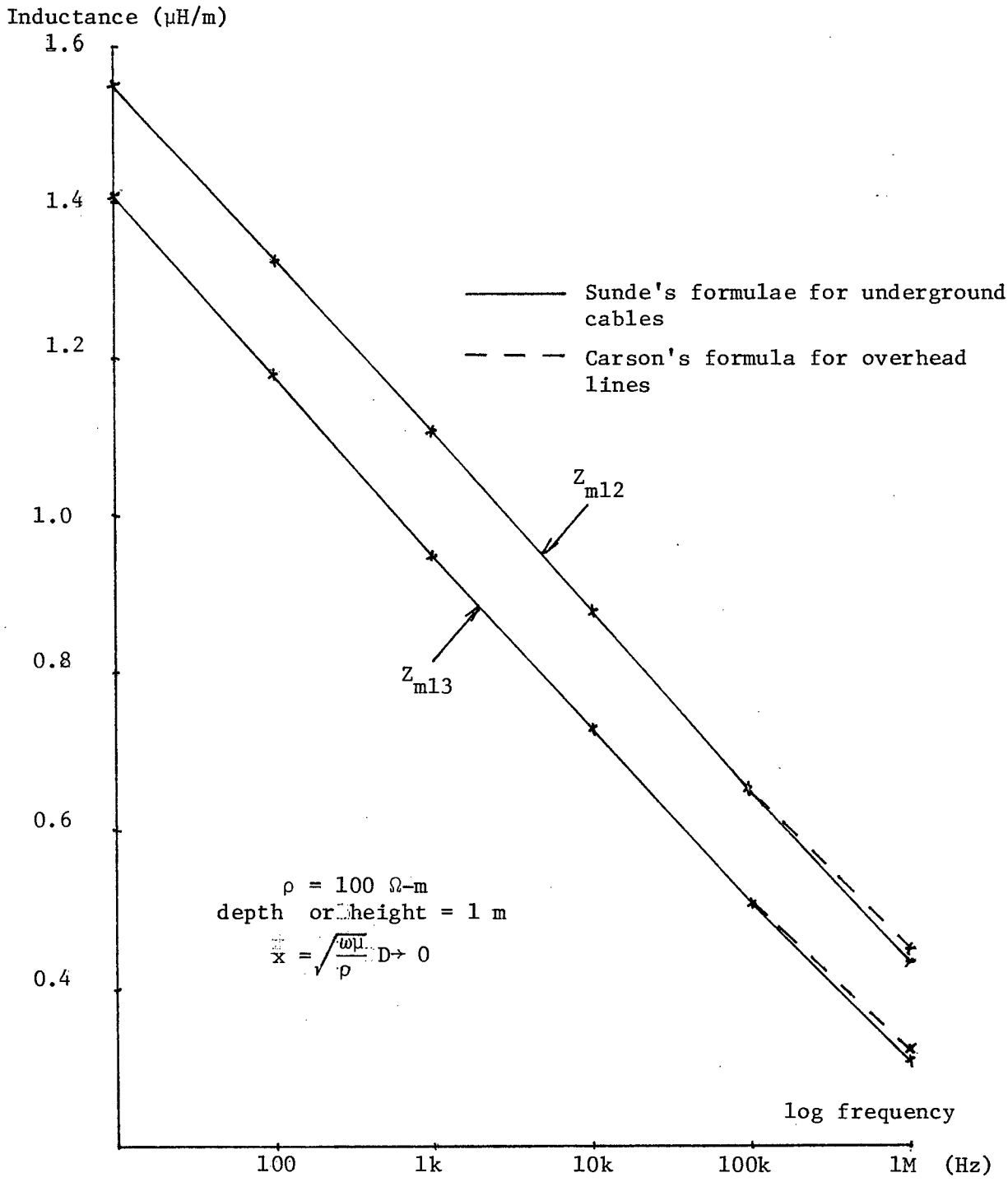

Figure 3.3: Approximations of mutual impedances between underground cables by Carson's formulae.

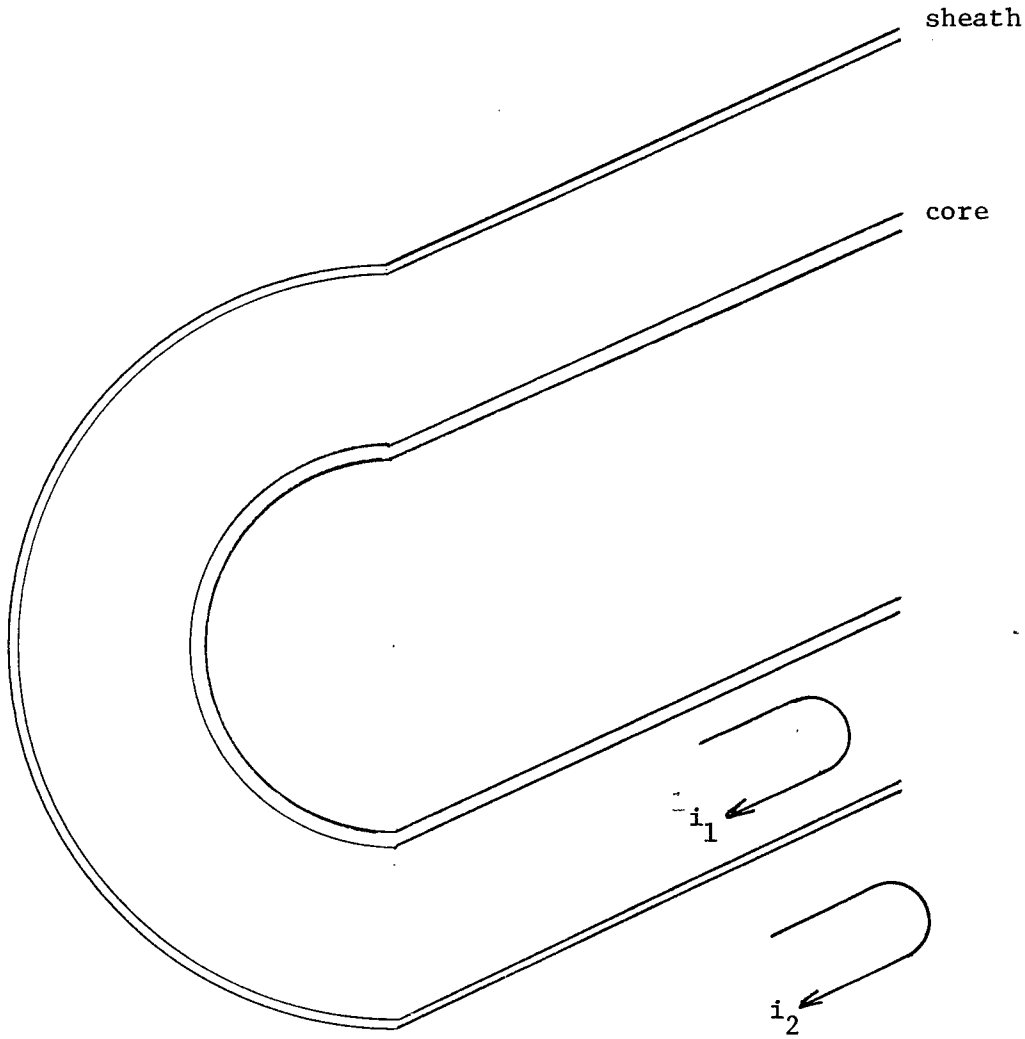

Figure 3.4: Current loops inside SF_6 cable for self impedance calculation.

The matrix elements of equation (3.21) can be obtained by considering the individual current loop components making up the corresponding loops 1 and 2 as

$$Z_{11} = Z_{\text{core-outside}} + Z_{\text{core/sheath insulation}} + Z_{\text{sheath-inside}} \quad (3.22)$$

$$Z_{22} = Z_{\text{sheath-outside}} + Z_{\text{earth-inside}} \quad (3.23)$$

$$Z_{12} = Z_{21} = -Z_{\text{sheath-mutual}} \text{ (minus sign since } i_1 \text{ and } i_2 \text{ in different direction).} \quad (3.24)$$

(N.B. Z_{12} is negligible when sheath thickness >> skin depth).

where the individual elements are

(Z1) $Z_{\text{core-outside}}$ = internal impedance of core with return through outside (sheath).

(Z2) $Z_{\text{core/sheath insulation}}$ = impedance of SF_6 insulation due to the time varying magnetic field.

(Z3) $Z_{\text{sheath-inside}}$ = internal impedance of sheath with return through inside (core).

(Z4) $Z_{\text{sheath-outside}}$ = internal impedance of sheath with return through outside (earth).

(Z5) $Z_{\text{earth-inside}}$ = self earth return impedance, this can be calculated by equations (3.7) & (3.7a), or can also be obtained by equation (3.25) with the approximation of infinite outside radius[33].

(Z6) $Z_{\text{sheath-mutual}}$ = mutual impedance of tubular sheath between loop 1 in inner surface and loop 2 in outer surface of sheath.

The individual self and mutual impedance terms can be again obtained by solving the Maxwell's equations for the coaxial conductors as similar to equations (3.2)&(3.3). They are a function of frequency as derived by Schkelkunoff[37] and Sunde[28] as

$$Z_{\text{tube-inside}} = \frac{m\rho}{2\pi q p} \left(I_0(mq)\, K_1(mr) + K_0(mq)\, I_1(mr)\right) \tag{3.25}$$

$$Z_{\text{tube-outside}} = \frac{m\rho}{2\pi r p} \left(I_0(mr)\, K_1(mq) + K_0(mr)\, I_1(mq)\right) \tag{3.26}$$

$$Z_{\text{tube-mutual}} = \frac{\rho}{2\pi q r p} \tag{3.27}$$

with $$p = I_1(mr)\, K_1(mq) - I_1(mq)\, K_1(mr) \tag{3.28}$$

where ω = angular frequency = $2\pi f$

μ = permeability = $\mu_r \mu_0$, μ_r = 1 for Al

q = outside radius of tubular conductor

r = inside radius of tubular conductor

$m = \sqrt{\frac{j\omega\mu}{\rho}}$, ρ = d.c. resistivity

I_0, I_1 = Bessel functions

and K_0, K_1 = Kelvin functions

After obtaining the individual terms of the loop equation matrix as shown in equation (3.21), we can then obtain the diagonal sub-matrix elements by applying the following circuit conditions:

$$V_1 = V_c - V_s \tag{3.30}$$

$$V_2 = V_s$$

$$i_1 = i_c \tag{3.31}$$

$$i_2 = i_c + i_s \tag{3.32}$$

The individual loop equations of equation (3.21) then becomes

$$-\frac{dV_c}{dx} + \frac{dV_s}{dx} = (Z_{11} + Z_{12})\, i_c + Z_{12}\, i_s \tag{3.33}$$

and

$$-\frac{dV_s}{dx} = (Z_{12} + Z_{22})\, i_c + Z_{22}\, i_s \tag{3.34}$$

Adding equation (3.33) to (3.34) gives

$$-\frac{dV_c}{dx} = (Z_{11} + 2Z_{12} + Z_{22})\, i_c + (Z_{12} + Z_{22})\, i_s \tag{3.35}$$

Thus, we can rewrite the self sub-matrix Z_s as

$$-\begin{bmatrix} \frac{dV_c}{dx} \\ \frac{dV_s}{dx} \end{bmatrix} = \begin{bmatrix} Z_{11} + 2Z_{12} + Z_{22} & Z_{12} + Z_{22} \\ Z_{12} + Z_{22} & Z_{22} \end{bmatrix} \cdot \begin{bmatrix} i_c \\ i_s \end{bmatrix} \tag{3.36}$$

5. Sheath current return characteristics for usual earth

As current flows along the core of the buried SF_6 bus, a return path is formed on its own sheath and possibly also on the surrounding soil and adjacent sheaths. Whether all the currents will return through its own sheath depends solely on the frequencies involved. Due to the skin effect in sheath material (Aluminum), all core current will return through its own sheath for frequencies above 1 k Hz.

In reality, the SF_6 cable is laid on the ground surface (e.g. inside the lead shaft) or is constructed above ground and grounded at certain intervals (e.g. inside the substation). This cable location even favor more current returning through the sheath than the ground as compared to buried cable case. One can thus investigate the limiting case with the cable buried underground. This cable location will favour least

core current returning through its own sheath.

In order to investigate the sheath current return characteristics and therefore the mutual coupling between cables, one has to use the series impedance matrix. One can consider cases in which adjacent sheaths are either included or excluded.

a. Sheath current return characteristics for single cable system

For this case, one only has to consider the self diagonal submatrix of the series impedance matrix as

$$-\begin{bmatrix} \frac{dV_c}{dx} \\ \\ \frac{dV_s}{dx} \end{bmatrix} = \begin{bmatrix} Z_{s11} & Z_{s12} \\ \\ Z_{s12} & Z_{s22} \end{bmatrix} \begin{bmatrix} i_c \\ \\ i_s \end{bmatrix} \tag{3.37}$$

Since the sheaths of the three individual SF_6 cables are solidly grounded at short joint intervals or laid on earth surface, or buried inside the earth, the sheath voltages can be considered to be zero for all practical purposes. Then Equation (3.37) becomes

$$0 = Z_{s12} \cdot i_c + Z_{s22} \cdot i_s$$

$$\text{or} \quad i_s = -\frac{Z_{s12}}{Z_{s22}} i_c = -i_c \tag{3.38}$$

(At high frequencies as sheath mutual impedance is negligible when sheath thickness greater than skin depth(See Appendix A).)

Thus, neglecting the other two sheaths, the current return characteristics of the SF_6 cable through its own sheath from the core can be calculated as in Equation (3.38). The obtained results are shown in Figure 3.4. For this case, essentially all the current through the core will return through its own sheath above the frequency of 10 Hz.

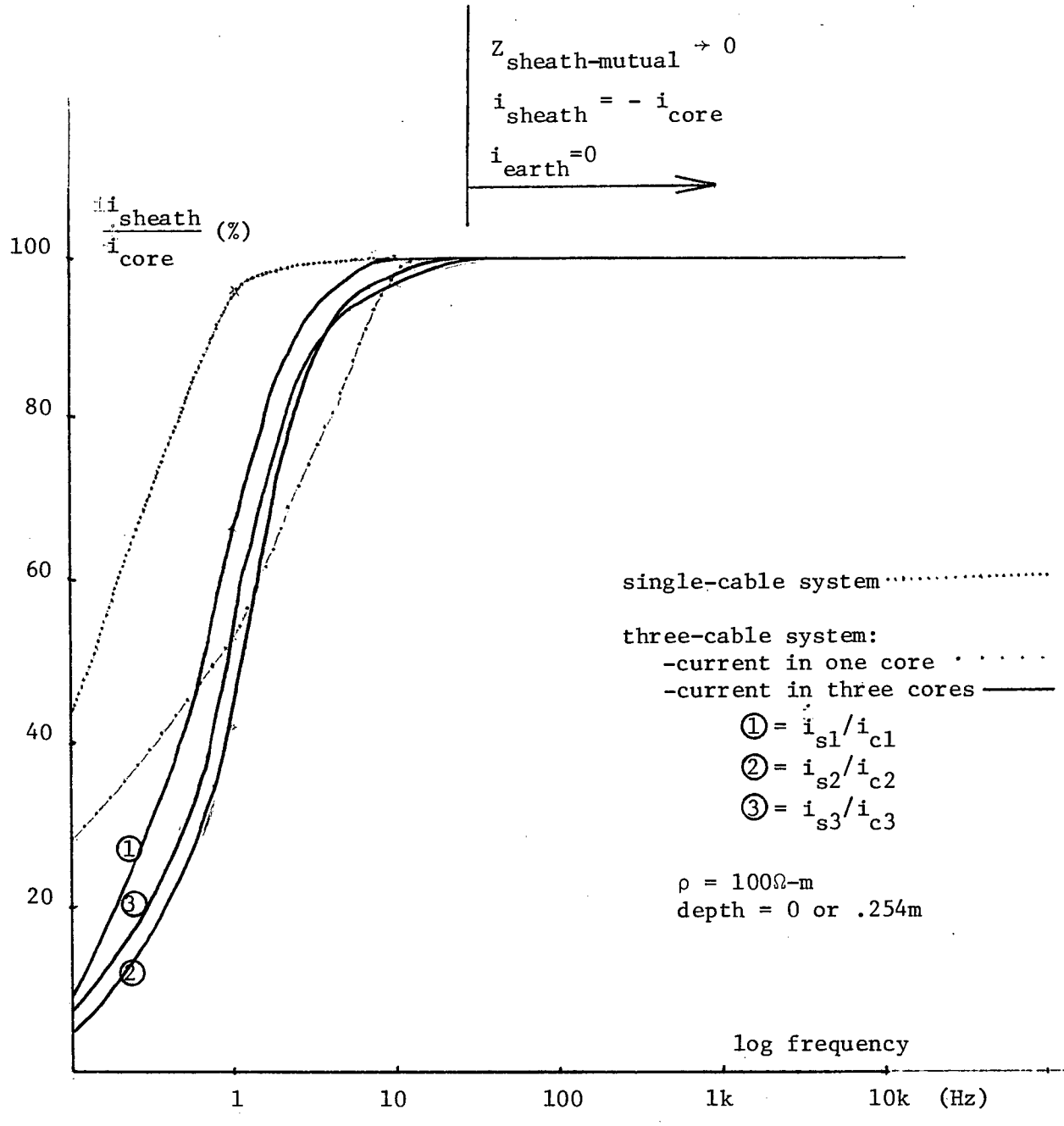

Figure 3.4: Ratio of core current return through own sheath for single-and three-cable system.

In other words, the sheath acts as a perfect magnetic shield above the frequency of 10 Hz. Because of this consideration, all SF_6 cables are decoupled from one another and can be represented as 3 single phase systems. It is also found that a change in depth (1 m to .254 m) of cable does not change the current return characteristics noticeably.

b. Sheath return characteristics for 3-cable system

Since all the 3 sheaths of the SF_6 bus are solidly grounded, the current will return through all the three sheaths at lower frequencies (< 60 Hz). At higher frequencies, however, all the core current will return through its own sheath because of the skin effect on the sheath. Here, again, one can conclude that the three SF_6 cables are decoupled from one another.

For this case of 3-cable system, one can also consider the sheath voltages to be zero. One can substitute this condition into equation (3.1) and obtain

$$-\begin{bmatrix} \frac{dV_{c1}}{dx} \\ 0 \\ \frac{dV_{c2}}{dx} \\ 0 \\ \frac{dV_{c3}}{dx} \\ 0 \end{bmatrix} = \begin{bmatrix} Z_{s11} & Z_{s12} & Z_{m12} & Z_{m12} & Z_{m13} & Z_{m13} \\ Z_{s12} & Z_{s22} & Z_{m12} & Z_{m12} & Z_{m13} & Z_{m13} \\ Z_{m12} & Z_{m12} & Z_{s11} & Z_{s12} & Z_{m12} & Z_{m12} \\ Z_{m12} & Z_{m12} & Z_{s12} & Z_{s22} & Z_{m12} & Z_{m12} \\ Z_{m13} & Z_{m13} & Z_{m12} & Z_{m12} & Z_{s11} & Z_{s12} \\ Z_{m13} & Z_{m13} & Z_{m12} & Z_{m12} & Z_{s12} & Z_{s22} \end{bmatrix} \cdot \begin{bmatrix} i_{c1} \\ i_{s1} \\ i_{c2} \\ i_{s2} \\ i_{c3} \\ i_{s3} \end{bmatrix} \quad (3.39)$$

(N.B. $Z_{m12} = Z_{m23}$ as symmetrical arrangement of cables as in Figure 3.1b)

Equating the zero sheath voltages for the 3 cables, we have

$$0 = Z_{s12}\, i_{c1} + Z_{s22}\, i_{s1} + Z_{m12}(i_{c2} + i_{s2}) + Z_{m13}(i_{c3} + i_{s3}) \tag{3.40}$$

$$0 = Z_{m12}(i_{c1} + i_{s1}) + Z_{s12}\, i_{c2} + Z_{s22}\, i_{s2} + Z_{m12}(i_{c3} + i_{s3}) \tag{3.41}$$

$$0 = Z_{m13}(i_{c1} + i_{s1}) + Z_{m12}(i_{c2} + i_{s2}) + Z_{s12}\, i_{c3} + Z_{s22}\, i_{s3} \tag{3.42}$$

If we assume phase B is energized, i.e., we assume

$$i_{c1} = i_{c3} \tag{3.43}$$

$$i_{s1} = i_{s3} \tag{3.44}$$

$$i_{c1} = i_{c3} = 0 \tag{3.45}$$

Then, substitute equations (3.43) to (3.45) into (3.40), we obtain

$$0 = Z_{s22}\, i_{s1} + Z_{m12}\, i_{s2} + Z_{m13}\, i_{s1} + Z_{m12}\, i_{c2}$$

$$= (Z_{m13} + Z_{s22})\, i_{s1} + Z_{m12}\, i_{c2} + Z_{m12}\, i_{s2}$$

or

$$\frac{Z_{m13} + Z_{s22}}{Z_{m12}} \frac{i_{s1}}{i_{c2}} + \frac{i_{s2}}{i_{c2}} = -1 \tag{3.46}$$

Also substitute equations (3.43) t0 (3.45) into (3.41), we obtain

$$0 = 2Z_{m12}\, i_{s1} + Z_{s22}\, i_{s2} + Z_{s12}\, i_{c2}$$

$$\frac{2Z_{m12}}{Z_{s12}} \frac{i_{s1}}{i_{c2}} + \frac{Z_{s22}}{Z_{s12}} \frac{i_{s2}}{i_{c2}} = -1 \tag{3.47}$$

By solving equations (3.46) and (3.47), we get

$$\frac{i_{s2}}{i_{c2}} = \frac{\begin{vmatrix} \frac{Z_{m13} + Z_{s22}}{Z_{m12}} & -1 \\ \frac{2Z_{m12}}{Z_{s12}} & -1 \end{vmatrix}}{\begin{vmatrix} \frac{Z_{m13} + Z_{s22}}{Z_{m12}} & 1 \\ \frac{2Z_{m12}}{Z_{s12}} & \frac{Z_{s22}}{Z_{s12}} \end{vmatrix}} = \frac{(Z_{m13} + Z_{s22})Z_{s12} - 2Z_{m12} \cdot Z_{m12}}{2Z_{m12} \cdot Z_{m12} - Z_{s22}(Z_{m13} + Z_{s22})} \qquad (3.48)$$

and

$$\frac{i_{s1}}{i_{c2}} = \frac{\begin{vmatrix} -1 & 1 \\ -1 & \frac{Z_{s22}}{Z_{s12}} \end{vmatrix}}{\begin{vmatrix} \frac{Z_{m13} + Z_{s22}}{Z_{m12}} & 1 \\ \frac{2Z_{m12}}{Z_{s12}} & \frac{Z_{s22}}{Z_{s12}} \end{vmatrix}} = \frac{-Z_{s12} \cdot Z_{m12} + Z_{s22} \cdot Z_{m12}}{2Z_{m12} \cdot Z_{m12} - Z_{s22}(Z_{m13} + Z_{s22})} \qquad (3.49)$$

The ratio of currents in sheath to core of phase B is calculated and plotted as a function of frequency in Figure 3.4. The result shows that at frequencies above 1 kHz as in lightning surges, all current through the core will return through its own sheath. Thus, one can conclude that the earth return current component is not important and therefore the mutual

coupling between cables can be ignored.

c. Sheath current return characteristics for 3 cable system with current in all 3 cores

For a case when currents flow in all the three cores of the three SF_6 cables, the return current through sheath will change accordingly. This suggests that such situations must also be investigated to deduce the mutual coupling effect among cables. Using the same equations as derived in Equations (3.40) to (3.42), one can now put in currents in the 3 cores by assuming

$$i_{c2} = 1.0 \angle 0 \tag{3.50}$$

$$i_{c3} = 1.0 \angle 120° \tag{3.51}$$

and

$$i_{c1} = 1.0 \angle -120° \tag{3.52}$$

Rewriting equations (3.40) to (3.42) as

$$Z_{s22}\, i_{s1} + Z_{m12}\, i_{s2} + Z_{m13}\, i_{s3} = -Z_{s12}\, i_{c1} - Z_{m12}\, i_{c2} - Z_{m13}\, i_{c3} = A_1 \tag{3.53}$$

$$Z_{m12}\, i_{s1} + Z_{s22}\, i_{s2} + Z_{m12}\, i_{s3} = -Z_{m12}\, i_{c1} - Z_{s12}\, i_{c2} - Z_{m12}\, i_{c3} = A_2 \tag{3.54}$$

$$Z_{m13}\, i_{s1} + Z_{m12}\, i_{s2} + Z_{s22}\, i_{s3} = -Z_{m13}\, i_{c1} - Z_{m12}\, i_{c2} - Z_{s12}\, i_{c3} = A_3 \tag{3.55}$$

Defining the determinant T as

$$T = \begin{vmatrix} Z_{s22} & Z_{m12} & Z_{m13} \\ Z_{m12} & Z_{s22} & Z_{m12} \\ Z_{m13} & Z_{m12} & Z_{s22} \end{vmatrix} = Z_{s22}^3 + 2Z_{m12}^2 \cdot Z_{m13} - Z_{s22}(Z_{m13}^2 + 2Z_{m12}^2) \tag{3.56}$$

We can then obtain the current through the three individual sheaths as

$$i_{s1} = \frac{A_1 Z_{s22}^2 + A_3 Z_{m12}^2 + A_2 Z_{m12} Z_{m13} - A_3 Z_{s22} Z_{m13} - A_2 Z_{m12} Z_{s22} - A_1 Z_{m12}^2}{T} \tag{3.57}$$

$$i_{s2} = \frac{A_2 Z_{s22}^2 + A_1 Z_{m12} Z_{m13} + A_3 Z_{m12} Z_{m13} - A_2 Z_{m13}^2 - A_3 Z_{m12} Z_{s22} - A_1 Z_{m12} Z_{s22}}{T} \tag{3.58}$$

$$i_{s3} = \frac{A_3 Z_{s22}^2 + A_2 Z_{m12} Z_{m13} + A_1 Z_{m12}^2 - A_1 Z_{m13} Z_{s22} - A_2 Z_{m12} Z_{s22} - A_3 Z_{m12}^2}{T} \tag{3.59}$$

After substituting the conditions for the 3 phase currents from equations (3.50) to (3.52) into equations (3.57) to (3.59), one can obtain the return currents through all individual sheaths. The magnitudes of the sheath currents are also shown in Figure 3.4. It is again confirmed here that at frequency above 60 Hz, all current flowing from core will return through its own sheath. Each core is completely shielded from the adjacent cores. Thus, the three SF_6 buses are completely decoupled from one another and should therefore be represented by single phases as in the case of lightning overvoltage propagation.

6. Sheath current return characteristics for substation earth with grounding grid network

In reality in the substation, the cable sheaths are grounded inside the substation with a grounding network grid consisting of copper bars which are connected across the whole substation. These grounding copper bars serve to reduce significantly the inside earth resistivity of the substation. This suggests that the sheath current return characteristics of this reduced earth resistivity should also be investigated as a reduction

in earth resistivity will favor more current returning through the earth.

The result for the sheath return current as a function of earth resistivity is shown in Figure 3.5. This figure shows that the sheath return current increases as the earth resistivity increases. This agrees with the manufacturers and utility companies of SF_6 substations who claim that current returning through sheath inside the substation is less than 75%. Based upon this criteria, a nominal earth resistivity of $0.3 \times 10^{-5} \Omega m$ is chosen.

After choosing a nominal value for earth resistivity, the sheath current return characteristic is then evaluated as a function of frequencies and depth, as shown in Figure 3.6. Fluctuations in overall sheath current results are shown in Figure 3.6. At about 1 K Hz, the sheath current is even found to be larger than the core current. This can be explained by the phasor diagram as shown in Figure 3.7. In Figure 3.7, only multi-cable systems with current in centre core are shown, but mutli-cable system with currents in all 3 cores would also give identical results. The present study again confirmed that all cores are decoupled from one another above 2 k Hz even for the adverse case of significantly reduced earth resistivity inside the substation.

It should be noted that the mutual impedance between cores, between sheaths and between corresponding cores and sheaths are all assumed to be equal by Wedepohl and Ametani. The shielding effect of the sheath is neglected. The validity of this assumption in cable parameter computations could be the topic of further research. It is of little concern for the purpose of this thesis. At the high frequencies encountered in lightning surge studies, core current always return completely through the sheath. In that case, the magnetic field becomes zero outside the sheath anyhow.

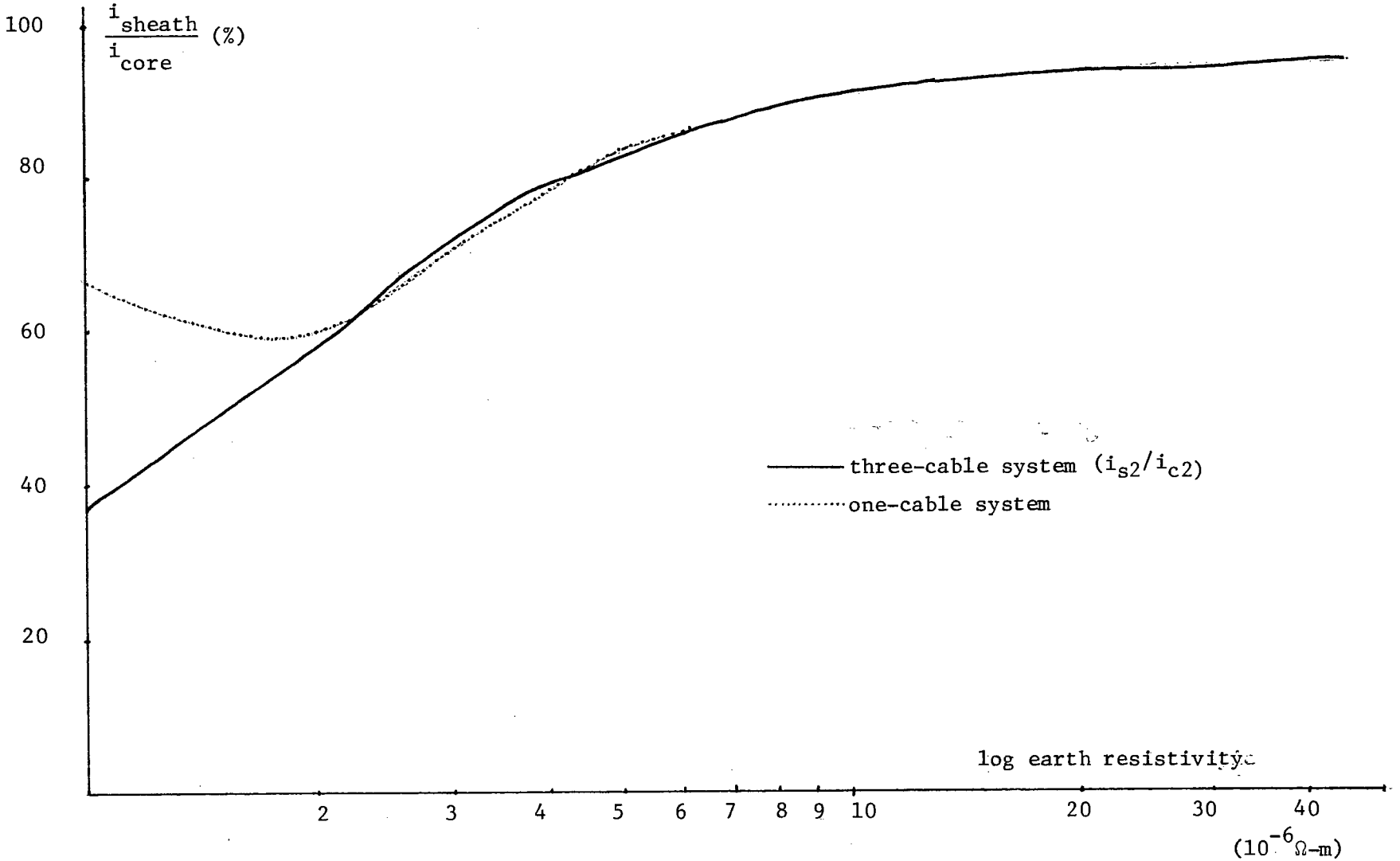

Figure 3.5: Ratio of core current return through sheath at 60 Hz for different earth resistivities.

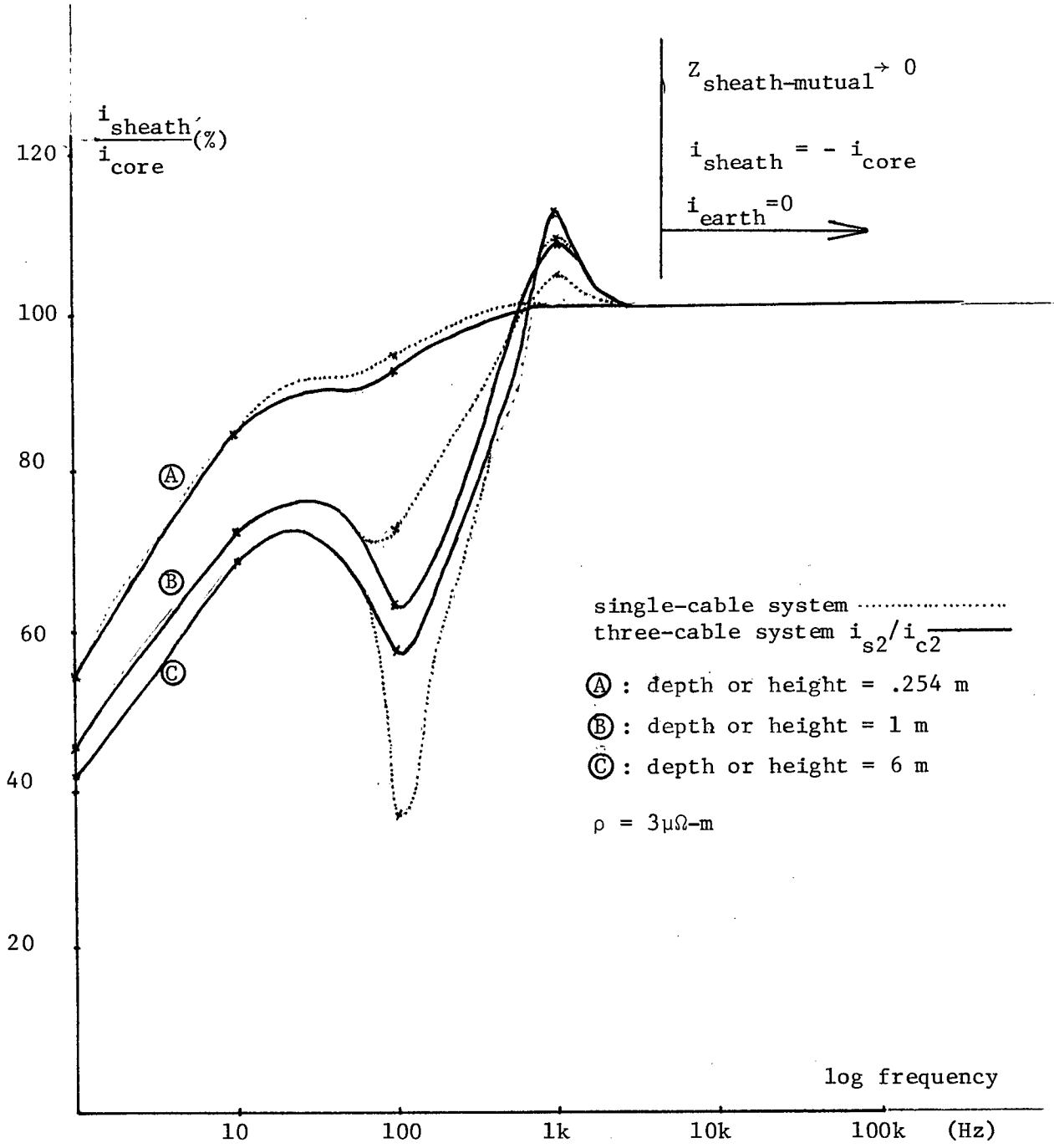

Figure 3.6: Ratio of core current return through own sheath for single- and three- cable system at reduced earth resistivity of 3 μΩ-m inside substation.

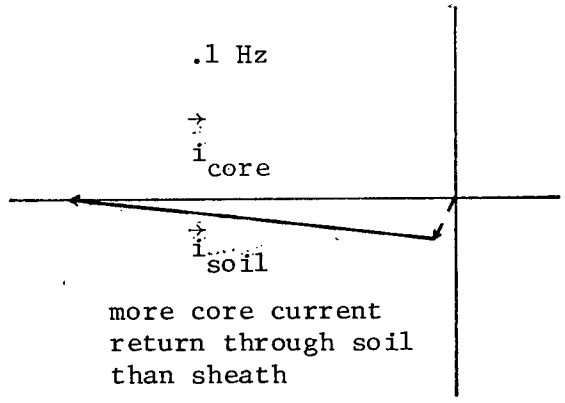

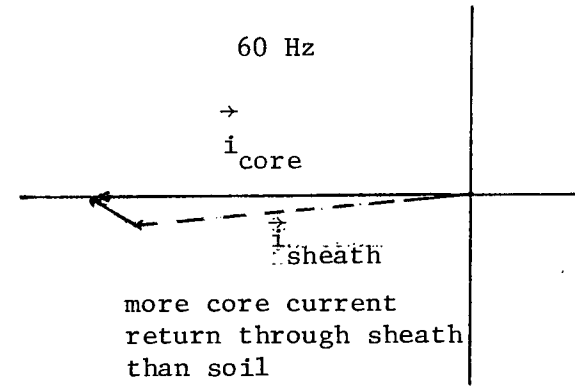

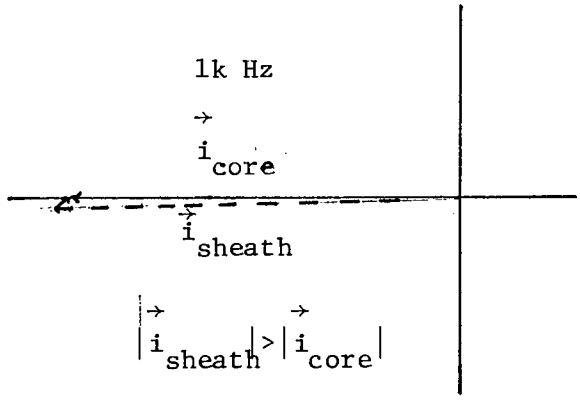

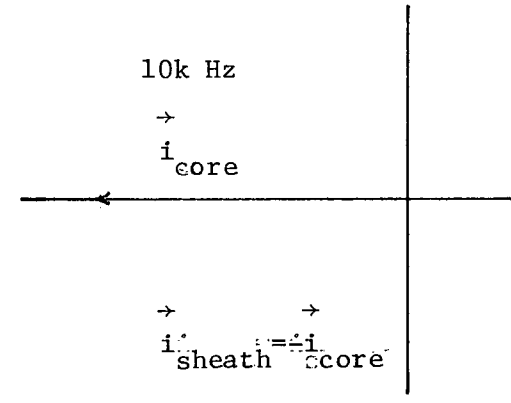

$$\vec{i}_{core} = \vec{i}_{sheath} + \vec{i}_{soil}$$

Figure 3.7: Phasor diagram of current return through sheath and earth.

7. Formation of shunt admittance matrix for SF_6 cables

For a usual 3-phase single core underground cable system, one can build a 6 x 6 shunt admittance matrix [Y] to describe the cable system as

$$[\frac{di}{dx}] = [Y] \quad [V]$$

i.e.

$$\begin{bmatrix} \frac{di_{c1}}{dx} \\ \frac{di_{s1}}{dx} \\ \frac{di_{c2}}{dx} \\ \frac{di_{s2}}{dx} \\ \frac{di_{c3}}{dx} \\ \frac{di_{s3}}{dx} \end{bmatrix} = \left[\begin{array}{cc|cc|cc} y_1 & -y_1 & 0 & 0 & 0 & 0 \\ -y_1 & y_1+y_2 & 0 & 0 & 0 & 0 \\ \hline 0 & 0 & y_1 & -y_1 & 0 & 0 \\ 0 & 0 & -y_1 & y_1+y_2 & 0 & 0 \\ \hline 0 & 0 & 0 & 0 & y_1 & -y_1 \\ 0 & 0 & 0 & 0 & -y_1 & y_1+y_2 \end{array}\right] \begin{bmatrix} V_{c1} \\ V_{s1} \\ V_{c2} \\ V_{s2} \\ V_{c3} \\ V_{s3} \end{bmatrix} \qquad (3.60)$$

Notice that the off-diagonal submatrix of [Y] are all zero due to the fact that the grounded sheaths in between acts as electrostatic shield between cables. For the SF_6 cable system as shown in Figure 3.1, the diagonal submatrix elements are

$$y_1 = j\omega c_1 = j\omega\, 2\pi\varepsilon_o \cdot \frac{1}{\ell n \frac{r_3}{r_2}}$$

$$y_2 = j\omega c_2 = j\omega\, 2\pi\varepsilon_o \cdot \frac{1}{\ell n \frac{r_4}{r_4}} = \infty$$

where y_1 is admittance due to internal SF_6 gas insulation, and

y_2 is admittance due to external sheath insulation.

(N.B. The external insulation is non-existent for the SF_6 cable.)

As has been confirmed by the author in previous finding for sheath current return characteristics, the core should be represented as single phase. Then, the admittance equation shown in Equation (3.60) should be reduced to

$$-\frac{di_c}{dx} = y_1 V_c$$

$$= j\omega \cdot 2\pi\varepsilon_o \cdot \frac{1}{\ell n \frac{r_3}{r_2}} \cdot V_c \qquad (3.61)$$

$$= y_{self} \cdot V_c \qquad (3.62)$$

8. Confirmation of numerical accuracy for cable parameter calculation and current return ratios

The numerical accuracy of the computation was confirmed when the cable parameters obtained by the developed cable constants program, and by the BPA cable constant program[32] agree consistently to more than three significant figures.

Then, a 500 kV submarine cable[38] was chosen as another test example. In this case, the cable parameters for the submarine cable was first calculated. The amount of core current returning through the sheath, armour and the sea was obtained by taking into account of zero potentials on the grounded sheath and the grounded armour. The ratios of magnitudes of core current returning through the sheath ,the armour, and the sea at 60 Hz were obtained as 14%, 87.8% and 5.6% respectively. These agreed to more than two figures to the results of other findings.[48]

9. Single phase representation parameters for multi-phase SF_6 cables

Since all phases of the SF_6 cables are decoupled from one another, single phase cable representation for studying lightning overvoltage wave

propagation in SF_6 cable is recommended. The self admittance element (y_{self}) can be calculated from the simple formula as shown in equations (3.61) and (3.62), whereas the self impedance matrix element can be calculated from equation (3.1) as

$$-\frac{dV_{c1}}{dx} = Z_{s11}\, i_{c1} + Z_{s12}\, i_{s1} + Z_{m12}(i_{c2} + i_{s2}) + Z_{m13}(i_{c3} + i_{s3}) \qquad (3.63)$$

and $$0 = Z_{s21}\, i_{c1} + Z_{s22}\, i_{s1} + Z_{m12}(i_{c2} + i_{s2}) + Z_{m13}(i_{c3} + i_{s3}) \qquad (3.64)$$

Subtracting Equation (3.64) from (3.63), we get

$$\begin{aligned} -\frac{dV_{c1}}{dx} &= (Z_{s11} - Z_{s21})\, i_{c1} + (Z_{s12} - Z_{s22})\, i_{s1} \\ &= (Z_{s11} - Z_{s21}(1 - \frac{i_{s1}}{i_{c1}}) - Z_{s22}(\frac{i_{s1}}{i_{c1}}))\, i_{c1}, \qquad (3.65) \\ &\doteq Z_{self} \cdot i_{c1} \end{aligned}$$

where the sheath to core current ratio can be obtained from equation (3.49) or equations (3.57) to (3.59).

Because all core current returns through the sheath at high frequencies, one has in such condition

$$\frac{i_{s1}}{i_{c1}} = -1, \text{ and } Z_{s12} = Z_{s22}$$

Substituting this into equation (3.65) or (3.37), one obtains

$$-\frac{dV_c}{dx} = (Z_{s11} - Z_{s22})\, i_c \qquad (3.66)$$

After having obtained the self series impedance for single phase cable as shown in Figure 3.1, one can then represent the cable by the surge impedance Z^{surge}, and the wave propagation velocity v, as given by

$$Z^{surge} = \sqrt{\frac{Z_{self}}{y_{self}}} = 61.4\ \Omega \tag{3.67}$$

$$v = \omega \sqrt{\frac{1}{Z_{self} \cdot y_{self}}} = 300\ m/\mu s \tag{3.68}$$

One should realize that the metallic sheath of the SF_6 cable always form a very good earth return path to the cable core. The series resistance is negligible compared to the reactance (See Fig.3.8).Thus, the SF_6 cable can be taken to be lossless. It should also be noted that for such a simple go-return circuit for a coaxial cable, the inductance can be given by the simple formula[15] as

$$L = \frac{\mu_o}{2\pi} \ln \frac{r_3}{r_2} \tag{3.69}$$

$$= 0.205\ \mu H/m$$

Consistent results for the inductance are obtained by equation (3.65) and (3.69) for frequencies above 10 Hz. Thus, the simple formula is in equation (3.69) is recommended for inductance calculation of SF_6 cable in the study of surge propagation characteristics. The surge impedance and the wave propagation velocity can be then obtained as

$$Z^{surge} = \sqrt{\frac{L}{C}} = \sqrt{\frac{\mu_o}{2\pi} \cdot \ln \frac{r_3}{r_2} \cdot \frac{1}{2\pi\varepsilon_o} \cdot \ln \frac{r_3}{r_2}}$$

$$= \sqrt{\frac{\mu_o}{\varepsilon_o} \cdot \frac{1}{4\pi^2}} \cdot \ln \frac{r_3}{r_2}$$

$$= 60 \ln \frac{r_3}{r_2} \tag{3.70}$$

where r_3 and r_2 are radius of sheath and core respectively.

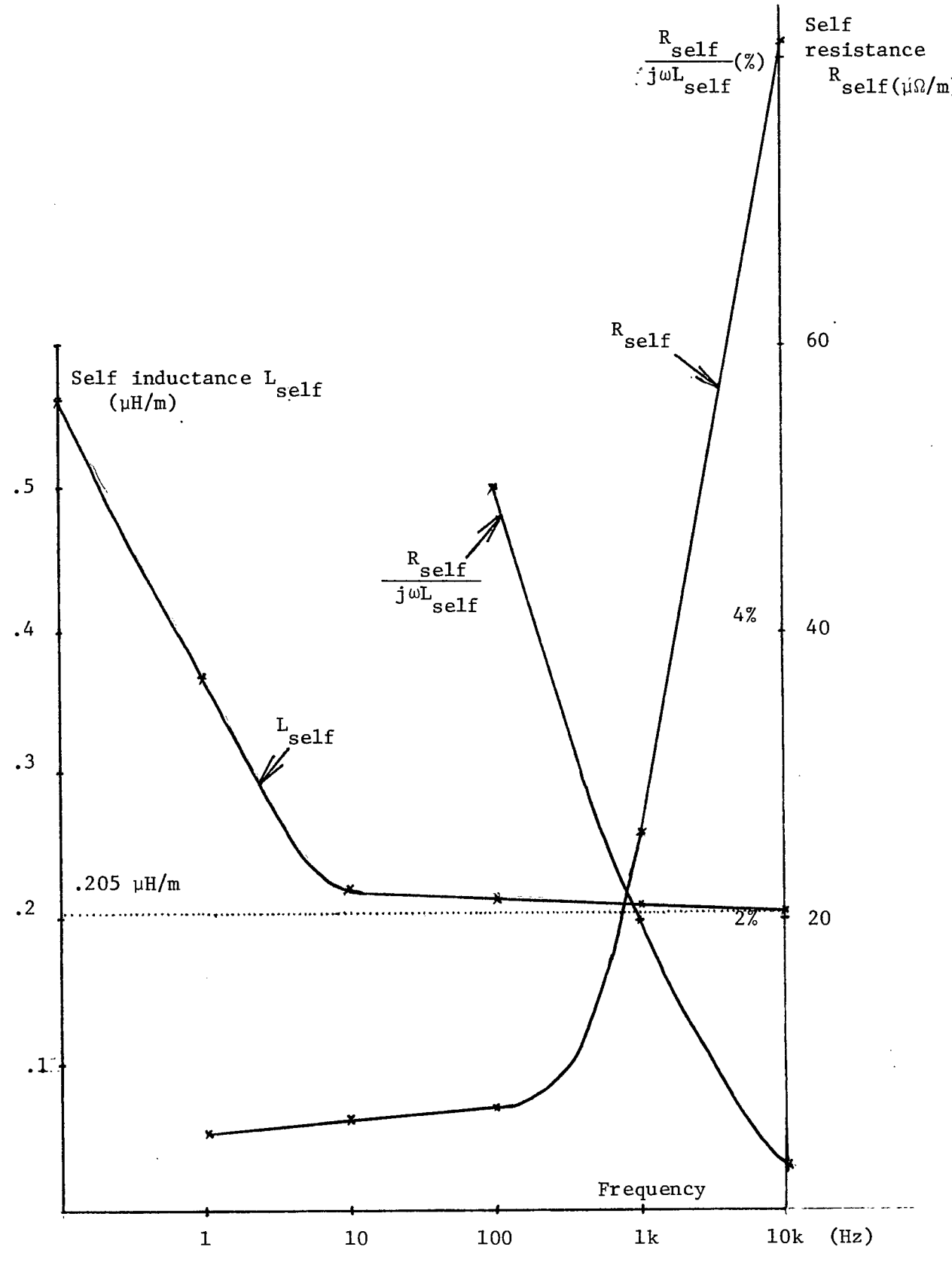

Figure 3.8: Self series inductance, resistance and resistance to reactance ratio for SF_6 cable.

and
$$v = \sqrt{\frac{1}{LC}} = \sqrt{\frac{2\pi}{\mu_o} \cdot \frac{1}{\ell n \frac{r_3}{r_2}} \cdot \frac{1}{2\pi\varepsilon_o} \cdot \ell n \frac{r_3}{r_2}} \qquad (3.70)$$

$$= \sqrt{\frac{1}{\mu_o \varepsilon_o}} = 300 \ ^{m}/\mu s$$

= velocity of light in vacuum

10. Wave propagation in SF_6 cables

Wave propagation characteristics in single core SF_6 cable can now be modelled by the surge impedance of 61.4 Ω, (typically about 60 to 75 Ω), and wave propagation velocity, (typically 300 $^{m}/\mu s$). A numerical simulation of overvoltage wave-shape in the receiving end of a SF_6 cable joining to a overhead transmission line is simulated.

The resulting voltage in the open-circuited SF_6 cable receiving end rises in a staircase fashion of diminishing amplitude, to a value of 2 p.u. (See Figure 3.9). This can be explained by using the reflection (C_ℓ) and refraction coefficient (C_R) of the system at the line-cable junction and the open-circuited cable end respectively.[39] For the line-cable junction at A, one has

$Z_2 = 312$, $Z_1 = 60\ \Omega$
(Wave incident from cable)
$$C_\ell = \frac{Z_2 - Z_1}{Z_1 + Z_2} = \frac{312 - 60}{312 + 60} = .68 \qquad (3.71)$$

(Wave incident from line)
$Z_2 = 60$, $Z_1 = 312\ \Omega$

and
$$C_R = \frac{2 \times Z_2}{Z_1 + Z_2} = \frac{2 \times 60}{312 + 60} = .32 \qquad (3.72)$$

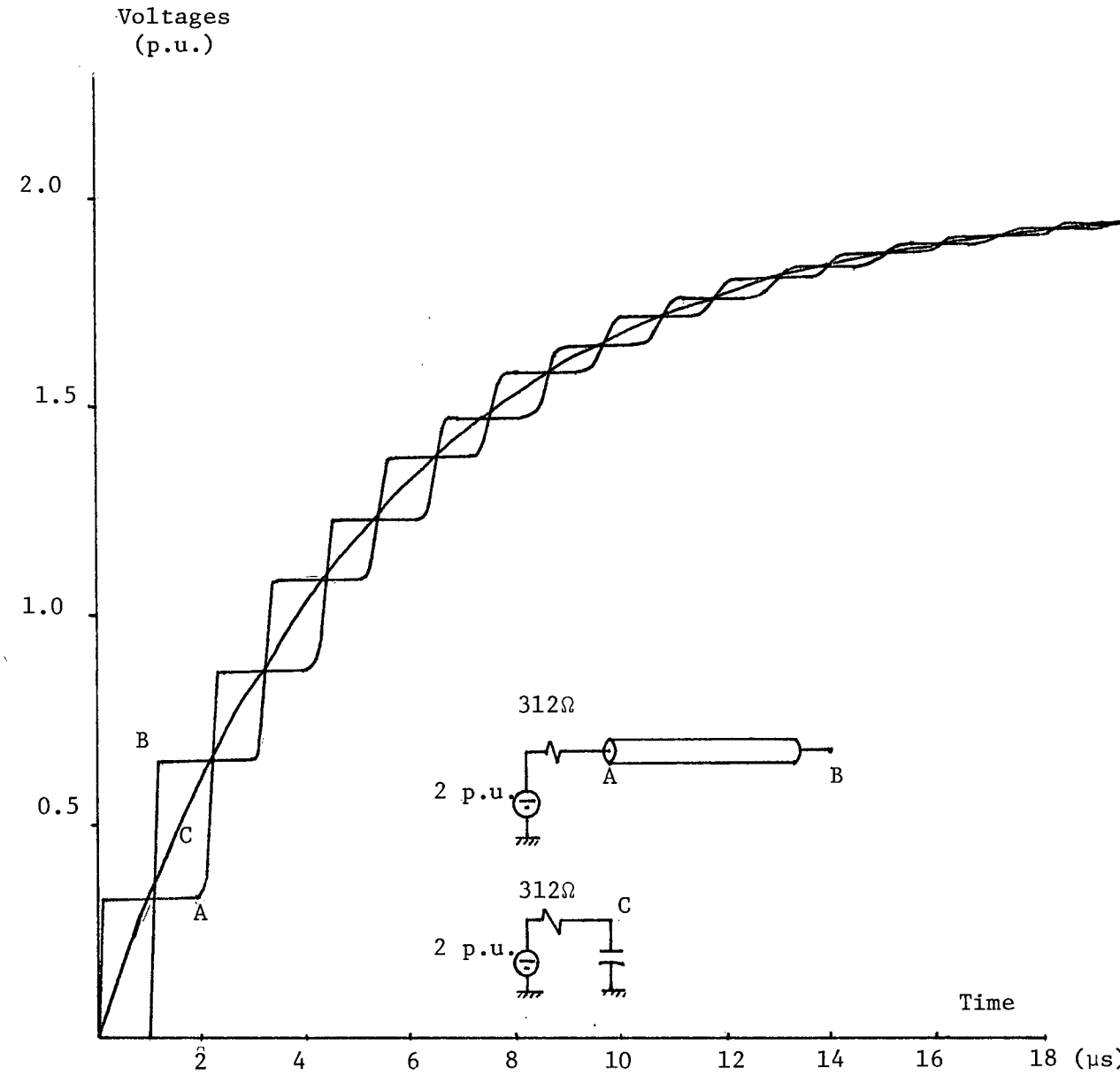

Figure 3.9: Overvoltage waveshapes at both ends of SF_6 cable joining from overhead transmission line.

For the open end of the cable, we have

$$C_{\ell}^{o} = \frac{Z_2 - Z_1}{Z_1 + Z_2} = \frac{\infty - 60}{\infty + 60} = 1$$

and $$C_{R}^{o} = \frac{2 \times \infty}{\infty + 60} = 2$$

(Wave incident from cable, $Z_1 = 60$, $Z_2 = \infty$)

Thus, the discrete rise in voltage wave shape can be expressed as

$$v = 2 \times .32 \ (1 + C_{\ell} + C_{\ell}^{2} + \ldots)$$

where each step addition accurs at discrete time intervals of 2 travel times.

On the other hand, this overall rise in overvoltages wave shape also agrees with the general exponential rise wave shape in charging of a capacitor. This is due to the inherent large self capacitance of cables. The overall rise in wave shape can be sketched by modelling the SF_6 cable as a lumped capacitor equivalent to the total capacitance for the length of cable, and ignoring the surge impedance of the cable (See Figure 3.9).

CHAPTER 4: CORONA ATTENUATION AND DISTORTION CHARACTERISTICS OF LIGHTNING OVERVOLTAGE IN OVERHEAD TRANSMISSION LINES.

1. Introduction

As the lightning voltage wave travels down the overhead transmission line, a high electric field is produced on the line conductor surface. When the electric field intensity exceeds the breakdown strength of air (~ 30 kV/cm), ionization of surrounding air molecules takes place. This phenomenon will dissipate the unwanted surge energy away from the system and thus reduces the magnitude and initial rate of rise of the lightning overvoltage.

In transient lightning overvoltage studies, several numerical methods have been employed to account for corona effects. Brown[44] applied the concept of corona radius to account for the corona envelope produced on the conductor surface. The coronated line capacitances at higher voltages are also obtained by extrapolation. Darveniza[12] also used lower wave propagation velocities higher voltages and different corona correction factor for different conductor configuration. However, both methods are not straightforward and are not totally successful in duplicating field rest results. Umoto and Hara[43] also transformed the transmission line equation for coronated lines into difference algebraic equations. However, this numerical approach is not efficient enough. Thus, an efficient and accurate numerical model for corona must be developed to predict the corona attenuation and distortion characteristics on lightning overvoltage propagations in overhead lines.

2. Physical properties of corona attenuation and distortion characteristics

The physical aspects and laws governing the behaviour of corona discharge have been investigated since the beginning of this century. However, most of the investigations and applications have been limited to power frequency steady state or at most to switching transient conditions. From

the published field measurements for lightning surges, it can be observed that the attenuation resulting from corona effects is much larger than that resulting from transmission line series resistance losses. The non-linear characteristics of the corona discharge can be considered as (see Figure 4.1):

a) Corona attenuation loss - From the quadratic law of corona loss proposed by Peek[41], the loss ($v\, i_k$) per unit length is proportional to the square of the voltage above the critical corona voltage v_{co} i.e.

$$vi_R = k_R \cdot (v - v_{co})^2, \tag{4.1}$$

where $k_R = \sigma_G \cdot \sqrt{\frac{r}{2h}} \times 10^{-11}$ mho/m

r , h = radius and height of conductor respectively

σ_G = Corona loss constant determined experimentally

This corona attenuation loss can be modelled with a resistive current loss i_R through the corona resistive branch to ground as

$$i_R = k_R \cdot \frac{(v - v_{co})^2}{v} \tag{4.2}$$

b) Increase in shunt capacitance - the retardation of the wave front by corona can be explained by an increase in shunt capacitance. Skilling[42] and Umoto[43] suggested that the increase in shunt capacitance is proportional to the voltage above the critical voltage v_{co}, i.e.

$$C_{corona} = 2k_c\left(1 - \frac{V_{co}}{V}\right), \tag{4.3}$$

where $k_c = \sigma_c \sqrt{\frac{r}{2h}} \times 10^{-11}$ F/m

σ_c = corona loss constant determined experimentally

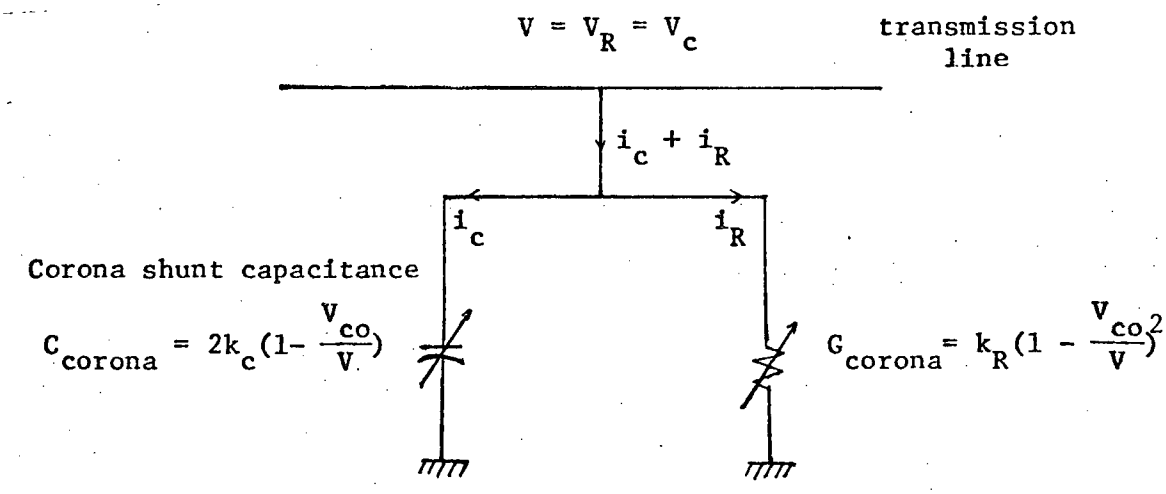

Figure 4.1: Nonlinear corona losses model.

This increase in capacitance can be modelled by a capacitance branch to ground with the capactive current loss i_c

$$i_c = 2k_c \cdot (1 - \frac{V_{co}}{V}) \frac{\partial v}{\partial t} \tag{4.4}$$

Corona discharge only occur if the voltage is greater or equal to the critical corona voltage, and if the voltage increase with time, i.e.

$$v \geq v_{co}, \text{ and } \frac{\partial v}{\partial t} > o.$$

This is due to the fact that, when the voltage begins to decrease, the space charge consisting of heavy ions in the ionization region remains practically constant in magnitude and position during a short period of time. This slow diffusion of ions results in little energy loss in the case of decreasing voltage conditions even when $v > v_{co}$.

3. Transmission line equations for coronated lines.

The corona phenomena can now be described by the modified line equations. With the introduction of digital computers, these phenomena can be studied accurately by solving the equations describing the electromagnetic wave propagations, taking corona into account as follows:

$$-\frac{\partial v}{\partial x} = L \frac{\partial i}{\partial t} \tag{4.5}$$

$$-\frac{\partial i}{\partial x} = C \frac{\partial v}{\partial t} + 2k_c \cdot (1 - \frac{v_{co}}{v}) \frac{\partial v}{\partial t} + k_R (1 - \frac{v_{co}}{v})^2 \cdot v \tag{4.6}$$

extra shunt capacitance due to corona

Extra shunt conductance due to corona

Umoto[43] and Inoue[45] solved the above equations by the difference method. The line equations (4.5) and (4.6) are transformed into algebraic equations of small increments of distance, Δx, and time, Δt. However, this method is not efficient to implement into the digital computer as the method requires Δx to be as small as 7 m, when using $\Delta t = .01$ μs.

4. Solution of line equation by compensation method with trapezoidal rules

The line equations (4.5) and (4.6) with corona losses can be solved by the compensation method.[47] In this method, the line equations are first solved without the extra corona terms. The Bergeron's method using travelling wave technique together with modal analysis(See Chapter 2) is applied. Then, the corona losses can be treated as non-linear shunt branches connected to ground. The trapezoidal rule can then applied to obtain the total current loss of the corona phenomena.

By applying the trapezoidal rule of linear interpolation to the corona resistive branch to ground, we have as shown in Figure 4.2,

$$i_{t+\Delta t} = i_t + d(v_{t+\Delta t} - v_t)$$

$$\text{i.e.} \quad v_{t+\Delta t} = \frac{1}{d} i_{t+\Delta t} + (v_t - \frac{1}{d} i_t)$$

$$\text{where} \quad d = \frac{i_{t+\Delta t} - i_t}{v_{t+\Delta t} - v_t} \tag{4.7}$$

as d = slope of graph at time t.

Also, d can be obtained by considering the equation (4.2)

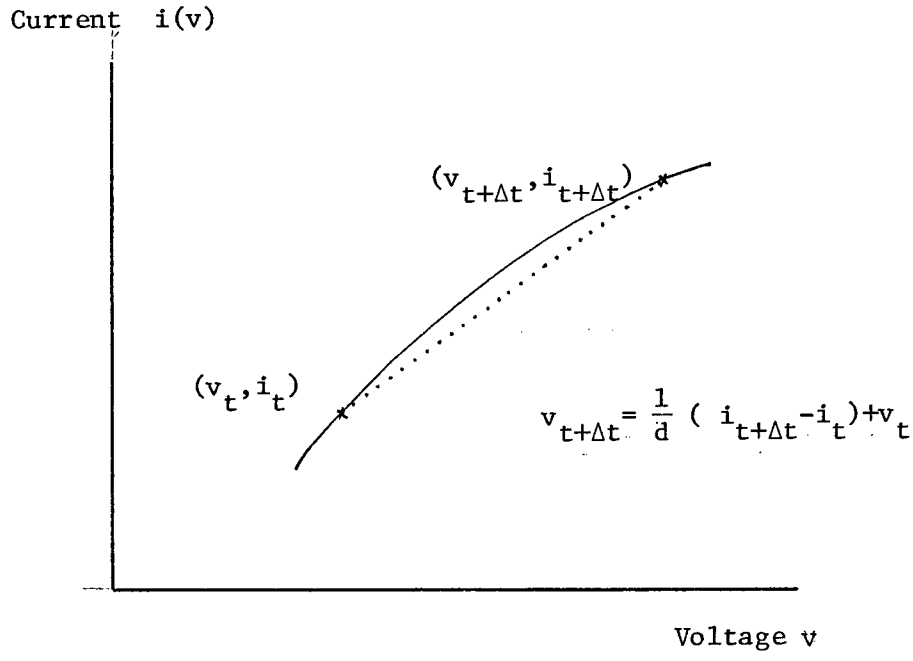

Figure 4.2: Linear interpolation for resistance corona branch.

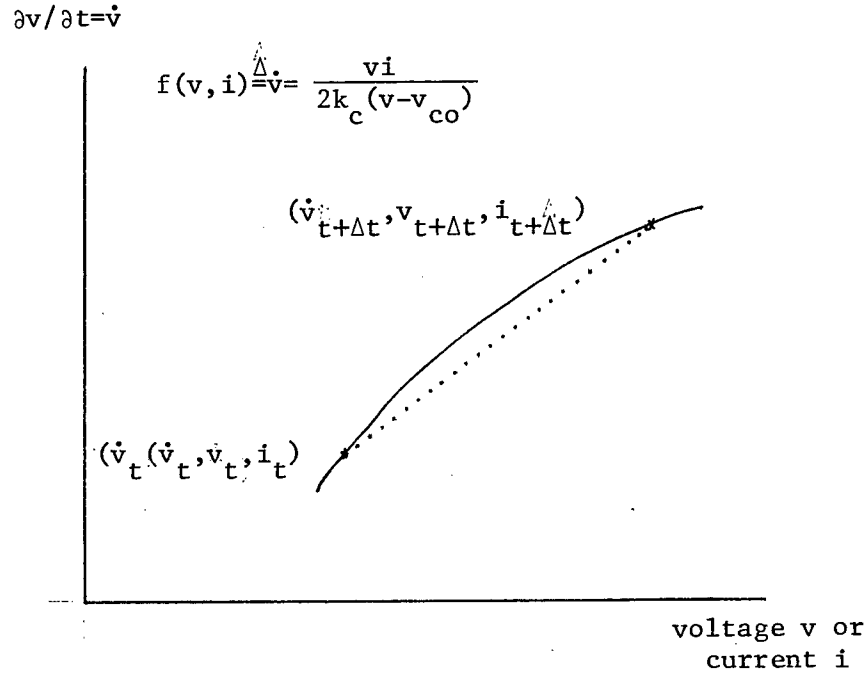

Figure 4.3: Linear interpolation for capacitive corona branch.

$$i_t = k_R \frac{(v_t - v_{co})^2}{v_t}$$

$$= k_R v_t + k_R \frac{v_{co}^2}{v_t} - 2k_R v_{co}$$

or $$d = \frac{di_t}{dv_t} = k_R - k_R \frac{v_{co}^2}{v_t^2} \tag{4.8}$$

Thus, we eventually have

$$v_{t+\Delta t} = \frac{1}{d} i_{t+\Delta t} + (v_t - \frac{1}{d} i_t) \tag{4.9}$$

$$= R_R \cdot i_{t+\Delta t} + v_o \tag{4.10}$$

where $v_o = v_t - \frac{1}{d} i_t$ (known from past history at time t)

and $R_R = \frac{1}{d}$ (known from past history at time t)

Similarly, since the corona capacitive branch current loss is given by

$$i = \frac{2k_c}{v} (v - v_{co}) \frac{\partial v}{\partial t}$$

or $$\frac{\partial v}{\partial t} = \frac{v \quad i}{2k_c(v - v_{co})} \triangleq f(v, i)$$

Applying linear interpolation of the 2 variables (i.e. from first term of Taylors' series), we have as shown in Figure 4.3

$$f(v, i)\Big|_{t+\Delta t} = f(v, i)\Big|_t + \frac{\partial f}{\partial v}\Big|_t (v_{t+\Delta t} - v_t) + \frac{\partial f}{\partial i}\Big|_t (i_{t+\Delta t} - i_t)$$

(4.11)

$$\therefore \quad \left.\frac{\partial f}{\partial v}\right|_t = \left.\frac{i_t}{2k_c}\frac{(v - v_{co}) - v}{(v - v_{co})^2}\right|_t$$

$$= \frac{-i_t}{2k_c}\frac{v_{co}}{(v_t - v_{co})^2} \tag{4.12}$$

$$\text{and} \quad \left.\frac{\partial f}{\partial i}\right|_t = \left.\frac{v}{2k_c(v - v_{co})}\right|_t$$

$$= \frac{v_t}{2k_c(v_t - v_{co})} \tag{4.13}$$

Thus, we obtain

$$f(v, i)\Big|_{t+\Delta t} = \left.\frac{\partial v}{\partial t}\right|_{t+\Delta t} = \frac{v_{t+\Delta t} - v_t}{\Delta t}$$

$$= \frac{v_t \cancel{i_t}}{2k_c(v_t - v_{co})} - \frac{v_{co}\, i_t}{2k_c}\frac{1}{(v_t - v_{co})^2}(v_{t+\Delta t} - v_t) +$$

$$\frac{v_t}{2k_c(v_t - v_{co})} \cdot (i_{t+\Delta t} - \cancel{i_t}) \tag{4.14}$$

Re-arranging equation (4.14) will give the linearized equation as

$$v_{t+\Delta t} = R_c\, i_{t+\Delta t} + v_1 \tag{4.15}$$

where $$R_c = \frac{1}{1 + \dfrac{v_{co}\, i_t \cdot \Delta t}{2k_c(v_t - v_{co})^2}} \cdot \frac{\Delta t \cdot v_t}{2k_c(v_t - v_{co})}$$ (known from past history)

and $$v_1 = \frac{1}{1 + \dfrac{v_{co}\, i_t \cdot \Delta t}{2k_c(v_t - v_{co})^2}}\left(v_t + \frac{\Delta t \cdot v_{co}\, i_t\, v_t}{2k_c(v_t - v_{co})^2}\right)$$ (known from past history)

Combining equations (4.10) and (4.15) for the voltages and currents in both corona resistive and capacitive branches by taking into account

$$v_c = v_R = v$$

and $$i = i_c + i_R$$

we can obtain

$$\left(\frac{1}{R_c} + \frac{1}{R_R}\right) v = (i_c + i_R) + \left(\frac{v_1}{R_c} + \frac{v_o}{R_R}\right) \tag{4.16}$$

or $$v = R'i + k' \tag{4.17}$$

where $$R' = \frac{R_c R_R}{R_c + R_k}$$

and $$k' = \frac{R_R v_1 + R_c v_o}{R_c + R_R}$$

Having the corona loss branches represented by a linear model as described in equation (4.17), the compensation method can then be applied to solve the transmission line equations including corona losses.

In the compensation method, the transmission line is first reduced to a Thevinin equivalent (See Figure 4.4) and is described by

$$v = v_o + A_2 i, \tag{4.18}$$

where A_2 is a negative number.

Then, this equation is solved simultaneously with the linearized equation for corona loss, as in equation (4.17). Thus, the resulting corona voltage and discharge current can be obtained as

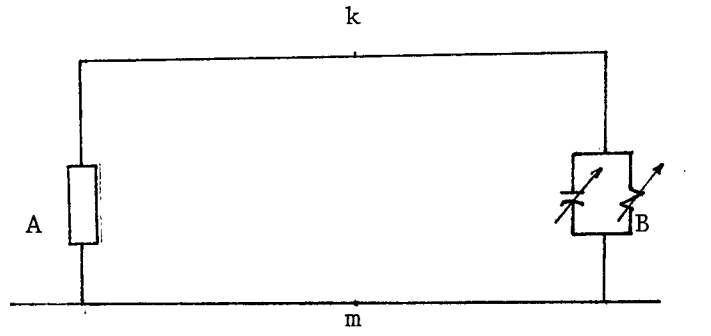

A : Thevinin equivalent network for transmission line without corona losses

$$v_{km} = v_o + A_2\, i$$

B : Nonlinear corona losses model

$$v = R'\, i + k'$$

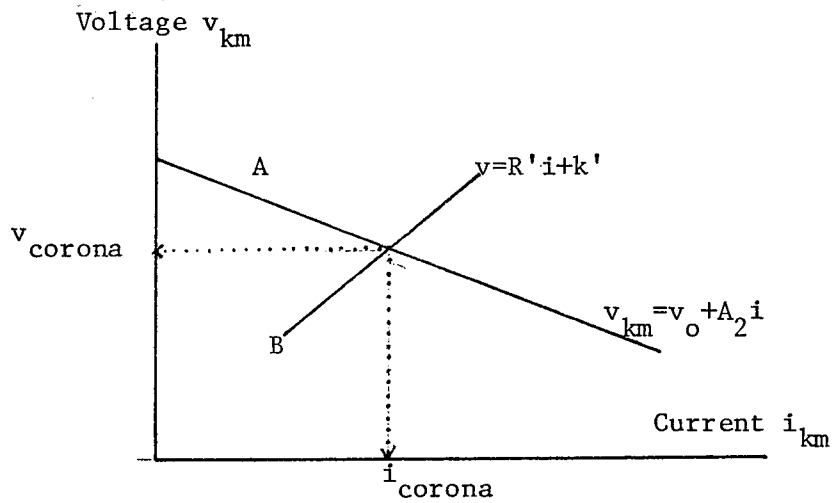

Figure 4.4: Compensation method for non-linear corona model

$$i_{corona} = \frac{v_o - k'}{R' - A_2} \tag{4.19}$$

and

$$v_{corona} = \frac{R'v_o - A_2k'}{R' - A_2} \tag{4.20}$$

5. Influence on corona by adjacent sub-conductors in the same bundle

Extra-high voltage phase conductors are designed to consist of several sub-conductors bundled together in order to reduce corona losses. The electric field on a sub-conductor surface is affected appreciably by the adjacent sub-conductors in the same bundles. The corona phenomenon is consequently influenced.

The electric field on the sub-conductor surface due to the sub-conductor itself is given by[46]

$$\left| \bar{E}_{max} \right| = \frac{Q}{2\pi \varepsilon_o r} \quad , \; Q := \text{charge/length}$$

$$= \frac{\bar{cv}}{2\pi \varepsilon_o r} \tag{4.21}$$

where

c = effective capacitance/length

v = voltage of conductor

r = radius of sub-conductor

However, for a bundled conductor with 4 individual sub-conductors, the maximum electric field is given by[7] (See Figure 4.5)

$$\left| \bar{E}_{max} \right| = \frac{Q'}{2\pi \varepsilon_o} \left(\frac{1}{r} + \frac{2}{S\sqrt{2}} + 2\,\frac{2}{S} \sin 45^o \right)$$

$$= \frac{Q'}{2\pi \varepsilon_o r} \left(1 + \frac{6r}{S\sqrt{2}} \right) \tag{4.22}$$

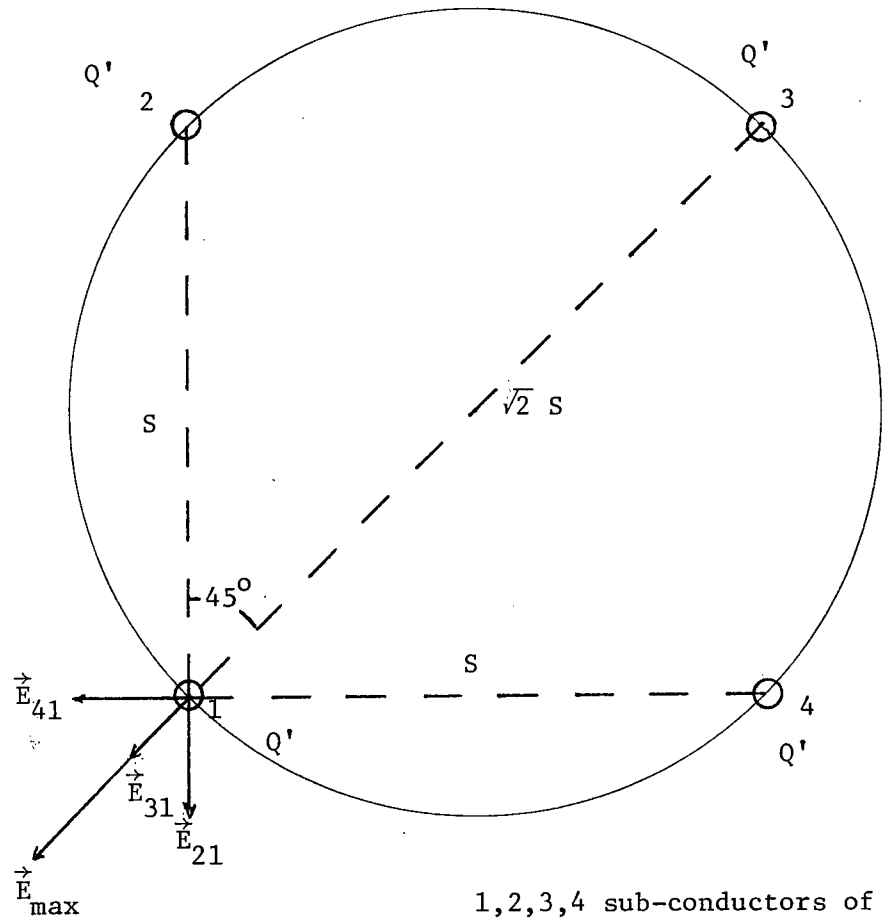

1,2,3,4 sub-conductors of radius r

$$\vec{E}_{max} = \frac{Q'}{2\pi\varepsilon_o r}\left(1 + \frac{6r}{\sqrt{2}S}\right)$$

where $Q' = \frac{C_{effective}V}{4}$

Figure 4.5: Critical voltage calculation by evaluation of maximum electric field on a 4-conductor bundle.

After the maximum electric field on the conductor surface is obtained, the critical voltage for corona discharge can be computed by equating the maximum electric field to 30 kV/cm or 3 x 10^6 v/m, the electric breakdown strength in air. A typical critical voltage for a single conductor has been found to be 277 kV, and that for a 4-conductor bundle to be 558 kV.

6. Influence on corona by adjacent phase conductors

Since the conductors in each phase are mutually coupled to one another, voltages are always induced in the adjacent conductors. Thus the maximum electric field on the conductor surface is affected. However, due to the design of transmission lines for extra high voltage levels, separating between phase conductors are usually large compared with radius of individual conductors. This effect usually change the overall critical overvoltages by less than 10%. But this change in critical voltage produces negligible effects on the overall corona attenuation and distortion characteristics on overvoltage wave (See Figure 4.6).

7. Optimal lumping locations and number of corona branch legs

The equations with corona phenomenon is now solved by the compensation method with the corona loss legs lumped at a few places along the transmission line. However, the optimal locations and optimal number of lumped elements has to be determined.

At first, 20 corona loss branches 70 m apart from one another were lumped between five transmission towers. Then, a separation of 350 m between the corona loss branches was used. This increase in separation increased the deviation of the predicted wave shape from field measurements appreciably (See Figure 4.7), from about 5 to 10%. This suggests that

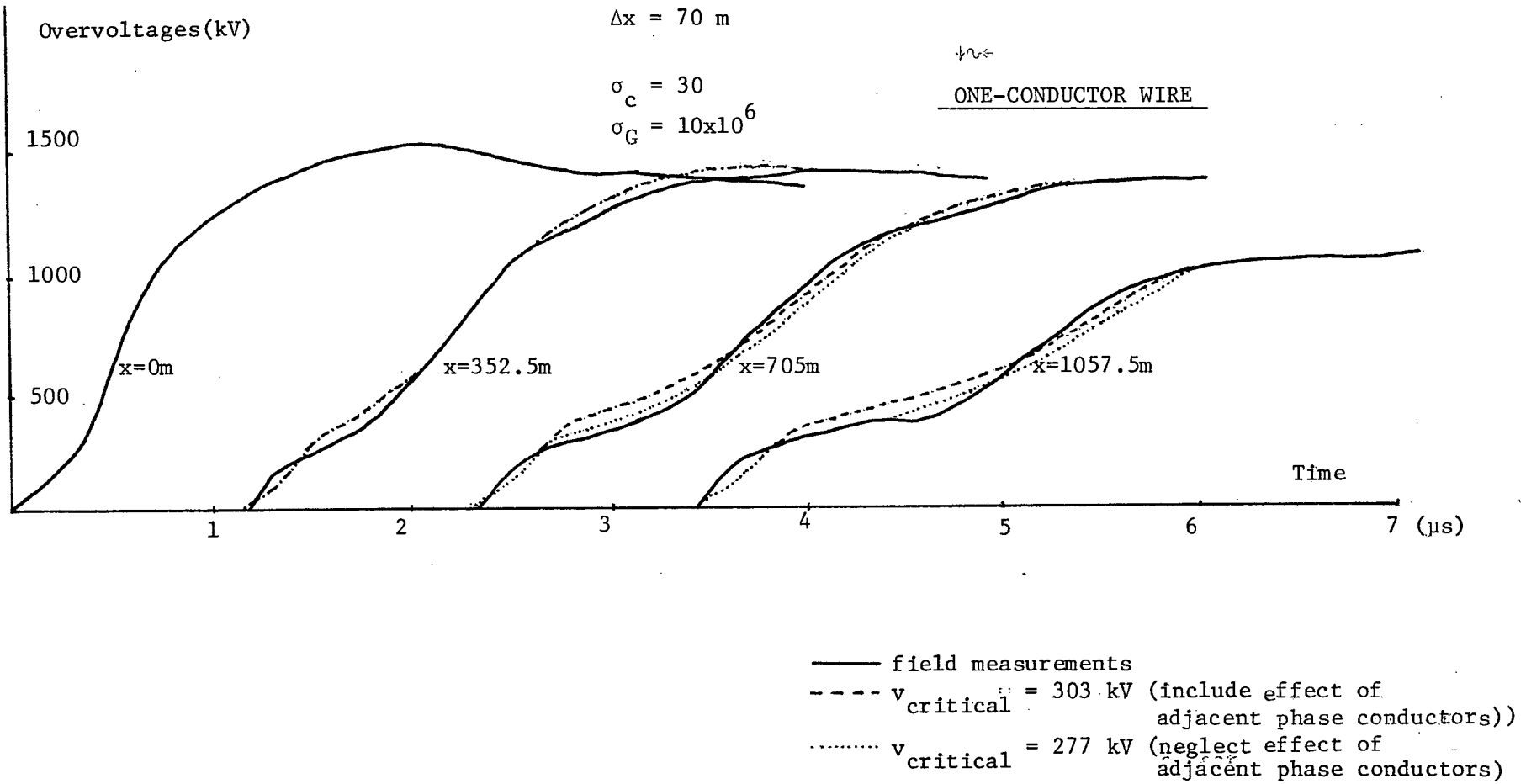

Figure 4.6: Effect of adjacent phase conductors on corona losses.

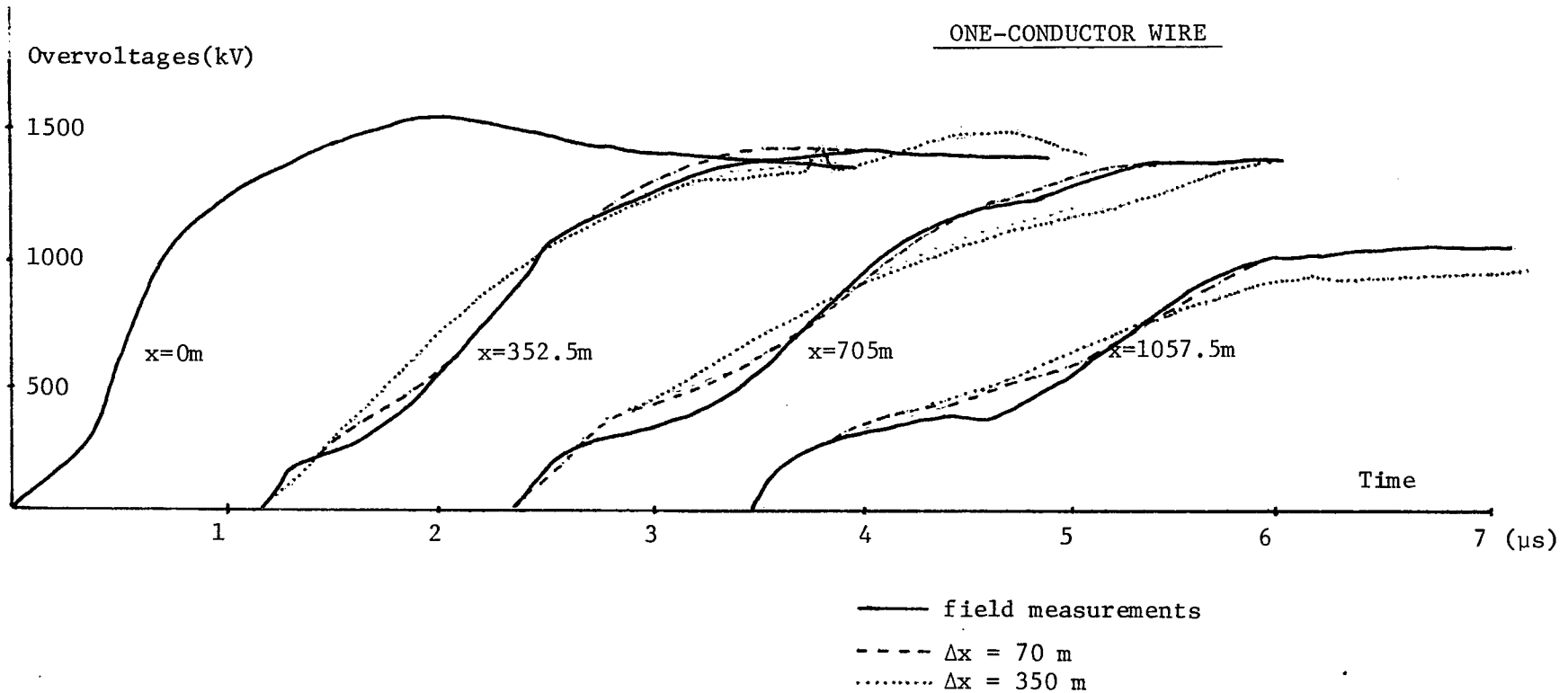

Figure 4.7: Effect of lumping distances on corona.

the optimal separation should be about 70 m.

The field measurement for a 4-conductor bundled was then simulated. In using the corona loss constants (for case of 1-conductor bundle)

$$\sigma_c = 30$$

$$\sigma_G = 10 \times 10^6$$

slightly higher overvoltages were obtained. Then, a new set of corona constants (for case of 4-conductors bundle)

$$\sigma_c = 30$$

$$\sigma_G = 20 \times 10^6$$

was used to give results consistent with those from field measurements (See Figure 4.8).

Finally, the negative impulse overvoltage was also simulated for the 4-conductor bundle case. The corona loss in this case was found to be much less than the positive impulse case. The corona loss constants were determined to be

$$\sigma_c = 15$$

$$\sigma_G = 10 \times 10^6$$

With these sets of corona constants, the field test measurement was again replicated closely (See Figure 4.9).

8. Overall numerical modelling for corona effects

The field test results of corona attenuation and distortion characteristics on a 500 kV test line were replicated by the method

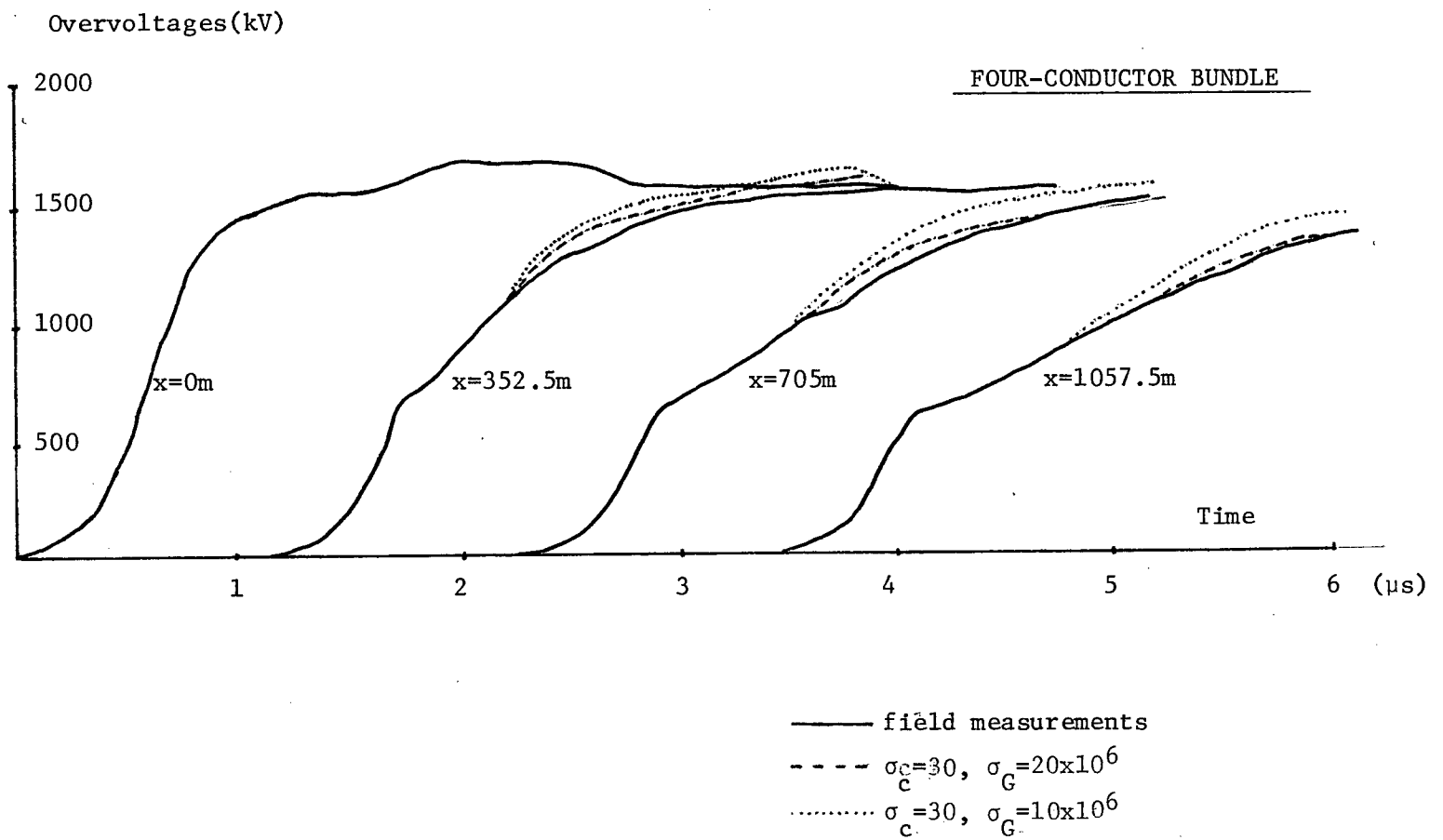

Figure 4.8: Positive impulse on 4- conductor bundle.

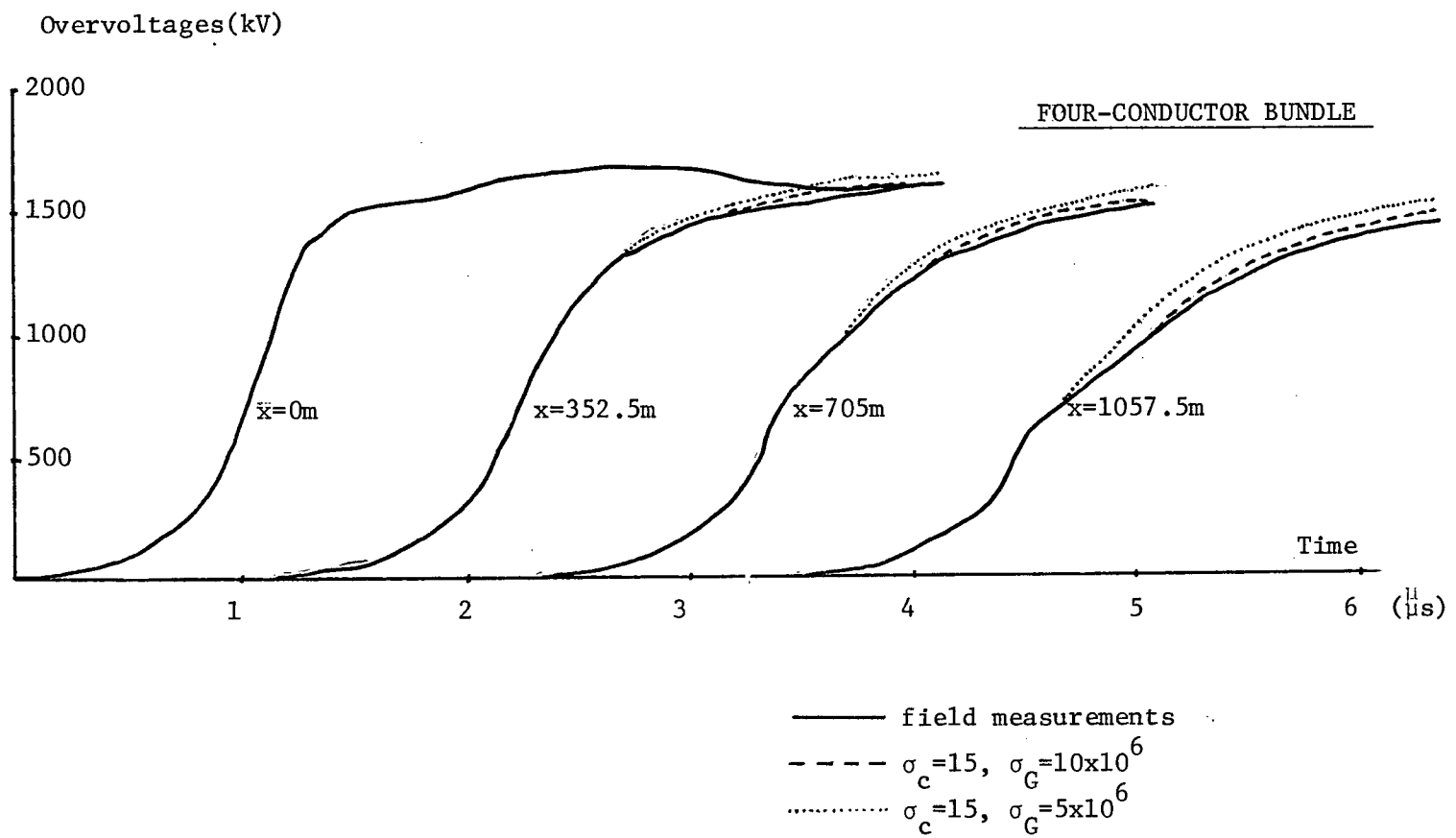

Figure 4.9: Negative impulse on 4- conductor bundle.

developed earlier. This method examined corona characteristics in both single and bundled conductor lines. From the performed study, one can conclude that the effects of bundling of conductors is efficient in increasing critical corona voltage. Furthermore, influence of adjacent phase conductors is negligible on corona effects. Thus, it is concluded that single phase line representation is sufficient for corona studies. Finally, it is determined that separation between the corona loss leg can be lumped at 70 m without sacrificing a loss of accuracy on the predicted coronated waveform. A reduction in distance between corona legs will not improve the accuracy of the simulated results.

It should be noted that lightning strokes will rarely hit more than one conductor at one time; thus corona phenomena have only been included for one conductor in this thesis, rather than for all three phases simultaneously.

CHAPTER 5: CONCLUSIONS

The attenuation and distortion of lightning overvoltage waves on multi-phase transmission lines and multi-phase single core SF_6 cables in compressed SF_6 gas-insulated substations was studied. Corona effects of lightning overvoltages on overhead lines were also investigated. Available field test results for corona effects were duplicated to within 5% accuracy.

Results obtained with the techniques developed by the author are useful for lightning insulation co-ordination studies[21] and other related studies[13,14,40]. The lightning surge wave front can be calculated at any location inside the substation, eg., inside the SF_6 bus or at the transformer terminal. Based on the studies described in the thesis the following recommendations are made for future insulation co-ordination design studies:

1. Multi-phase untransposed lines can be represented by single-phase line models using self parameters calculated at a high frequency of approximately 1 M Hz (See Table 2.4). Series resistance should be ignored. Frequency dependent effects are not important for propagation over distances less than 2 km.
2. Corona effects are important in reducing the magnitude and rate of rise of the incoming lightning overvoltage surge. Efficient solution techniques using compensation methods are developed to solve the non-linear corona attenuation and distortion phenomenon.
3. Multi-phase SF_6 single core cables can be represented by single phase cable models. Series resistance can be ignored. Cable parameter can be obtained with the simple formula for a go-return circuit for a coaxial cable with sufficient accuracy.

APPENDIX A: SKIN DEPTH ATTENUATION IN CONDUCTING MEDIUM WITH FINITE CONDUCTIVITY.

This section shows that the core current return characteristics through the sheath for the SF_6 cable could be obtained by a different approach. From the Maxwell's equations in a conducting medium, we have[50]

$$\nabla \times E = -j\omega\mu_o H \tag{A.1}$$

$$\nabla \times H = j\omega\epsilon E + \sigma E$$

$$= \sigma E, \text{ for good conductors} \tag{A.2}$$

where σ is conductivity of medium.

From equations (A.1) and (A.2), we can get

$$\nabla \times \nabla \times E = \nabla(\nabla \cdot E) - \nabla^2 E = -\nabla^2 E \text{ (for homogeneous medium)}$$

$$= -j\omega\mu\nabla \times H$$

$$= -j\omega\mu\sigma E$$

$$= -m^2 E$$

where

$$m = \sqrt{j\omega\mu\sigma}$$

$$= \frac{1 + j}{\sqrt{2}} \cdot \sqrt{\omega\mu\sigma}$$

This equation is identical to the diffusion equation with solutions

$$\frac{J_x}{\sigma} = E_x = E_o e^{-mZ}, \tag{A.3}$$

$$= E_o e^{-j\sqrt{\frac{\omega\mu\sigma}{2}} \cdot Z} \cdot e^{-j\sqrt{\frac{\omega\mu\sigma}{2}} \cdot Z} \tag{A.4}$$

$$= E_o e^{-jZ/\delta} \cdot e^{-jZ/\delta} \tag{A.5}$$

where $$\delta = \frac{1}{\sqrt{\frac{\omega\mu\sigma}{2}}} = \frac{1}{\sqrt{\pi f\mu\sigma}} \equiv \text{skin depth}$$

Thus, the tangential electric field E_x or the tangential current density J_x will be attenuated by $\frac{1}{e} = \cdot 368$ when the depth of penetration Z equals to the skin depth. For aluminum, we have the skin depth δ as

$$\delta = \frac{1}{\sqrt{\pi f\mu\sigma}} \tag{A.6}$$

$$= \frac{1}{\sqrt{\pi f(4\pi x10^{-7})(3\cdot 8x10^{7})}}$$

$$= \frac{8\cdot 1}{\sqrt{f}} \quad \text{cm}$$

Therefore, for frequency above 1 kHz, the electric field is essentially attenuated and negligible flux outside the sheath. Thus, since characteristic frequencies of lightning strokes exceeds 1 kHz, the above results indicate that each phase of the cable is decoupled from other phases as was shown previously in Chapter 3.

After the tangential current density for one medium is obtained by equations (A.3) to (A.5), the tangential current density for another medium on the boundary to the first medium can be obtained by

$$E_{1t} = E_{2t}$$

or $$J_{1t} = \frac{\sigma_1}{\sigma_2} J_{2t}$$

Thusm the total current flowing in different components of the cable system can be obtained by

$$I = \int J dA$$

BIBLIOGRAPHY

1. W. Diesendorf, 'Insulation coordination in high voltage electric power systems', Butterworth Co. London 1974.

2. M. Uman, 'Understanding lightning', Bek Technical Publication Inc., Pennsylvania, 1971.

3. 'Transmission and Distribution Reference Book', Westinghouse Electric Corporation, Pennsylvania,1964.

4. F. Popolansky, 'Frequency distribution of amplitude of lightning currents', Report No. SC 33-71 (WG01) IWD, presented at CIGRE Meeting, Lugano, 1971.

5. L.V. Bewley,'Travelling waves on transmission systems', Dover Publication, N.Y. 1951.

6. 'The Principle and Practice of Insulation Co-ordination', Canadian Standard Assoc. C308, presented to the CEA Meeting, March 1979.

7. 'Transmission line reference book - 345 kV and above', Electric Power Research Institute, Palo Alto, 1979.

8. G.W. Brown, 'Lightning Performance I - shielding failure simplified', IEEE Trans. PAS-97, pp. 33-38, January/February 1978.

9. K.C. Lee, 'Propagation of the wave front on untransposed overhead and underground transmission lines', UBC M.A.Sc. Thesis, April 1977.

10. J.C. Cronin, R.G. Colclaser, R.F. Lehman, 'Transient lightning overvoltage protection requirement for a 500 kV gas-insulated substation', IEEE Trans. PAS-97, pp. 68-78, January/February 1978.

11. Mitsubishi Electric Corporation, 'A conditon of insulation co-ordination study on Revelstoke Power Station 500 kV System', B.C. Hydro and Power Authority Report HAT-5159-B, HAT-5319, August 27, 1979.

12. Darveniza et al, 'Modelling for lightning performance calculations', IEEE Trans. PAS-98, pp. 1900-19 8, November/December 1979.

13. K.C. Lee, H.W. Dommel, 'Additions of untransposed - distributed parameter line models to the UBC Electromagnetic Transient Program', Progress Report to the System Engineering Division of B.C. Hydro and Power Authority, August 1979, (56 pages).

14. K.C. Lee, H.W. Dommel, 'Addition of modal analysis to the UBC Line Constants Program' ibid., January 1980, (39 pages).

15. UBC Computing Centre, 'UBC CEIGN' April 1972.

16. P.C. Magnusson, 'Travelling waves on multi-conductor open-wire line - a numerical survey of the effect of frequency dependence on modal decomposition', IEEE Trans. PAS-92, pp. 999-1008, 1973.

17. W.S. Meyer, H.W. Dommel, 'Numerical modelling of frequency - dependent transmission line parameters in an electromagnetic transients program', IEEE Trans. PAS-93, pp. 1401-1409, 1974.

18. J. Marti, UBC Ph.D Thesis (to be completed).

19. A. Ametani, 'Surge propagation on a 500 kV untransposed line: Field Test Results', CIGRE WG 13-05, 13-74 (WG•05) 36 IWD, October 1974.

20. A. Ametani, 'Surge propagation on Japanese 500 kV untransposed transmission line', Proc IEE-121, pp. 136-138, 1974.

21. K.K. Nishikawara, N. Cuk, H.W. Dommel, K.C. Lee, T. Nitta, Y. Shibuya, T. Tanabe, M. Imataki, 'Development of insulation co-ordination requirement for high voltage SF_6 CGI substations of B.C. Hydro and Power Authority', presented to Canadian Electrical Association Spring Meeting, Montreal, March 1980, also abstracted in Modern Power and Engineering p. 31 May 1980, (26 pages).

22. L.M. Wedepohl, 'Radio interference fields in multi-conductor overhead transmission line', Proc. IEE pp. 1875-1879, 1969.

23. R.D. Handel, 'Design of the MICA Hydro Electric Project', IEEE Trans. PAS-96, pp. 1535-1543, September/October 1977.

24. M. Mitani, 'Analysis of lightning surge phenomena and examination of insulation co-ordination in a 3-core type GI cable', presented to the 1979 IEEE PES Summer Meeting A79 401-1.

25. G.W. Brown, R.G. Rocamora, 'Surge propagation in the 3-phase pipe type cable, 'IEEE Trans. PAS-95, pp. 89-95, January/February 1976.

26. E. Comellini et al, ' A computer program for determining electrical resistance and reactance of any transmission line', IEEE Trans. PAS-92, pp. 308-314, March-April 1973.

27. K.O. Abledu, 'Impedance calculation of cable using sub-division of the cable conductors', UBC M.A.Sc. Thesis, September 1979.

28. E.R. Sunde, 'Earth conduction effects in transmission systems', Dover Publication, N.Y. 1968.

29. F. Pollaczek, 'Sur le champ produit par un conducteur simple infinement long parcouru par un courant alternatif', Revue gen. Elec. vol. 29 pp. 851-867, 1931.

30. L.M. Wedepohl, D.J. Wilcox, 'Transient analysis of underground power transmission systems', Proc. IEE vol. 120, pp. 252-260, 1973.

31. A. Ametani, 'A general formulation of impedance and admittance matrix of cables', IEEE Trans. PAS-99, pp. 902-910, May/June 1980.

32. A. Ametani, 'Performance of a theoretical investigation in multi-phase power system cables', Bonneville Power Administration Contract No. 14.03 6049 N, July 1976.

33. G. Bianchi, G. Luoni, 'Induced currents and losses in single-core submarine cables', IEEE Trans. PAS-95, pp. 49-58, January/February 1976.

34. H.W. Dommel, 'Line Constants of overhead lines and underground cables', UBC EE 553 notes, May 1978.

35. UBC Computing Centre, 'UBC Function CBESK', December 1977.

36. M. Abramowitz, I.A. Stegun, 'Handbook of Mathematical Functions', National Bureau of Standards, Applied Mathematics Series 55, November 1970.

37. S.A. Schelkunoff, 'The electromagnetic theory of coaxial transmission lines and cylindrical shells', Bell System Technical Journal, vol. 13, pp. 532-579, 1934.

38. T. Ono and H. Matsubara, 'Surge voltages in HVDC submarine cables', Electrical Engineering in Japan, vol. 94, pp. 42-49, 1974.

39. A. Greenwood, 'Electrical transients in Power systems', Wiley Interscience, N.Y. 1971.

40. K.C. Lee, H.W. Dommel, 'Calculation of cable parameters of a single core SF_6 cable', Progress Report to the System Engineering Division of B.C. Hydro and Power Authority, April 1980.

41. F.W. Peek, 'Laws of corona I II III', AIEE Trans. vol. 30, p. 1889, 1912.

42. H.H. Skilling et al, 'Distortion of travelling waves by corona', AIEE Trans, vol. 50, p. 850, 1937.

43. J. Umoto et al, 'Numerical analysis of surge propagation in single conductor system considering corona losses', Electrical Engineering in Japan, vol. 89, p. 21, 1968.

44. G.W. Brown, 'Lightning Performance II - updating backflash calculations', IEEE Trans. PAS-97, pp. 34-51, January/February 1978.

45. A. Inoue, 'High voltage travelling waves with corona discharge on bundle conductors', presented to the IEEE 1978 Winter Meeting A78 170-3.

46. W. Hayt, 'Engineering Electromagnetics', McGraw Hill , N.Y. 1974.

47. H.W.Dommel, W.S.Meyer, 'Computation of electromagnetic transients' , Proc. IEEE vol.62, pp.983-993, July 1974.

48. H.W.Dommel, private communication July 1979.

49. G. Strang, 'Linear algebra and its applications',Academic Press N.Y. 1976.

50. A.T.Adams, ' Electromagnetics for engineers', Ronald Press Company, New York, N.Y. 1971.

51. G.L. Ford, E.P.Dick, ' Study of fault-produced overvoltages as related to grounding practise for SF_6-insulated substations', Canadian Electrical Association Contract No. 071T101, Sept. 1979.

52. ' Lightning protection design guide book for power stations and substations', Central Research Institute of Electric Power Industry CRIEPI Report No. 175034, Tokyo, Japan 1976. (in Japanese)